U.PORTO

U.PORTO
FEUP FACULDADE DE ENGENHARIA
UNIVERSIDADE DO PORTO

Analysis of ply damage using computational micro-mechanics: transverse shear failure mechanisms

Tiago Vaz Maia Vieira

Dissertation submitted to
Faculdade de Engenharia da Universidade do Porto
for the degree of:

Mestre em Engenharia Mecânica

Advisor:
Prof. Dr. Albertino Arteiro

Secção de Mecânica Aplicada (SMAp)
Departamento de Engenharia Mecânica (DEMec)
Faculdade de Engenharia da Universidade do Porto (FEUP)

Porto, 2020

The work presented in this dissertation was performed at the
Section of Applied Mechanics
Department of Mechanical Engineering
Faculty of Engineering
University of Porto
Porto, Portugal.

Tiago Vaz Maia Vieira
E-mail: up201709031@fe.up.pt

Albertino José Castanho Arteiro
E-mail: aarteiro@fe.up.pt

Faculdade de Engenharia da Universidade do Porto
Departamento de Engenharia Mecânica
Secção de Mecânica Aplicada
Rua Dr. Roberto Frias s/n, Edifício L, Sala L303
4200-465 Porto
Portugal

Abstract

Qualification of fibre-reinforced polymers for the manufacturing of structural components in the aeronautical industry is usually associated with extensive and costly experimental campaigns. The burden of testing is immense and materials should be characterised under different loading stress states (tensile, compressive, shear) to assess their structural integrity during service conditions. Recent developments in microscale simulation, together with increased computational power and improvements in modeling tools, can be used to alleviate this scenario.

The effect of ply thickness on the onset of ply damage, in terms of matrix cracking, is extremely important for the prediction of the mechanical response of laminated composite structures. This is of particular significance when dealing with the most recent spread-tow, ultra-thin plies, where ply thickness can be extremely low.

By reducing the ply thickness in a multidirectional laminate, an *in-situ* effect occurs consisting of matrix cracking suppression, which provides high strength and delays damage onset, thereby enhancing the fatigue life of a composite laminate.

During the last few years, computational micro-mechanics proved to be a reliable tool for understanding of the *in-situ* effect. In this dissertation, a micro-mechanical model is used to study the effect of ply thickness on constrained 90° plies subjected to transverse shear loading, thus extending the current understanding of such phenomenon.

The micro-mechanical framework proposed in this work is able to accurately represent the micro-mechanical response of ultra-thin plies when subjected to transverse shear loading, including (i) the mechanics of transverse shear cracking onset and propagation, (ii) a consistent orientation of the fracture plane of the 90° lamina, (iii) the constraining effect observed in the lamina embedded in a multidirectional laminate (iv) the gradual, slow stress relaxation and progressive transverse cracking observed in very thin plies, and consequent increase of the crack density, and (v) an *in-situ* effect in transverse shear.

Keywords: Thin-ply composite laminates, *In-situ* effect, Matrix cracking, Ply damage, Computational micro-mechanics, Finte Element Analyses.

Resumo

A caracterização de polímeros reforçados com fibras para a produção de componentes estruturais na indústria aeronáutica é usualmente associada a campanhas experimentais extensas e dispendiosas. A dificuldade no teste deste tipo de materiais é imensa, e estes devem ser caracterizados sob diferentes tipos de solicitação (tração, compressão, corte), de forma a avaliar a sua integridade estrutural nas suas condições de serviço. Desenvolvimentos recentes na simulação à micro-escala, juntamente com o aumento do poder computacional e melhorias em ferramentas de modelação, podem ser usadas para aliviar este cenário.

O efeito da espessura da camada na iniciação de dano, em termos de fendas na matriz, é extremamente importante para a previsão do comportamento mecânico de estruturas laminadas compósitas. O mesmo é de particular interesse quando se está perante os mais recentes compósitos de camadas ultrafinas, onde a espessura da camada é extremamente pequena.

Ao reduzir-se a espessura da camada num laminado multidirecional, um efeito *in-situ* ocorre, consistindo na supressão de fendas na matriz, que conduz a uma maior resistência mecânica e atrasa o início do dano, deste modo aumentando a resistência e a vida à fadiga do laminado compósito.

Ao longo dos últimos anos, a micromecânica computacional provou ser uma ferramenta robusta para se compreender o efeito *in-situ*. Nesta dissertação, um modelo micromecânico é usado para estudar o efeito da espessura da camada, em camadas a 90° embebidas e submetidas a uma carga de corte transversal, estendendo assim o atual conhecimento deste fenómeno.

A abordagem micromecânica proposta neste trabalho é adequada para a representação precisa da resposta micromecânica de camadas ultrafinas quando sujeitas a uma solicitação de corte transversal, incluindo (i) a mecânica de início e propagação de uma fenda por corte transversal, (ii) uma orientação do plano de fratura da camada a 90° consistente, (iii) o efeito de restrição observado na camada embebida num laminado multidirecional, (iv) uma gradual relaxação de tensão e progressiva fissuração transversal observada em camadas muito finas, e consequente aumento da densidade de fissuração, e (v) um efeito *in-situ* em corte transversal.

Keywords: Laminados compósitos de camadas ultrafinas, Efeito *in-situ*, Fendas na matriz, Dano da camada, Micro-mecânica computacional, Análise de Elementos Finitos.

To my parents,
and my beloved goddaughter Maria Beatriz.

'And however difficult life may seem,
there is always something you can do, and succeed at.
It matters that you don't just give up.'

Stephen Hawking

Acknowledgements

This dissertation ends up a five-year academic route in Mechanical Engineering, where I had contact with the most extraordinary people I ever saw. I sincerely believe that these people not only strongly contributed to the quality of the present work, but also to the whole intellectual development I got during these years. I hope that somehow I have already expressed my praise to all of them, which are certainly not limited to those mentioned here.

Firstly, a special gratification should be given to my advisor, Prof. Dr. Albertino Arteiro, for his scientific rigor, organization, and outstanding capacity in solving problems. This opportunity to work in a team with him was highly motivating for me, as I was conscious I was working with a great professional. I am pretty sure that this was an experience that I will never forget.

Secondly, I would also express my heartfelt gratitude to the Section of Applied Mechanics from the Faculty of Engineering of the University of Porto. Particularly I would like to thank Prof. Dr. Paulo Tavares de Castro, Prof. Dr. José Dias Rodrigues, Prof. Dr. Pedro Ponces Camanho, Prof. Dr. Renato Natal Jorge, and Prof. Dr. José Soares Esteves, for their constant effort in teaching and captivating students to the branch of Machine Design and Structural Engineering.

I too owe a special thanks to my friends, António Couto Carneiro and Miguel Couto Aires, for never letting one single doubt unclarified, and helping me with the smallest things that eventually made a big difference in the present work.

Finally, I want to thank all the people that were an important part of my life during the past five years.

To my long time friends André Parente, Miguel Ângelo, Orlando Carriço and Rui Rajão, for the genuine friendship we established since the beginnings of college. Part of what we are today, we owe to this friendship, where the jokes, the football games, the study, and mainly the personal support, were always the pillars of such relationship.

To all the friends I made in FEUP and accompanied me throughout this journey, especially João Filipe, Luís Ramos, Miguel Dantas, Pedro Camacho and Tiago Teixeira. This is a farewell to the academic life, however, an introduction to a new stage awaits us, thus, it is only a “see you soon”. You can always count on me, and I wish you all the best.

To my nuclear family, my greatest acknowledgments are adressed. To my parents Maria das Dores and Manuel Vieira, the humblest human beings I ever met, for teaching me the value of honest work, for their unconditional love and support, and for always believing in my capacities. The man I am today I owe you. To my sister Maria Vaz, for being always present in my life, and helping me in taking care of our beloved parents. To my brother in law Samuel Dantas and my uncle José Rodrigues, whose their silent example, taught me that, inside the engineering world, the humility and hard work need to be present, both at the same level, on our daily routine. Finally, to my beloved goddaughter Maria Beatriz, that although being a baby, is capable of either putting a ripped smile on the godfather's face, or motivating him to give his best.

Last, but not least, to Marta Pires, my lucky charm, whose, although has not accompanied me this journey since the beginning, was crucial to its conclusion. For her tremendous patience in these last months always accompanied by incessant gestures of affection and true love.

My sincere esteem to you all,

Tiago Vaz Maia Vieira

Contents

List of Figures

List of Tables

Nomenclature

General Abbreviations

2D	**B**i-**D**imensional
3D	**T**hree-**D**imensional
BK	**B**enzeggagh-**K**enane
CFRP	**C**arbon **F**ibre-**R**einforced **P**olymer
CMM	**C**omputational **M**icro-**M**echanics
COD	**C**rack **O**pening **D**isplacement
DIC	**D**igital **I**mage **C**orrelation
ERR	**E**nergy **R**elease **R**ate
FAW	**F**ibre **A**real **W**eight
FPF	**F**irst-**P**ly **F**ailure
FRP	**F**ibre-**R**einforced **P**olymer
FE	**F**inite **E**lement
LEFM	**L**inear **E**lastic **F**racture **M**echanics
LPF	**L**ast-**P**ly **F**ailure
NCF	**N**on-**C**rimp **F**abrics
PBC	**P**eriodic **B**oundary **C**ondition
SEM	**S**canning **E**lectron **M**icroscope
RVE	**R**epresentative **V**olume **E**lement
UD	**U**ni**d**irectional

Latin Variables

a	RVE width (y-direction)
b	RVE thickness (z-direction)
c	RVE length (x-direction)
c_d	Dilatational wave speed in a FE
D_f	Fibre diameter
E	*Young's* modulus
E_1	Longitudinal *Young's* modulus
E_2	Transverse *Young's* modulus
E_I	Internal energy
E_V	Viscous energy dissipated
E_{FD}	Frictional energy dissipated

E_{KE}	Kinetic energy
E_{IHE}	Internal heat energy
E_W	Work done by externally applied loads
E_{PW}, E_{CW}	Work done by contact and constraint penalties
E_{MW}	Work done by propelling added masses
E_{HF}	Heat energy through external fluxes
E_{total}	Total energy
G	Shear modulus
G_{12}	In-plane shear modulus
G_{23}	Transverse shear modulus
$\mathcal{G}_c$	Critical energy release rate
$\mathcal{G}_{\mathrm{I}c}$	Critical ERR in mode I
$\mathcal{G}_{\mathrm{II}c}$	Critical ERR in mode II
$\mathcal{G}_{\mathrm{III}c}$	Critical ERR in mode III
h	Embedded homogenised material size
h_c	Transverse crack height
K	Stiffness
k	RVE integration point
L_{min}	FE characteristic length
N_p	RVE total number of integration points
S_L	In-plane shear strength
S_L^{is}	*In-situ* in-plane shear strength
S_T	Transverse shear strength
S_T^{is}	*In-situ* transverse shear strength
T_0	Stress-free temperature
t	Ply thickness
t_{out}	Outer ply thickness
V	RVE volume
V_f	Fibre volume fraction
V^k	Associated volume of the RVE integration point
w	Applied vertical (z-direction) displacement on the RVE
$\dot{w}$	Applied vertical (z-direction) velocity on the RVE
X_T	Tensile strength
X_C	Compressive strength
Y_C^{is}	*In-situ* transverse compressive strength
Y_T^{is}	*In-situ* transverse tensile strength

Greek Variables

α	Thermal expansion coefficient
α_0	Fracture angle
α_{11}	Longitudinal thermal expansion coefficient
α_{22}	Transverse thermal expansion coefficient

α_{FP}	Fracture plane angle
β	Shear stress-strain relation non-linearity parameter
γ_{23}	Transverse shear strain
$\bar{\gamma_{23}}$	Applied transverse shear strain
γ_{23}^{0}	Homogenised transverse shear strain
$\gamma_{23}^{0,\mathrm{Eq}}$	Equivalent applied transverse shear strain
γ_{23}^{k}	Transverse shear strain determined at an integration point
Δt	Step time increment
η	Mixed-mode interaction parameter
η_L	Longitudinal friction coefficient
$\eta_{L,is}$	*In-situ* longitudinal friction coefficient
η_T	Transverse friction coefficient
$\eta_{T,is}$	*In-situ* transverse friction coefficient
θ	Orientation of the outer plies
λ, μ	Lamé constants
ρ	Mass density
ν	*Poisson's* ratio
ν_{12}	Major in-plane *Poisson's* ratio
ν_{23}	Transverse *Poisson's* ratio
ν_p	Plastic *Poisson's* ratio
τ_1^0,τ_2^0	Interfacial shear strengths
τ_3^0	Interfacial normal strength
τ_{23}	Transverse shear stress
$\bar{\tau_{23}}$	Applied transverse shear stress
τ_{23}^{0}	Homogenised transverse shear stress
τ_{23}^{k}	Transverse shear stress determined at an integration point
ϕ	Ply configuration parameter
ω_{max}	Maximum eigenfrequency of an assembled mesh
ω_{max}^{e}	Highest eigenfrequency of an individual FE in the mesh

Chapter 1

Introduction

This introductory chapter provides the context for the current dissertation. A brief introduction to the increasing importance of composite materials in the design and development of new structural components, particularly for the aeronautical, automotive and marine industries, is presented. Then, a new manufacturing technology for composite laminates is exposed, which introduces the motivation of the present research, whose objectives are formally defined afterwards. Finally, the thesis layout is provided at the end of the chapter.

1.1 Background

A composite material is the result of a macroscopic combination between two or more different materials. Such combination is advantageous, as it leads to a material that exhibits superior properties than those of the individual constituent materials acting independently [1; 2]. Most man-made composite materials are made from two materials: a reinforcement material typically in the form of fibres, and a base matrix material. The stiffness and strength present in the composite come from the reinforcement, while the matrix is responsible to keep the fibres together, protect them against environmental threats, and transfer the load between them. Typically, the composite materials emerge on nature under three diferent types: fibrous composites, which consist of continuous or discontinuous fibres in a matrix material; particulate composites, which are composed of macro size particles in a matrix; and laminated composites, which are made of layers of different materials, including composites of the first two types [3]. The processing flexibility and low-density of polymer materials, turn the so-called FRPs the most common composite materials in industry, especially for structural applications that require high performance. Advanced FRPs are often fabricated in the form of laminates, consisting of a number of thin layers, called laminae or plies, stacked together, each one oriented in a given direction. The thickness and the orientation of each ply, along with the stacking sequence or layup and the interlaminar strength between plies, are factors that influence the mechanical behaviour of a composite laminate - see Figure 1.1.

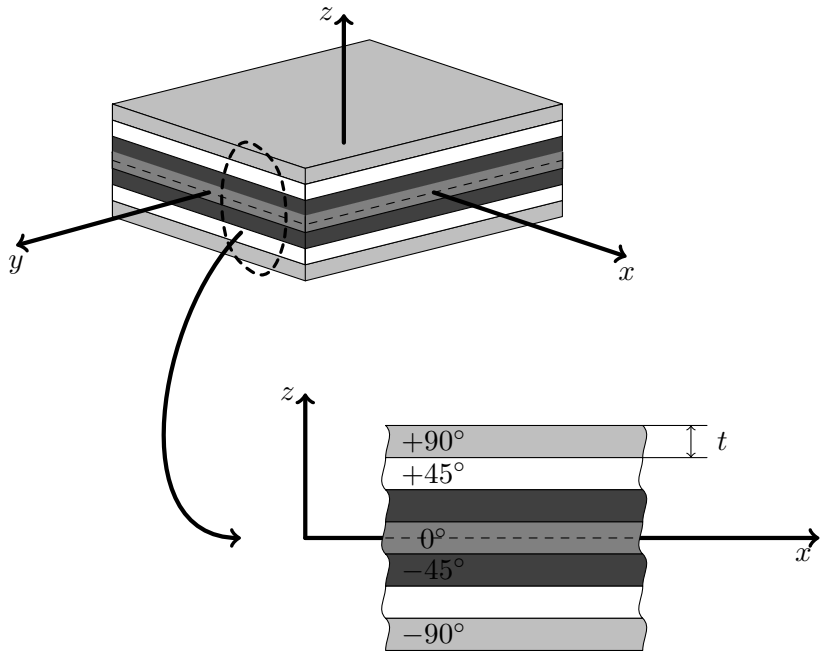

Figure 1.1: Schematic representation of a FRP composite laminate.

Over the last few years, composite materials have seen an increase in structural applications, namely on aeronautical, automotive, and marine industries. Such applicability is gradually evolving from secondary, non-critical applications to lightweight primary load-bearing structural applications. Regarding the aeronautical industry, the incorporation of this technologically advanced materials is tremendous and evident, as nearly all airplanes use composites extensively, having been now introduced in primary structural components in the most recent long-range airplanes such as the center wing box, the fuselage or the wings [4]. In the automotive industry, the new advanced powertrain systems for hybrid and electric vehicles lead to a weight increase, thus the application of advanced FRPs in primary structural components is also becoming increasingly important [5; 6]. Finally, in the marine industry, the demanding in-service conditions due to environmental phenomena also motivate application of this type of advanced materials in structural components. Advanced FRPs are ubiquitous in pleasure boat and racing yacht construction and are widely used in the construction of fast ferries, naval and coastguard patrol craft, fishing and workboats, and in offshore oil and gas platforms [7].

One reason for this wider application of FRPs is because components made of composite materials can be engineered to offer outstanding mechanical (stiffness and strength), fatigue, ballistic, thermal, acoustic, corrosion, and electromagnetic properties, typically with reduced weight. Such characteristics promote the use of renewable energy and generally result in a far more sustainable lifestyle. Currently this is becoming even more apparent as the significance of life cycle assessment is being recognised. Another reason is due to all existing processing techniques. Composites give designers and engineers tremendous freedom in terms of both form and function. Compound curves and complex geometries can be readily incorporated, maximizing structural integrity and performance. Furthermore, composites also favour the development of integrated design when a part or component is suitable to be manufactured in "one-shot", avoiding laborious joining and fitting operations.

1.2 Motivation

1.2.1 New composite materials technologies

Knowledge of constituent material properties is an important aspect when defining a composite structural component for a given application and in understanding how that component will respond to the various stimuli likely to be imposed on it. When the development of new manufacturing technologies leads to new composite materials, understanding their potential advantages and disadvantages concerning manufacturing, processing, mechanical behaviour, design and cost-effectiveness is crucial for their successful and safe introduction into new markets and applications.

In the domain of commercial aircraft, advanced laminated composites, namely CFRPs, have seen an increasing use in structural applications in the airframe and other aeronautical structures, mainly because when compared to other materials, CFRP-based aero-structures offer: weight saving, which leads to fuel saving, increase in payload, and/or increase in range, improving performance; good fatigue resistance, which leads to enhanced life and savings in the long-term cost of the component; and good corrosion resistance, which means fewer requirements for inspection, resulting in savings on maintenance cost [1; 8]. However, in order to ensure safe operation, there is a huge concern when designing composite structures, thus, currently, large safety margins are present in the design process. This is due to the lack of deep knowledge and predictive capability of the mechanical response and complex failure behaviour of composite materials, which limits full exploitation of their benefits. This is also due to the high susceptibility of CFRPs to sub-critical damage mechanisms, which degrade their mechanical performance without showing any external evidence of damage.

Since laminated composites are heterogeneous materials, their damage behaviour is quite different from that of commonly used materials (metals, for instance), generally more complicated, and dependent on several factors, such as the properties of the constituent materials, the fibre orientation, the stacking sequence, or the nature of loading, to mention just a few [9]. The typical damage behaviour of laminated composites includes transverse micro-cracking, fibre breakage and delamination. Usually, transverse micro-cracking through the thickness of the ply occurs as FPF mode, followed by delamination. Fiber breakage usually happens at the last stage of the failure process. However, laminated composites can totally lose their structural integrity only due to matrix-dominated damage (both micro-cracking and delamination), without any fibre breakage [9].

Accordingly, when promising new composite technologies appear, the aeronautical industry tries to follow up their development, aiming to improve the performance of the aero-structures. One new technology of interest, which is already available comercially, is the spread-tow thin-ply technology.

1.2.2 Spread-tow thin-ply technology

The spread-tow thin-ply technology is a recent technique that is used to continuously and stably open thick fibre tows and obtain uniform plies significantly thinner than the conventional ones [10; 11]. A careful control of the tension in the tows allows to cost-effectively produce flat and straight plies with a dry ply thickness as low as 0.020 mm

without damaging the filament fibres. There are several potential advantages regarding the use of such ultra-thin plies:

- On one hand, the use of thinner plies allows the production of thinner and lighter laminates and composite structures. On the other hand, per given laminate thickness, more plies can be accommodated, increasing the design space and leading to a possibility of using smaller relative fibre angles between adjacent plies, which is considered beneficial when it comes to delamination between plies [12].
- By reducing the ply thickness in a multidirectional laminate, the *in-situ* effect characterised by an increase in transverse strength of a lamina constrained between two plies with a different fibre orientation gains additional importance. Matrix cracking is suppressed without the use of special resins, providing high strength, enhancing fatigue life, and improving resistance to leakage events [13; 14]. In fact, thin-ply laminates are intrinsically stronger than thick-ply laminates.
- Spread-tow plies exhibit improved fibre orientation and distribution, potentially leading to fewer weak zones.

The availability of such thin plies with a ply thickness equal to or below 0.100 mm opens a broad range of new possibilities in composites design, but also new challenges in understanding how ply thickness will affect the mechanical behaviour of composite laminates. Studies assessing the mechanics of thin-ply laminates have been carried out recently, and preliminary conclusions have been reached. Some studies were carried out to assess the *in-situ* effect and its consequences on ply damage [15–21]. These studies were performed considering transverse, tensile [15; 17–21] and compressive [16] loading scenarios. However, this effect, and its consequences, are not completely characterised. Similar studies considering shear loading scenarios, are scarce, but would be important to further understand the *in-situ* effect under more general stress states.

1.3 Objetives

The main objective of this dissertation is to study, in a micro-mechanical context, matrix cracking development considering shear loading scenarios, therefore, providing a more comprehensive analysis of ply damage within FRP composite laminates under complex loading conditions that would otherwise be very difficult or impossible to assess, for example, through direct experimental observations. In particular, it is the objective of this work to assess the effect of ply thickness on the transverse shear response of UD laminae embedded in multidirectional laminates.

To accomplish this objective, the following tasks were carried out in the context of this work:

- Literature review concerning the introduction and application of thin-ply composite laminates in structural design, the effect of ply thickness on the mechanical behaviour of composite laminates in terms of matrix cracking and the *in-situ* effect, and the application of CMM to study this deterministic size effect;
- Development of a CMM model for the analysis of ply damage, based on the constitutive models of the constituent materials of advanced FRPs;

- Micro-mechanical analysis of ply damage in polymer composite laminates subjected to a transverse shear stress state;

- Assessment of the effect of ply thickness on the micro-mechanical response of embedded UD laminae subjected to a transverse shear stress state.

1.4 Thesis layout

This thesis is organized in 5 chapters. After this first introductory chapter, the structure of this thesis is as follows:

- **Chapter 2 - State-of-art and literature review**
  A brief description and contextualization of the main topics of this study is presented in this chapter. Firstly, thin-ply composite laminates are introduced, followed by a discussion of the effect of ply thickness on the mechanical behaviour of composite laminates in terms of matrix cracking and *in-situ* effect. Then, the general aspects of CMM and its applicability to study the *in-situ* effect are reviewed.

- **Chapter 3 - Computational micro-mechanics. Model formulation**
  This chapter is devoted to the formulation of the micro-mechanical FE model. Firstly, the models that represent the constituent materials of advanced FRPs are introduced. Then, the modelling techniques employed on the FE model, in terms of mesh discretisation, loading and boundary conditions, and the strategy adopted to characterise the transverse shear strain of the RVE are described. Lastly, the model execution definitions necessary to perform the micro-mechanical analysis are presented.

- **Chapter 4 - Micro-mechanical analysis of ply damage under transverse shear stress. Numerical results**
  This chapter presents the numerical results obtained by micro-mechanical analysis. Firstly, the mechanics of the transverse shear cracking in the embedded UD laminae is described. Following, the effect of ply thickness is analysed by means of a normalised crack height. Finally, an *in-situ* effect in transverse shear is documented.

- **Chapter 5 - Conclusion**
  A summary of the main conclusions and most relevant contributions of this thesis are presented in this final chapter. In addition, suggestions for future work based on the results of this dissertation are briefly described.

- **Appendix A - Analysis of ply damage using computational micro-mechanics - In-plane shear**
  This appendix intends to present a suggestion to perform a similar micro-mechanical analysis to further assess the effet of ply thickness on the in-plane shear response of UD laminae embedded in multidirectional laminates.

Chapter 2

State-of-art and literature review

In this chapter, firstly, a brief introduction to thin-ply composite laminates, and the opportunities, in terms of manufacturing and design, brought by this new generation of composite laminates, is presented. Then, a comprehensive literature review concerning the effect of ply thickness scaling on the mechanical response of multidirectional composite laminates, in terms of matrix cracking and the *in-situ* effect, is discussed. A possible way through for the understanding of this effect is the use of CMM. Therefore, lastly, an introduction to CMM, along with a brief literature review of the studies of ply thickness effects using this computational technique, are also presented.

2.1 Thin-ply composite laminates

2.1.1 Introduction

Conventional composite laminates are made of plies with a FAW higher than $100\,\mathrm{g\,m^{-2}}$. However, a new generation of composite laminates has been introduced in the market — thin-ply composite laminates. This type of laminates is made of plies with a FAW below $100\,\mathrm{g\,m^{-2}}$, typically $50\,\mathrm{g\,m^{-2}}$ or even $25\,\mathrm{g\,m^{-2}}$. The plies are manufactured by a method known as spread tow thin-ply technology, in which large fibre tows are continuously spread to a flat thinner tape. Reduced ply thickness leads to better dispersion of the fibres throughout the composite laminate, which results in a more homogeneous material than conventional composite laminates — see Figure 2.1.

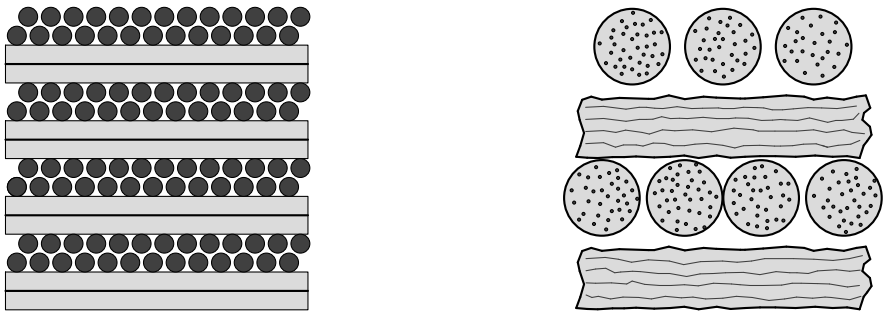

(a) Thin-ply laminate (b) Thick-ply laminate

Figure 2.1: Schematic representation of a thin-ply and thick-ply morphology (adapted from [22]).

The use of thin-ply composite laminates offers a large set of advantages over the conventional ones. Besides the general advantages presented in Section 1.2.2, the employment

of this new generation of composite laminates also renders several opportunities in manufacturing and design of composite laminates. Therefore, it is not surprising to see that the interest of the scientific and industrial communities in the spread-tow thin-ply technology has increased drastically in the last years. A review concerning opportunities in manufacturing and design with thin-ply composite laminates is presented in the next sections.

2.1.2 Opportunities in manufacturing and design

On first sight, it might appear that structural part production using thin-ply laminates will result in a clear disadvantage, as per laminate thickness, more plies will have to be accommodated. However, novel reinforcement architetures enabled by the unique uniformity of thin plies allow their efficient use in laminate design, due to a reduced degree of waviness in NCF and reduced crimp angle and tow flexure in woven fabrics [23]. Moreover, heavier tow yarns (with 100 k or 200 k fibre counts) can be used to reduce the cost of the source fibre tows and balance the additional cost of the spreading step required before the stabilisation and the laying or weaving steps. Due to easier homogenisation, there are opening perspectives for automated and continuous lay-up on the structural part production, thus also significantly reducing production costs [15].

The unique ply uniformity of thin plies also leads to an excellent surface appearance which may imply a reduction in the production costs of structural parts in terms of surface finishing and painting. During manufacturing, improved fibre distribution and wider inter-fibre spacing allows easy impregnation by either thermosetting resins or thermoplastic matrices, leading to fewer defects such as voids or resin-rich areas, despite lower fibre volume fractions [23].

In addition, reduced ply thickness favours the suppression of thermally-induced damage [23] as a result of an *in-situ* effect (please refer to Section 2.2.2). For instance, in an experimental programme conducted by Fernberg and Joffe [24], very few to no transverse cracks in spread-tow fabric laminates after manufacturing were observed, as opposed to conventional woven fabrics. Another advantage of ply thinness is the design of ply drops, which become much smoother — see Figure 2.2. By such design, not only the appearance is improved, but also the structural integrity of the laminates, due to the resultant lower ERR present at the interfaces between ply drops [23].

(a) Ply drop with thin plies (b) Ply drop with thick plies

Figure 2.2: Schematic illustration of ply drops with thin and thick plies (adapted from Arteiro et al. [23]).

By employing thinner plies, for the same laminate thickness, more plies can be accommodated. On one hand, there is an opportunity to widen the design space due to the increased flexibility in accommodating plies of different orientations. On the other hand, laminate homogenisation through the repetition of sub-laminates is easier to reach for the typical laminate thickness currently required in advanced structural design. In particular, mid-plane symmetry becomes irrelevant, since thermal warpage is negligible; as a consequence optimisation may rely only on topological optimisation [23; 25]. In addition, simpler lay-up processes are enabled, since reversing the stacking sequence at the mid-plane is no longer needed. Thereby continuous stacking becomes possible, and ply drops no longer need to be symmetric, thus the processing time, cost, waste and stacking errors are reduced. Furthermore, by avoiding the symmetry rule, the laminate design space widens further and the optimisation for out-of-plane loading and damage tolerance, where non-symmetric laminates can perform better, becomes easier [23].

Through the allowance of a higher number of repeated sub-laminates, the potential for a general laminate thickness reduction on buckling- and damage tolerance-driven laminate design also increases. Additionally, minimum gauge structures are expected to benefit from the introduction of thin plies, as it leads to lower discrete steps in terms of ply thickness; when the theoretical minimum gauge corresponds to a non-integer number of plies, by simply adding one thin ply will lead to a thinner, and therefore, lighter structure than adding one conventional ply [23].

As already mentioned in Section 1.2.2, having more plies per laminate thickness leads to the possibility of using smaller relative ply orientations between adjacent plies, further improving delamination [12], as well as impact resistance [23; 26]. It is also observed that sub-laminates with smaller relative ply orientations reduce the gap between FPF and LPF in such a way that matrix cracking can be completely suppressed before the ultimate failure strain of the laminate (please refer to Section 2.2.2).

Thin carbon plies also favour the development of hybrid composite solutions with superior toughness and a non-catastrophic failure behaviour [23]. Moreover, hybrid composites ensure that the resistance of the CFRP thin plies, which approaches the tensile strain-to-failure of the fibres, is fully exploited [23].

The laminate-level homogenisation and absence of sub-critical damage mechanisms such as matrix cracking and delamination (Section 2.2.2) before the ultimate failure strain of thin-ply laminates make the analysis and design much faster and simpler. The simplest methods are based on FPF analysis, designing against the ocurrence of transverse cracking. However, for the most conventional laminates, the FPF strain is much lower than the ultimate failure strain of the laminate, thus the high specific strength of the composite material is compromised [23]. In thin-ply composite laminates, the gap between FPF and LPF is reduced, and the high performance usually associated to composite laminates can be fully exploited by employing closed-form and fast solutions. The suitability of simpler analysis models combined with the intrinsic superior strength and increased design space of thin-ply laminates allow optimisation for enhanced performance and lead to a higher consistency in defining safety factors, with great potential for weight savings and, consenquently, cost reduction either during the conceptual and detailed design stages, either during service life.

2.2 Ply thickness scaling and its effect on composite laminates

2.2.1 Introduction

Thin plies have intrinsic advantages in terms of the mechanical response of composite laminates [23; 27]. Higher *in-situ* strength is one clear benefit that leads to an improved mechanical response of thin-ply laminates when compared with the conventional ones. In high-performance applications, such as the ones found in the aeronautics industry, if micro-cracking can be supressed or eliminated, there is a further incentive to use thin-ply laminated composite structures in favour of other structural materials, like metals. However, these benefits must be properly quantified, and other potential advantages identified in a systematic manner by means of detailed experimental programmes, complemented by analytical models and numerical, FE-based analysis, which should be carried out to improve understanding of the mechanical behaviour of thin-ply laminates. In the past years, several studies have adressed the effect of stacking sequence and ply thickness scaling on several aspects of the mechanical response of composite laminates. These studies, which involved detailed experimental campaigns and/or analysis methods, have contributed to the understanding of the effect of ply thickness scaling on the nature of the damage mechanisms that cause laminate failure. However, the introduction of spread-tow thin plies makes this analysis more pertinent than ever, since the majority of the studies carried out in the past addressed ply thickness effects by means of ply scaling restricted to a minimum nominal ply thickness of 0.125 mm, considerably above what can be obtained nowadays using tow spreading. A review concerning the effect of ply thickness scaling on the mechanical response and structural integrity of composite laminates, in terms of matrix cracking and *in-situ* effect, is presented in the next sections.

2.2.2 Matrix cracking and *in-situ* effect

When embedded in a multidirectional laminate, the laminae whose fibre orientation is perpendicular to the loading direction generally develop matrix cracks at strains lower than the ultimate failure strain of the laminate [13; 14; 28] — see Figure 2.3. These matrix cracks are responsible for the deterioration of the mechanical performance of the laminate, originating other damage modes (e.g. delamination), and creating pathways for chemicals and other substances (critical for applications such as chemical tanks and pressure vessels) [29]. Either under static or fatigue loading, damage onset is generally the result of the nucleation, propagation and multiplication of transverse cracks [30].

Nevertheless, it is observed that the development of these matrix cracks (which define the actual strength of the transverse plies) occurs at applied stresses greater than the transverse strength measured in UD coupons; in fact, the actual strengths of transverse plies are not only higher than those measured in UD coupons, but they reportedly increase with decreasing ply thickness [28; 31–33]. The crack density in embedded transverse plies is also known to increase with decreasing ply thickness [13; 15; 16; 34]. This is a deterministic size effect that occurs at the meso-scale, known as the *in-situ* effect. The neighbouring plies cause a constraining effect on the embedded ply, reducing the available elastic energy and delaying damage propagation in the matrix [14; 15; 35–37]. Therefore, the ply strengths cannot be treated as intrinsic lamina properties [31; 38], but as *in-situ* properties, that depend on the material and geometry of the laminate [32; 33; 39].

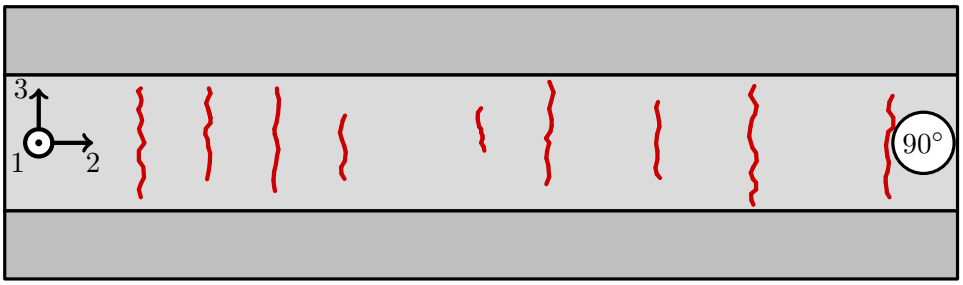

Figure 2.3: Transverse matrix cracks in a cross-ply laminate, where 1 stands for the longitudinal (fibres) direction, 2 the transverse direction and 3 the through-thickness direction of the embedded 90° lamina (adapted from Sebaey et al. [28]).

2.2.3 *In-situ* strengths

Several experimental studies in the literature show that the transverse tensile strength and the in-plane shear strength of an embedded ply depend on the ply thickness [28; 31; 38; 40–43], on the orientation of the adjacent plies [31; 38] and on the ply location in the laminate [33; 44; 45]. Indirect observations also show that the transverse shear strength [46–50] and the transverse compressive strength [16; 46; 47] are *in-situ* properties too. More recently, a direct experimental demonstration of the transverse shear strength was performed, to further understand this deterministic size effect in other stress states [51].

In-situ tranverse tensile strength

The first studies addressing matrix transverse cracking appeared in the late 1970s, when Bailey and co-authors [40–42] studied the formation of matrix transverse cracking in different glass FRP cross-ply composite laminates subjected to tensile tests. It was observed that, as the thickness of the transverse (90°)-plies is reduced, transverse cracking changes from multiple occurences to slow crack growth, small edge cracks and, finally, complete crack supression, clearly evidencing matrix cracking constraining in the 90° plies — see Figure 2.4.

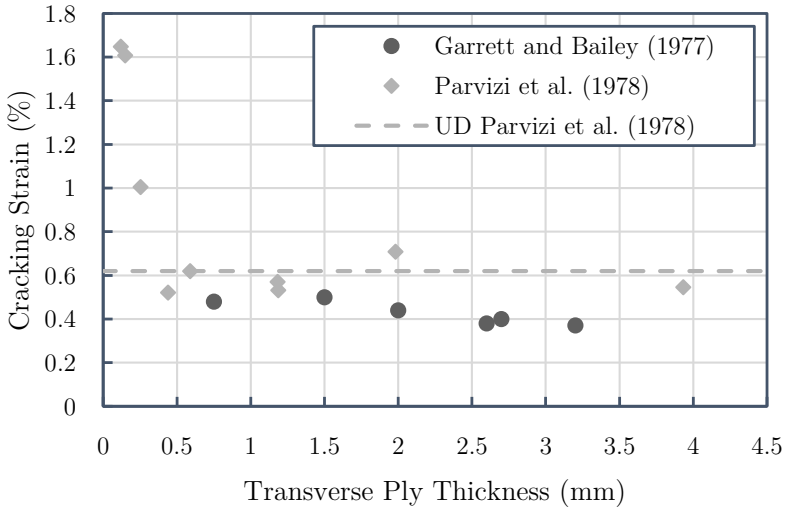

Figure 2.4: Cracking strain of different glass fibre-reinforced polymer cross-ply laminates (adapted from Garrett and Bailey [40] and Parvizi et al. [41]).

Flaggs and Kural [31] experimentally showed that the transverse stress at the onset of transverse matrix cracking in the 90° laminae of $[\pm\theta/90_n]_s$ carbon/epoxy laminates not only strongly depends on the 90° laminae thickness, but also on the orientation of the adjacent $\pm\theta$ laminae, suggesting that transverse tensile strength should not be considered as an instrinsic lamina property — see Figure 2.5. Accordingly, the transverse stress at the onset of matrix cracking increases with decreasing ply thickness and increasing stiffness of the adjacent laminae. In addition, it was the first time that a reference to the existence of an *in-situ* effect on the tranverse tensile strength was mentioned. Similar results for the influence of ply thickness on the transverse tensile strength of carbon/epoxy laminates were obtained later by Boniface et al. [43] for distinct resin systems, namely single phase and toughened resins.

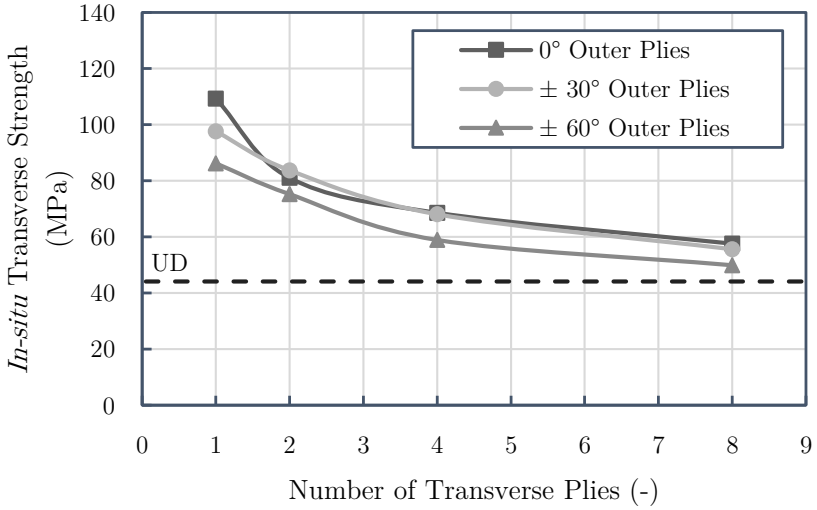

Figure 2.5: *In-situ* effect on the transverse tensile strength of an embedded 90° ply (adapted from Flaggs and Kural [31]).

In the early 1980s, in a experimental study about the effect of ply thickness on the mechanical response of angle-ply laminates, Herakovich [44] has shown that the ultimate stress, the strain to failure and the toughness (measured as the area under the experimentally obtained stress-strain curves) of angle-ply laminates is higher when plies of the same orientation are dispersed through the laminate instead of blocked together due to a delay in matrix cracking that caused a strong change in the nature and sequence of the failure mechanisms. More recently, Fuller and Wisnom [52] showed that matrix cracking parallel to the fibre direction in angle-ply laminates can be completely suppressed using a spread-tow thin-ply composite material, leading to a brittle type of net-section fibre dominated failure mode.

Dvorak and Laws [32] developed an analytical model to predict the *in-situ* transverse tensile strength as a function of the ply thickness, based on LEFM. This analytical model was validated by a comparison with experimental results on T300/934 carbon/epoxy composite laminates. The authors showed that the *in-situ* transverse tensile strength increases with decreasing inner 90° ply thickness, and that analytical models based on fracture mechanics are able to accurately predict this *in-situ* effect — see Figure 2.6.

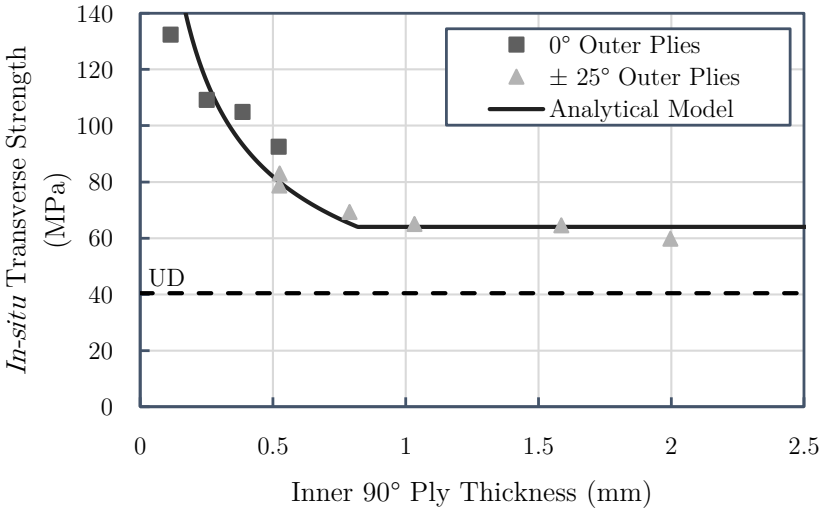

Figure 2.6: *In-situ* transverse tensile strength of an inner 90° ply (adapted from Dvorak and Laws [32]).

Later, Camanho et al. [33], based on the derived expression for the interaction energy of a ply with an elliptical slit crack proposed by Laws [53], and consequent expressions for the ERRs for the cases of crack propagation in the transverse and longitudinal directions proposed by Dvorak and Laws [32], predicted, based on LEFM, that the *in-situ* transverse tensile strength and the *in-situ* in-plane shear strength also depend upon its location in the laminate, i.e., if the ply is an embedded ply (inner ply), constrained by another ply or group of plies, or if the ply is at the surface of the laminate (outer ply) — see Figures 2.7a and 2.7b. In addition, these predictions were compared with experimental results for several materials and a good correlation was observed.

Around the 1990s, Chang et al. [54] conducted a parametric study, using a progressive damage model formulated taking into account the *in-situ* effect, to evaluate the effect of ply clustering on the strength and failure mode of angle-ply and cross-ply laminated composites containing an open hole under tensile loading. This model revealed high efficiency, and it accurately captured the reduction in the maximum failure load due to ply clustering. Adolfsson and Gudmundson [35] performed an experimental investigation concerning the evolution of the elastic properties in glass/epoxy cross-ply laminates, considering different stacking sequences, due to matrix cracking. A severe degradation of the elastic properties with increasing transverse ply thickness was observed. Lavoie et al. [55] reported that stress concentrations on the 0° plies arising from transverse cracking in thick 90° ply blocks can have a measurable effect on the strength of the 0° ligaments and induce premature laminate failure too. Lavoie and Adolfsson [56], based on experiments on carbon/epoxy multidirectional laminates, showed that laminates with thicker ply blocks developed matrix cracks due to existent thermal residual stress, as opposite to laminates with thinner ply blocks, where no thermally induced matrix cracks could be identified.

More recently, an increasing number of studies have demonstrated that the applied stress corresponding to the occurrence of the first transverse crack increases with decreasing ply thickness [29; 45; 57–62], and that a reduction of the stiffness of the adjacent plies promotes transverse cracking [29; 57], both resulting from the presence of an *in-situ* effect.

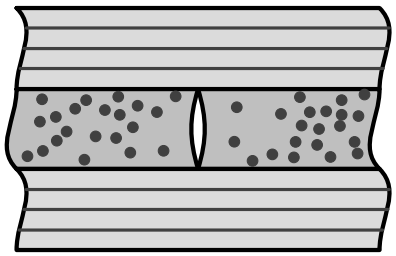

(a) Schematic view of an embedded ply

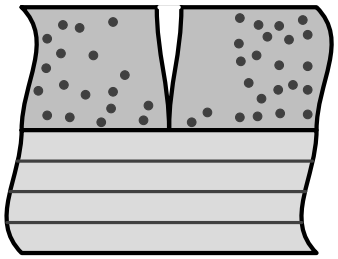

(b) Schematic view of an outer ply

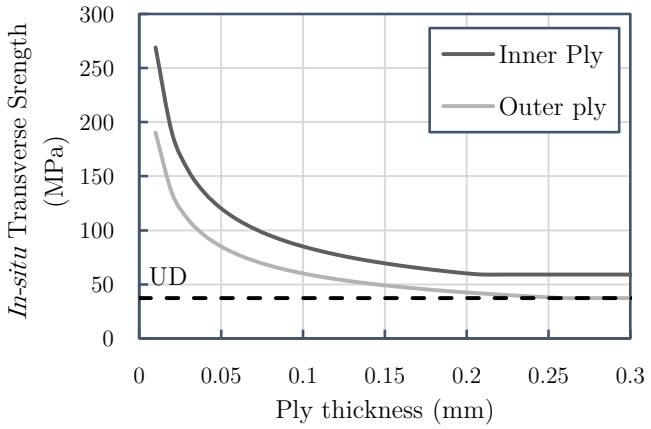

(c) *In-situ* transverse tensile strength of an embedded (inner) and outer ply

Figure 2.7: Schematic views of embedded (inner) and outer plies and *in-situ* transverse tensile strength prediction (adapted from Camanho et al. [33]).

The first studies adressing transverse cracking in spread-tow thin plies appeared in the early 2000s. Uniaxial tensile quasi-static tests on unnotched and open-hole multi-directional laminates [9; 13; 21; 24; 37; 50; 63–67] showed that FPF is delayed nearly up to ultimate failure, as observed by free-edge observations, SEM visualization, accoustic emission and/or DIC, and often supported by numerical analyses [64; 65].

Particularly, the results from the experimental programme performed by Saito et al. [13], assessing transverse crack constraining in thin-ply carbon/epoxy cross-ply laminates, and from complementary numerical analysis [14], were later supported by a CMM analysis performed by Arteiro et al. [15] (please refer to Section 2.3.3).

In-situ in-plane shear strength

Even though most of the studies addressing ply *in-situ* effects have been focused on matrix cracking in tension, this deterministic size effect was also observed under other loading scenarios. For example, experimental programmes suggest a significant ply thickness and orientation effect on the in-plane shear strength of embedded plies [38; 68; 69].

Chang et al. [68] performed a simple experimental study, through shear tests on carbon/epoxy symmetric cross-ply laminates, $[0/90]_s$, using a rail shear testing fixture, to measure the in-plane shear strength of the laminate. In order to study the ply orientation effect, laminates with different ratios of 0° plies were tested (corresponding to the number of 0° plies divided by the total number of plies). It was reported that the shear

strength depends on this ratio. For ratios above 50%, the shear strength decreases. Therefore, when this ratio is higher than 50%, the corresponding shear strength should be used in calculating the failure strength and the failure mode. Another important issue was observed. The shear stress to shear strain relationship was nonlinear, thus, the assumption of a linear stress-strain relation may result in some error in the calculated values of the failure strength, especially for laminates consisting predominantly of [0/90] and [±45] sub-laminates.

A few years later, Chang and Chen [38] extended the experimental tests performed by Chang et al. [68], to include the study of the ply thickness effect on the in-plane shear strength of the laminate. The ply orientation effect was studied too. An important conclusion was reached; as the ply thickness increased, the shear strength decreased and reached a lower plateau, clearly demonstrating that the ply thickness has a significant effect on the shear strength. The authors presented a reason for this decrease in shear strength, the inherent flaws in the laminates, which could be introduced through the lay-up process, and the thicker the laminate, the higher the possibility of introducing flaws. Regarding the ply orientation effect, it was concluded that the symmetric cross-ply laminates [0/90] offered higher shear strength than the UD ones, again demonstrating that the ply orientation effect interferes on the shear strength of the laminate.

More recently Liu et al. [69] also investigated the effect of ply thickness and orientation on the shear response of composite laminates using V-notched rail shear specimens subjected to shear tests. Different ply thickness and ply orientation were employed on four specimens, each one composed by a different composite lay-up sequence, $[(0/90)_4/0]_s$, $[(0_2/90_2)_2/0]_s$, $[(0_4/90_4)/0]_s$ and $[(0/+45/90/-45)_2/0]_s$. A DIC system was used to detect the strain evolution on the surface of the specimens. It was reported that laminates with larger ply thickness exhibited lower laminate shear modulus and strength. Regarding the ply orientation effect, it was observed that the samples containing ±45° plies presented higher shear strength when compared to the samples containing 0° or 90° plies, as expected. Lastly, a nonlinear shear stress-strain relationship was also detected.

The relation between the *in-situ* in-plane shear strength and the ply thickness can be taken into account using fracture mechanics analytical models and the transverse intralaminar mode II fracture toughness [32; 33].

Camanho et al. [33] proposed an analytical closed-form model to predict the *in-situ* in-plane shear strength of composite laminates:

$$S_L^{is} = \sqrt{\frac{(1+\beta\phi G_{12}^2)^{1/2}-1}{3\beta G_{12}}} \tag{2.1}$$

where β is a parameter that defines the nonlinearity of the shear stress-shear strain relation, G_{12} is the shear modulus and the parameter ϕ is defined according to the configuration of a given ply. For a thick embedded ply, ϕ is given as [33]:

$$\phi = \frac{12(S_L)^2}{G_{12}} + \frac{72}{4}\beta(S_L)^4 \tag{2.2}$$

and for a thin embedded ply as [33]:

$$\phi = \frac{48\mathcal{G}_{\mathrm{IIc}}}{\pi t} \tag{2.3}$$

where $\mathcal{G}_{\mathrm{IIc}}$ is the fracture toughness associated with intralaminar fracture of the transverse ply (parallel to the fibre direction) in mode II and t is the ply thickness. Similarly, for a thin outer ply, ϕ is given as [33]:

$$\phi = \frac{24\mathcal{G}_{\mathrm{IIc}}}{\pi t} \tag{2.4}$$

and for a thick outer ply, there is not a constraining *in-situ* effect caused by the neighbouring plies, thus S_L^{is} can be considered as [33]:

$$S_L^{is} = S_L \tag{2.5}$$

The special case of a linear shear behaviour is obtained when β tends to zero. Therefore, the *in-situ* shear strength of embedded plies considering a linear shear response can be obtained as [33]:

$$S_L^{is} = \lim_{\beta \to 0} \sqrt{\frac{(1+\beta\phi G_{12}^2)^{1/2} - 1}{3\beta G_{12}}} = \sqrt{\frac{\phi G_{12}}{6}} \tag{2.6}$$

Considering the definitions of the parameter ϕ — Equations 2.2-2.4,— Equation 2.6 can be rewritten, for a thin embedded ply, as [33]:

$$S_L^{is} = \sqrt{\frac{8 G_{12} \mathcal{G}_{\mathrm{IIc}}}{\pi t}} \tag{2.7}$$

for a thick embedded ply as [33]:

$$S_L^{is} = \sqrt{2} S_L \tag{2.8}$$

and for a thin outer ply as [33]:

$$S_L^{is} = 2\sqrt{\frac{G_{12} \mathcal{G}_{\mathrm{IIc}}}{\pi t}} \tag{2.9}$$

A comparison between the predictions of the *in-situ* strength, using linear and non-linear shear stress-shear strain relations, can be seen in Figure 2.8, for the cases of a thin embedded inner and outer ply. It can be seen that there is a significant difference in the predicted *in-situ* strengths with linear and non-linear shear response; in this case, the nonlinear shear response typically observed in FRPs [68; 69] must be included in the fracture mechanics model.

In-situ transverse shear strength

Experimental programmes have also shown that a substantial reduction in longitudinal compressive and transverse shear strengths can result from transverse cracking (earlier references can be seen in Ref. [31]). Therefore, an *in-situ* effect on other matrix-dominated failure mechanisms is expected to exist, namely on transverse shear cracking, wedge transverse compressive fracture, and fibre kinking.

Very recently, García-Rodríguez et al. [51] performed an experimental demonstration of the *in-situ* effect under transverse shear, by combining interlaminar shear strength tests with X-ray tomography inspections, thus comparing the damage sequence of $[45/0/-45, 90]_s$ short-beam specimens manufactured with standard NCF and thin-ply NCF. In both specimens, the authors associated the onset of instability to a shear crack tunnelling across the central [90] ply-cluster. The intersection of this crack with the ones developing in the adjacent layers induced interlaminar delaminations. Furthermore, a 3D elasto-plastic

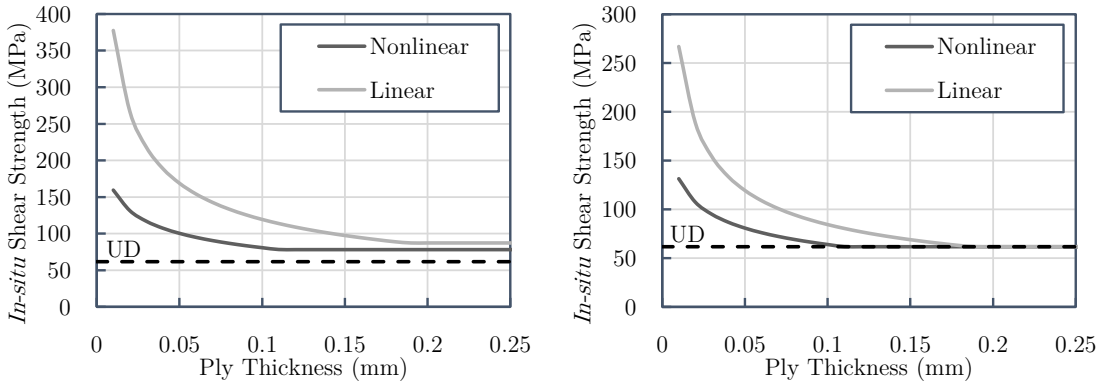

(a) Inner ply (b) Outer ply

Figure 2.8: Linear and nonlinear predictions for the *in-situ* in-plane shear strength of an embedded (inner) and outer ply (adapted from Camanho et al. [33]).

numerical model predicted that, for the same applied shear load, the ply-cluster of both laminates would display a similar maximum principal stress distribution. However, the authors concluded that the thin-ply samples improved the interlaminar shear strength by 34%, evidencing the so called *in-situ* effect.

Similarly to in-plane shear, experimental analyses assessing the ply thickness effect are difficult to perform in transverse shear, specially because of the difficulties in imposing shear loading scenarios. Thus the referred experimental evidence performed by García-Rodríguez et al. [51] is, to the author's knowledge, the only direct and unambiguous experimental evidence of an *in-situ* effect in tranverse shear. However, analytical models can predict this deterministic size effect [46–48].

The application of 3D phenomenological failure criteria has been proposed to estimate and take into account the *in-situ* effect on the transverse shear and transverse compressive strengths of thin embedded plies [46; 47]. According to these models, when embedded in a multidirectional laminate, not only Y_T^{is} and S_L^{is} are assumed *in-situ* properties (calculated using the models proposed by Camanho et al. [33]), but also Y_C^{is} and S_T^{is}.

Catalanotti et al. [46] proposed a 3D failure criteria, considering both longitudinal and transverse failure mechanisms, where the effect of ply thickness on the material strength is taken into account. Focusing on transverse compression failure, the proposed criterion is based on Puck's criterion [70; 71], assuming a modified failure index, in order to take into account the *in-situ* effect. Considering pure transverse compression, starting from a modified failure index expression, S_T^{is} is explicitly given as [46]:

$$S_T^{is} = \frac{1}{2} \frac{(2\sin^2(\alpha_0) - 1) S_L^{is}}{\sqrt{1 - \sin^2(\alpha_0)} \sin(\alpha_0) \eta_{\mathrm{L}}} \tag{2.10}$$

where α_0 is the fracture angle under uniaxial transverse compressive failure and η_{L} is the friction coefficient of the composite material [46].

Camanho et al. [47] developed 3D failure criteria based on the transversely isotropic yield function proposed by Vogler and co-authors [72; 73]. The referred criteria have

an invariant quadratic formulation based on structural tensors that account for the preferred directions of the anisotropic material. With this formulation, the typical anisotropy present in FRPs is derived using structural tensors and not symmetric conditions based on a reference coordinate system. The so-called structural tensors represent the material symmetries of the respective anisotropy class as an intrinsic material property, which enables an elegant coordinate system-free description of anisotropy using isotropic tensor functions. According to these criteria, the *in-situ* transverse shear strength and the *in-situ* biaxial transverse tensile strength are numerically calculated imposing [47]:

$$\begin{cases} \eta_L^{(+)} = \eta_{L,is}^{(+)} \\ \eta_T^{(+)} = \eta_{T,is}^{(+)} \end{cases} \tag{2.11}$$

where η_L and η_T are, respectively, the slopes in the $\sigma_{22}-\sigma_{12}$ and $\sigma_{22}-\sigma_{23}$ failure envelopes when $\sigma_{22}=0$. Camanho et al. [47] assumed that η_L and η_T are not *in-situ* properties — see Figure 2.9. Accordingly, solving the system of equations present in 2.11, the *in-situ* transverse shear strength can be written as [47]:

$$S_T^{is} = S_L^{is}\frac{S_T}{S_L} \tag{2.12}$$

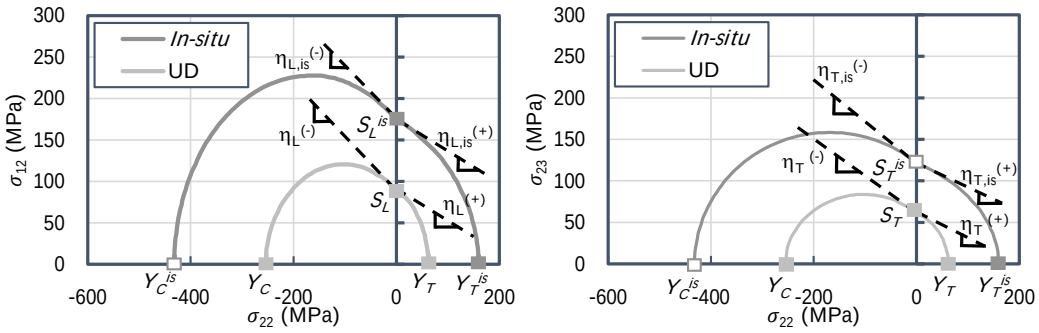

(a) $\sigma_{22}-\sigma_{12}$ failure envelope. (b) $\sigma_{22}-\sigma_{23}$ failure envelope.

Figure 2.9: Definitions of the parameters η_{L} and η_{T} (adapted from Camanho et al. [47]).

Olsson [48] proposed an analytical model for damage prediction due to large mass impact on thin-ply composites. He assumed that in multidirectional laminates, the S_T^{is} is governed by the growth of transverse shear cracks, which typically appear as inclined mode I transverse shear cusps, sandwiched between two comparatively stiff plies and deflect into delaminations — see Figure 2.10. Similarly to constrained transverse plies loaded in tension, the constraining effect of the stiffer adjacent plies reduces the available elastic energy within the ply, delaying transverse shear crack growth in the matrix [14; 35–37]. According to the author, the *in-situ* transverse shear strength is given for a thick embedded ply as [48]:

$$S_T^{is} = 1.12\sqrt{2}Y_T \tag{2.13}$$

and for a thin embedded ply as [48]:

$$S_T^{is} = 1.4\sqrt{\frac{\mathcal{G}_{\mathrm{Ic}}E_2}{2(1+\nu_{23})t}} \tag{2.14}$$

where $\mathcal{G}_{\mathrm{Ic}}$ is the intralaminar fracture energy in mode I, E_2 is the transverse *Young's* modulus (perpendicular to the fibres direction), ν_{23} is the transverse Poisson's ratio of the composite material, and t is the ply thickness.

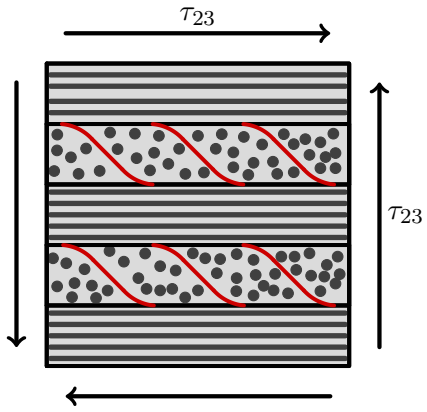

Figure 2.10: Transverse shear cracking scenario in multidirectional laminates (adapted from Olsson [48]).

A comparison of the predictions of the *in-situ* transverse shear strength of an embedded ply according to the criteria specified above can be seen in Figure 2.11. Some differences can be observed, but no direct or indirect validation is available yet for any of these criteria.

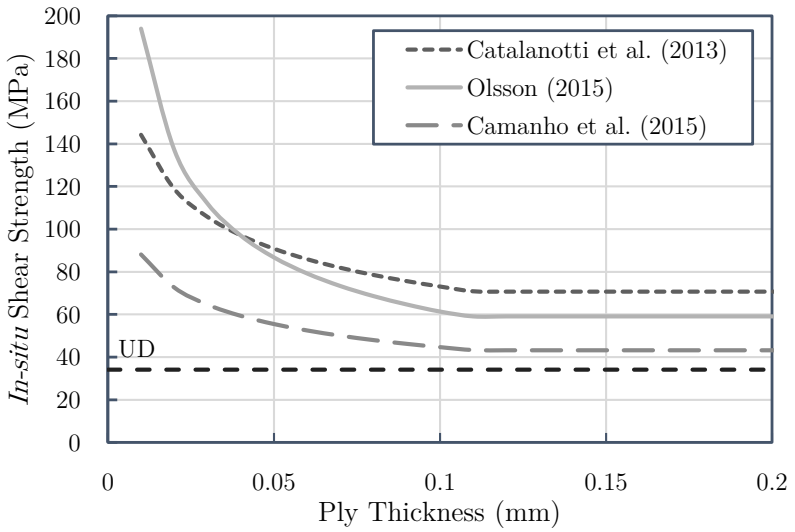

Figure 2.11: Predictions for the *in-situ* transverse shear strength of a thin embedded ply.

In-situ transverse compressive strength

There is no direct experimental evidence of an *in-situ* effect in transverse compression. However, recent studies, which adressed directly or indirectly the effect of ply thickness on the compressive properties of multidirectional laminates, indicate that ply thickness affects the compressive response of polymer composite laminates [45; 74; 75].

Kawabe et al. [74] studied the thin-ply effects on the compressive properties of multidirectional, quasi-isotropic composite laminates, by employing compression tests. Ply thicknesses starting from 0.045 mm were analysed. A clear *in-situ* effect in compression has been reported by the authors. Erçin et al. [45], reported a higher compressive unnotched strength for laminates having dispersed plies when compared to partially blocked-

ply laminates. The authors justified these results with the existence of an *in-situ* effect in compression too.

Arteiro et al. [75] have also shown a strength improvement in the compressive unnotched strength of quasi-isotropic laminates. These observations were later supported by a detailed representation of the mechanics of transverse compressive failure and associated *in-situ* effect using a 3D CMM framework [16]. A clear *in-situ* effect in transverse compression was identified (please refer to Section 2.3.3).

2.3 Computational micro-mechanics

Experimental analysis based on *in-situ* observations of very thin plies are extremely difficult, not only because it is hard to identify any transverse damage at this scale, but also because the applied strains needed to develop such damage mechanisms are so high that conduct to failure (or severe damage) of the constraining material [34]. CMM has, therefore, been proposed as a reliable way for the understanding of the *in-situ* effect.

2.3.1 Introduction

The capability of damage models to predict physical phenomena, such as the initiation and propagation of damage on composite laminates, strongly depends on the scale at which the damage mechanisms under consideration are modelled [76; 77] — see Figure 2.12. In fact, the conceptual idealisation of the damage process, i.e., the identification, characterisation and formulation of the governing physical equations of damage evolution, may span from molecular dynamics scales to structural mechanics scales, including the intermediate micro- and meso-scales [77]. In the case of composite laminates, where the in-plane dimensions exceed the length scale at which delamination, matrix cracking and fibre debonding take place by one to several orders of magnitude, the proper definition of the modelling scale is a fundamental aspect [76].

At lower structural scales, damage idealisations have higher resolution and higher kinematic freedom, and they are able to recreate all kinds of mechanisms, each of these captured with separate damage laws [77–79]. Micro-mechanical scale models, at the constituents level, represent what is normally the smallest scale of composite damage idealisation [77; 78; 80]. The experimental data of fibres and matrix material is necessary to establish the properties of, firstly, the lamina and, then, the composite laminate structure [80].

A computational micro-mechanics analysis allows for a detailed insight of the mechanical behaviour of a composite material by considering the influence of each constituent. If a proper constitutive model is developed for each constituent of the composite and special attention is given to the interface between constituents, a better understanding of the mechanical behaviour of composite laminates under complex load combinations is possible.

Within the present work, experimental data on the properties of the fibres and matrix materials, which are considered individual homogeneous materials, are used to study the constitutive behaviour and to obtain the macroscopic properties of a composite lamina [1; 78; 80], not only the elastic constants, but also the strength properties under diverse

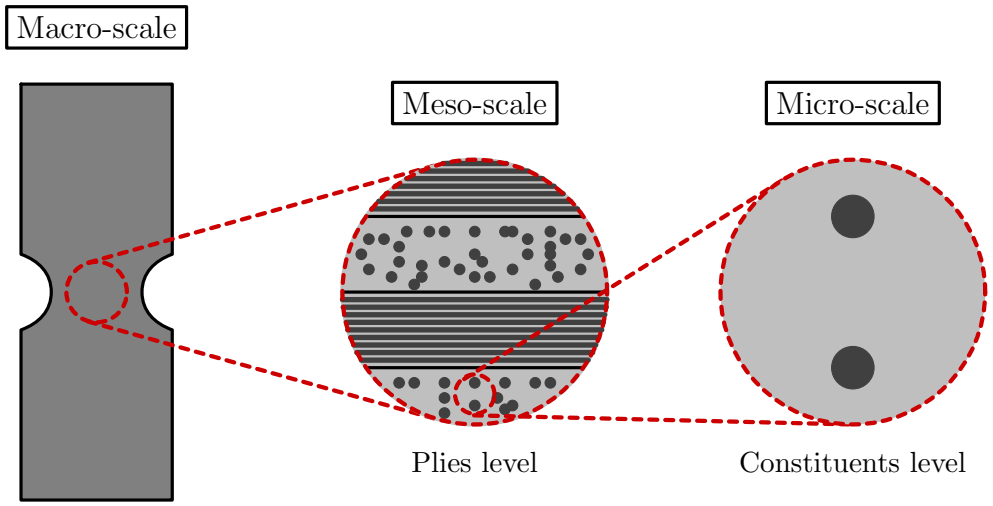

Figure 2.12: Length-scales for composite laminate damage modelling (adapted from Arteiro et al. [81]).

loading scenarios. Detailed matrix damage mechanisms, such as matrix plasticity and damage, and fibre-matrix interface cracking can be easily captured and represented through the numerical simulation of the deformation and failure of a RVE of the microstructure, where fibres, matrix and their interface are modelled according to appropriate constitutive equations. Therefore, the micro-scale is the ideal damage scale to analyse intralaminar fracture, in particular the ply thickness and constraining (*in-situ*) effects on matrix damage initiation and propagation.

At this scale, RVEs can be defined as the smallest volumes of material whose properties are representative of the entire mechanical performance of the material system [82; 83] — see Figure 2.13. Therefore, an important issue when using computational micro-mechanics is the minimum size of the RVE.

An RVE cannot be too large, as this would endanger the possibility to numerically analyse it, but it cannot be too small, since it should contain all the necessary information about the statistical description of the miscrostruture, so that the average properties of this RVE are independent of its size and position within the material [84; 85]. This critical RVE size depends on the phase and interface properties, as well as on the spatial distribution [84].

In addition to the size of the RVE, other important issues include fibre distribution, volume fraction and spatial arrangement of reinforcements in the matrix. This spatial arrangement is usually not periodic and it is highly dependent upon the manufacturing process of the composite system [85]. To accurately reproduce and capture the onset and evolution of damage in the matrix, it is crucial to represent properly the transverse randomness of the fibre distribution (i.e. distance to first neighbours, occurrence of clusters of fibres, etc.) [85; 86].

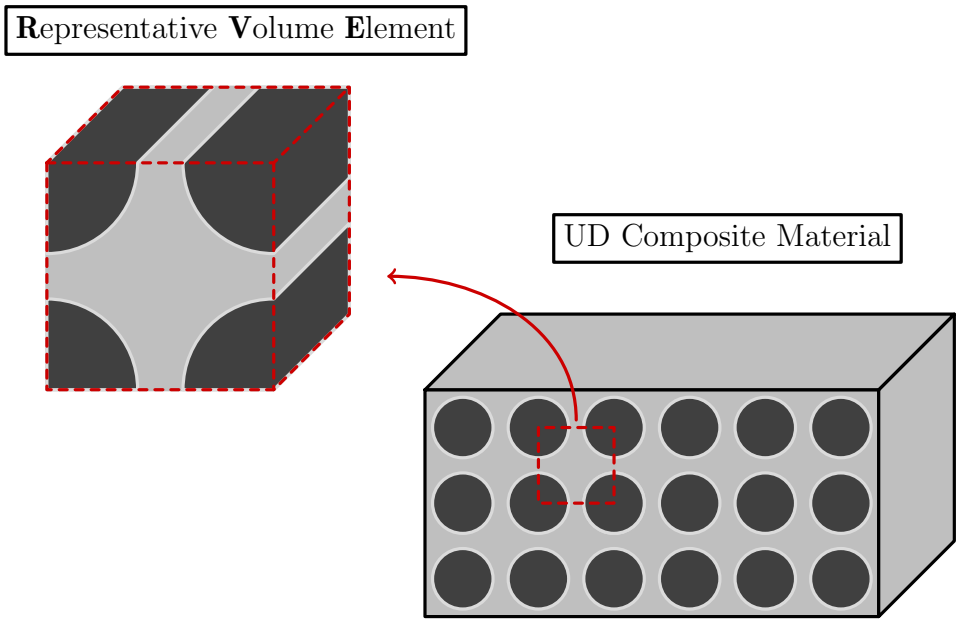

Figure 2.13: A schematic UD composite material and definition of representative volume element.

2.3.2 Micro-mechanical modelling

In recent years, micro-mechanical numerical analysis has made substancial advances. Proof of that is the outstanding increase in recent publications addressing the issue of micro-mechanical modelling of composite materials, making use of FE analysis to solve the most varied problems within computational mechanics [15–18; 20; 87–94].

The first issue which requires attention when modelling the micro-mechanical behaviour of a composite material is the distribution of reinforcements in the matrix material. Initially, a simplification was used, considering that the distribution of reinforcements followed a deterministic, ordered and regular pattern, for example, square or hexagonal [95]. Romanowicz [96] and Hobbiebrunken et al. [97] performed micromechanical analysis, considering an hexagonal distribution of the reinforcements. However, such distributions do not appropriately reflect the stress field in the matrix, namely the hydrostatic pressure imposed by the stiffer fibre material.

In a similar way, in order to understand if the assumption of a deterministic and ordered distribution conducts to worse results than the assumption of a random distribution of the reinforcements in the composite material, Trias et al. [98] compared the stress and strain distributions obtained between a periodic and a random model distribution for a CFRP. This comparison showed that periodic models can be used for the simulation of effective properties when the accuracy required is not so high (the difference in the *Young's* modulus was about 12% and in the Poisson's ratio about 6%); However, for any statistical analysis or for the simulation of local phenomena such as local damage or matrix cracking, random models must be considered. Clearly, this is an important feature to take into account in the micro-mechanical analysis of the *in-situ* effect.

To circumvent this problem, algorithms and special techniques were developed to generate spatial distributions of reinforcements. For instance, Vaughan and McCarthy [99] presented an experimental-numerical approach to generate statistically equivalent distributions of reinforcements in a composite material, while Melro et al. [85] developed an algorithm to quickly reproduce a statistically proven random distribution of reinforcements in the matrix material. This model is able to quickly and simply generate random fibre distributions, even for high values of fibre volume fractions, that are materially and statistically equivalent to real distributions in the transverse cross-section of laminated composites.

Another relevant aspect in the development of micro-mechanical models is the correct definiton of the constitutive behaviour of the constituents, in particular of the matrix material. For instance, epoxy resins, which are typically used in advanced composite laminates, are known to be pressure dependent and extremely ductile under shear loading.

In order to simulate these properties, many authors used standard non-linear models found in the literature to reproduce the constitutive behaviour of the matrix material [96; 100; 101]. Vaughan and McCarthy [100] and Totry et al. [101] applied the Mohr-Coulomb elasto-plastic model, Romanowicz [96] used the Drucker-Prager elasto-plastic model, and Canal et al. [102] considered the matrix to follow an alternative plastic model which does not consider any hardening effect. Independent experimental analysis have shown that these constitutive models are not suited for modelling the mechanical behaviour of epoxy resins [103].

Based on these conclusions, Melro et al. [87; 104] proposed and implemented a new pressure dependent, elasto-plastic thermodynamically consistent damage model, that is able to properly represent the most relevant characteristics of epoxy matrices, namely the pressure dependency on its yield and failure behaviour, and the shear nonlinear-almost perfectly plastic behaviour.

2.3.3 Analysis of the *in-situ* effect

In recent years, several researchers [15–21] have been employing computational micro-mechanics to further understand the *in-situ* effect, thus addressing the benefits of incorporating ultra-thin plies in composite laminates.

Arteiro et al. [15] performed a micro-mechanical analysis of the *in-situ* effect in polymer composite laminates, and studied the mechanical response of ultra-thin plies under transverse tensile loading by employing a micro-mechanical FE model of a composite laminate consisting of a RVE of a 90° thin lamina in-between two homogenised 0° plies. The proposed 3D computational micro-mechanics framework was able to accurately represent the micro-mechanical response of ultra-thin plies, including (i) the mechanics of transverse cracking onset and propagation, (ii) the constraining effect observed in the laminae embedded in multidirectional laminates, (iii) the gradual, slow stress relaxation and progressive transverse cracking observed in very thin plies, and consequent increase of the crack density, (iv) the reduction in COD of the transverse cracks with ply thickness, (v) the formation of thin necks of matrix material around the regions where interfacial damage is more pronounced, and (vi) the *in-situ* strength.

Mechanics of transverse cracking onset and propagation As expected, a matrix crack developed along a direction transverse to the applied load in the embedded 90° ply. Similarly to what was previously observed experimentally from *in-situ* observations [13] damage started in the narrower portions of matrix between the closest adjacent fibres aligned with the loading direction at approximately the same applied strain, first as fibre-matrix decohesions, then followed by matrix cracking. The *in-situ* observations presented in Ref. [13] have also shown that, for the thicker 90° embedded plies, once a transverse crack is formed, it rapidly penetrates through the thickness. This aspect was also observed in the simulations.

Kohler et al. [21] performed a numerical study, by employing a FE model, which was built using a multi-scale "embedded cell" modelling approach, in which a finely discretised region corresponding to the 90° ply was embedded in a larger continuum model of the laminate, where the total model length was at least three times the embedded cell length. This model was employed to assess the effect of ply thickness scaling on ply damage. The sequence of damage events was similar to the one reported by Arteiro et al. [15]. A ply thickness independence on the onset of fibre-matrix debonding was reported, which leads to local stress concentrations in the matrix, plastic damage accumulation and eventually transverse matrix cracking through coalescence of micro-damage.

In a micro-mechanical analysis assessing matrix crack-induced delamination in cross-ply laminates under longitudinal tensile loading, Fu and Wang [18] reported a similar behaviour concerning transverse cracking onset and propagation, i.e., damage appeared as fibre/matrix interface debonding in the narrower regions between two neighboring fibres aligned with the loading direction. Then, plastic deformation and damage of the matrix at the vicinity of the fibre/matrix interface debonding occured, leading to the formation of matrix micro-cracks. Followed by the coalescence of the fibre/matrix interface debonding and matrix micro-cracks at different locations, a thin crack ran quickly through the thickness of the transverse lamina and stopped in the resin-rich interlaminar region. Finally, delamination initiated from the matrix crack tips in the resin-rich region where local stress concentrations existed and propagated along the ply interface in the form of matrix plasticity and cracking.

Guillén-Hernández et al. [20], in a micro-mechanical analysis assessing fracture events in cross-ply laminates under in-plane monotonic transverse tensile loading, obtained a similar behaviour for transverse crack onset and propagation, i.e., cracks mainly evolved along the direction transverse to the external loading. A special focus to the different stages of matrix cracking, onset and propagation, was given. Three different stages were identified, as in Arteiro et al. [15], firstly the onset of a debond at the fibre-matrix interface, secondly the appearance of several debonds at different fibre-matrix interfaces, and lastly an initial stage of damage.

Constraining effect observed in the laminae embedded in multidirectional laminates Experimental evidence in Ref. [13] demonstrated that, in the case of the thinner transverse plies, crack extension slows down with increasing applied strain. In the numerical simulations carried out by Arteiro et al. [15], the same trend was observed. The authors established a relation between a normalised crack length and the applied strain for different 90° ply thicknesses — see Figure 2.14. Clearly, there is a constraining effect in the laminae embedded in the multidirectional laminate.

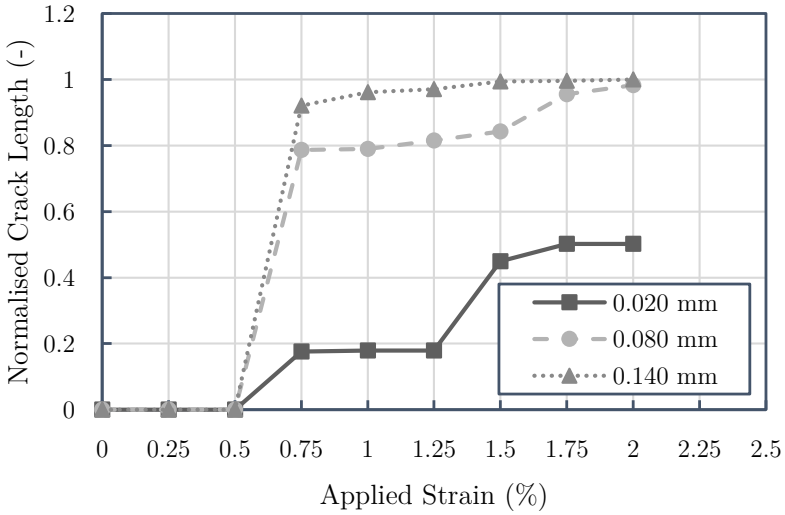

Figure 2.14: Normalised crack length as a function of applied strain for different 90° ply thicknesses (adapted from Arteiro et al [15]).

Gradual, slow stress relaxation and progressive transverse cracking observed in very thin plies. Increease of the crack density Also, as reported by Saito et al. [13], for the thickest transverse laminae, the sudden matrix crack extension leads to stress relaxation, whereas the thinner transverse laminae show a gradual extension of the tranverse cracks, eventually without completely penetrating through the thickness. Therefore, stress relaxation is much more difficult in the last case. Again, this fact was clearly verified by the micro-mechanical analysis performed by Arteiro et al. [15]. As discussed in Ref. [13], this higher stress field in the thinner transverse laminae results in an increase of the crack density of the thinner plies. An observation of this phenomenon was also obtained by simulation.

After the onset of damage, which occurs approximately at the same applied strain (as observed elsewhere [13; 14]), softening is more gradual for the thinner transverse plies, becoming steeper and with more pronounced jumps or sudden variations as the ply thickness increases — see Figure 2.15.

In a similar study, Naderi and Iyyer [17] performed a micro-mechanical analysis assessing the damage mechanisms under transverse tension of $[0/90]_s$ thin-ply composite laminates. A similar homogenised stress-strain relation for the embedded 90° ply was also observed. Naderi and Iyyer [17] attributed the gradual softening observed on thinner transverse plies to a higher likelihood distribution of weaker fibre-matrix interface properties, in terms of strength and fracture energy, as it tends to increase in the thicker embedded 90° plies. To further understand the effect of the fibre-matrix interface properties on damage evolution mechanisms, Naderi and Iyyer [17] performed additional analyses considering different values of the fibre-matrix interface fracture strength. It was noted that in terms of homogenized stress-strain curves for the embedded 90° ply, an earlier deviation from the linear response was associated with lower values of interface fracture strength.

Fu and Wang [18] also reported an increase in matrix crack density with the decreasing ply thickness.

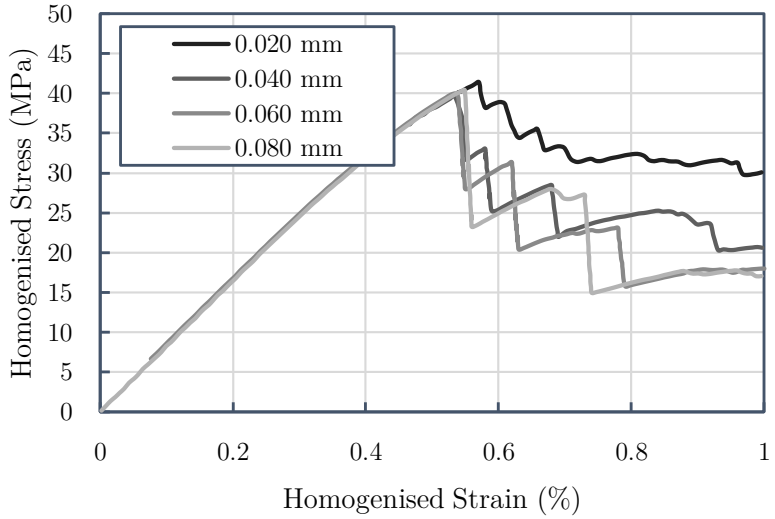

Figure 2.15: Homogenised stress-strain curves of the embedded 90° ply for different ply thicknesses (adapted from Arteiro et al [15]).

Reduction in COD of the transverse cracks with ply thickness Another very interesting finding reported by Saito et al. [13] in their experimental work and also observed by Arteiro et al. [15] is related with the COD of the transverse cracks in 90° plies of different thicknesses. Due to the constraining effect imposed by the adjacent 0° plies, the COD in the thinner 90° plies was much smaller than the one observed in thicker ones — see Figure 2.16.

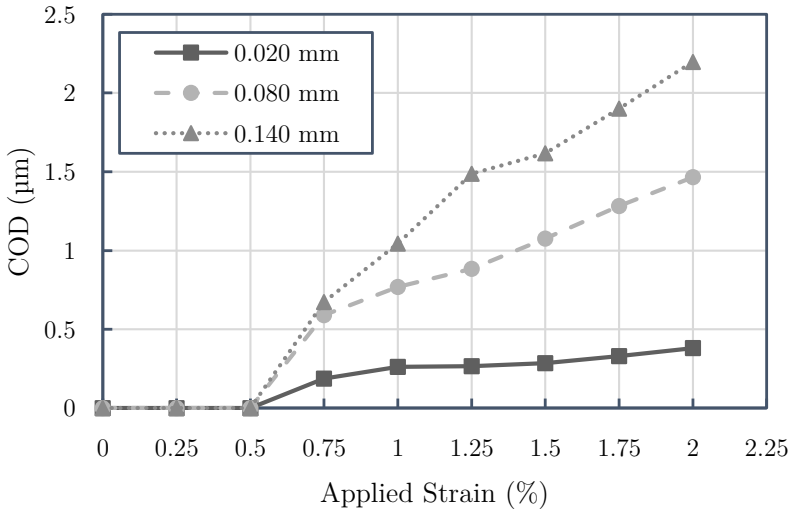

Figure 2.16: COD as a function of applied strain for different 90° ply thicknesses (adapted from Arteiro et al [15]).

Formation of thin necks of matrix material around the regions where interfacial damage is more pronounced The numerical simulations employed also led to another interesting result, which had been previously confirmed by experimental work [13] and by numerical analyses presented by Melro et al. [87]: the formation of thin necks of matrix material

around the regions where interfacial damage is more pronounced. The *in-situ* observations presented by Saito et al. [13] suggest that this phenomenon is potentiated by increasing ply thicknesses, also confirmed by Arteiro et al. [15].

In the micro-mechanical analyses performed by Naderi and Iyyer [17], a similar observation concerning the formation of thin necks of matrix material around the regions where interfacial debonding was dominant was also observed.

***In-situ* strength** Lastly, a relation between the *in-situ* transverse tensile strength versus the ply thickness, based on the micro-mechanical analysis, was determined [15] — see Figure 2.17. This relation was compared with the analytical model of the *in-situ* transverse tensile strength, based on fracture mechanics, proposed by Camanho et al. [33]. In fact, the trends, of the analytical and computational micro-mechanics models were in reasonable agreement, thus, it was clearly possible to identify a substancial increase in the *in-situ* transverse tensile strength with decreasing ply thickness.

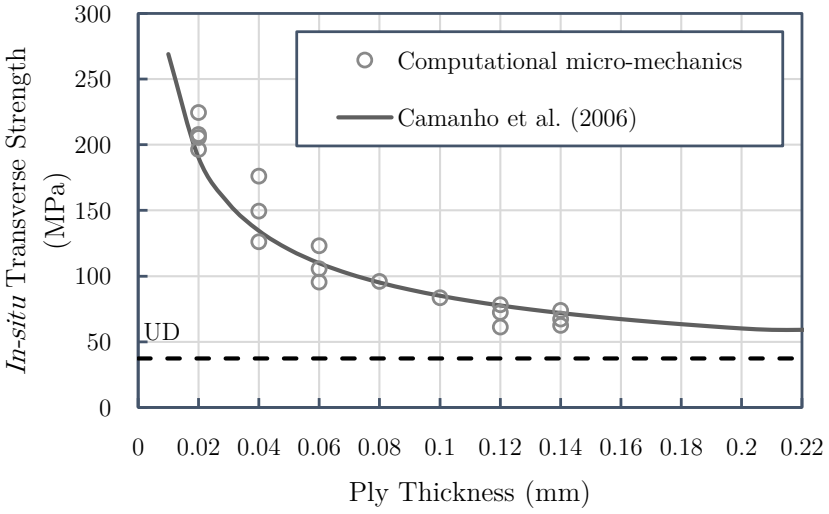

Figure 2.17: *In-situ* transverse tensile strength as a function of the ply thickness (adapted from Arteiro et al. [15]).

Following the study of the mechanical response of ultra-thin plies under transverse tensile loading [15], Arteiro et al. [16] performed a micro-mechanical analysis, using the same micro-mechanical model, to study the effect of ply thickness on constrained 90° plies subjected to transverse compressive loading. The results of the micro-mechanical model, when compared with the predictions from analytical models [46; 47], predicted the same trends.

- For cross-ply sublaminates with conventional, standard-thickness 90° plies, failure was dominated by fibre-matrix interface cracking and large localised plastic deformation of the matrix, forming a localised band of damage in a plane not aligned with the loading direction. The predicted wedge shaped transverse fracture was in agreement with what has been described in the literature [71; 87]. In the case of cross-ply sublaminates with ultra-thin plies, a similar damage pattern could be identified, but developing at higher applied strains. In fact, a transverse crack suppression effect

could be clearly identified. As the ply thickness decreases, damage progression becomes more and more gradual, and through-thickness fracture is delayed. This fact indicates that there is an *in-situ* effect in transverse compression.

- Following the previous conclusion, it was noted that, unlike conventional 90° plies subjected to transverse compressive loading, constrained ultra-thin plies showed a dispersed damage mechanism, combining wedge cracking with ply fragmentation/separation, or just ply fragmentation/separation for the thinnest plies. This dispersed type of damage on thin-ply sublaminates is the result of a less pronounced stress relaxation due to the stronger constraining effect imposed by the surrounding plies. This results in the development of progressive ply damage instead of discrete transverse cracking. Therefore, a transverse crack supression effect could be observed.

- Lastly, the *in-situ* transverse compressive strength, as a function of the ply thickness, determined from the micro-mechanical model prensented in the current study, was plotted and compared with the analytical predictions proposed by Catalanotti et al. [46] and by Camanho et al. [47] — see Figure 2.18. Similar trends were observed, which indicated not only that the analytical models were sufficiently accurate, but also that there is an *in-situ* effect in the transverse compressive failure of polymer composites.

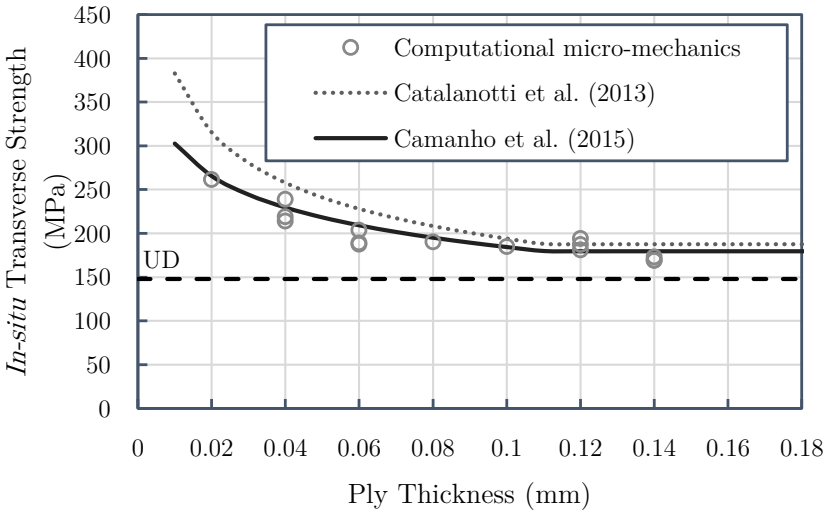

Figure 2.18: *In-situ* transverse compressive strength as a function of ply thickness (adapted from Arteiro et al. [16]).

Chapter 3

Computational micro-mechanics. Model formulation

In this chapter, the 3D CMM model formulated for the analysis of the *in-situ* effect is presented. The referred FE model consists of three main parts, a micro-mechanical RVE of a 90° thin lamina, two adjacent homogenised plies, and the interfaces between the 90° lamina and the adjacent homogenised plies. The constitutive models referring to each one of these parts are presented, followed by a comprehensive description of the FE modelling strategy used, to appropriately develop a FE analysis of the *in-situ* effect.

3.1 Constitutive modelling

The RVE of the 90° thin lamina includes a discrete representation of the carbon fibres, the epoxy matrix, and the interfaces between fibres and matrix. A random distribution of the carbon fibres is generated using an adaptation of the algorithm proposed by Melro et al. [85], with imposed fibre continuity along the faces perpendicular to the y-direction — see Figure 3.1. Here, the x-direction coincides with the longitudinal direction of the discretised transverse ply, the y-direction coincides with the in-plane transverse direction of the discretised transverse ply, and the z-direction coincides with the out-of-plane transverse direction.

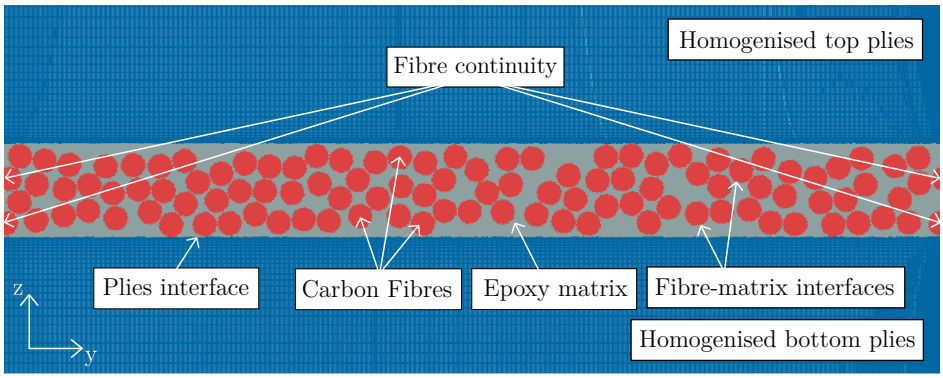

Figure 3.1: RVE of a laminate with a discretised 0.02 mm thick 90° lamina (adapted from Arteiro et al. [16]).

Unlike 3D random RVEs with PBCs, for the micro-mechanical analysis of UD composites [87; 104], in the present work, the entire thickness of the discretised transverse ply is represented, so its effect in the response of the thin-ply sublaminate can be taken into

account. The faces of the discretised transverse ply perpendicular to the z-direction will be connected to the homogenised outer plies, and, therefore, in the generation of the RVE, fibres are not allowed to intersect these faces — see Figure 3.1.

The homogenised outer plies are intended to simulate the mesoscopic elastic behaviour of the surrounding laminae and its effect on the mechanical response and on the damage initiation and growth in the intermediate 90° thin lamina. The interfaces between the 90° lamina and the homogenised outer plies, and the corresponding interlaminar damage onset and propagation, are simulated using a cohesive element formulation. The constitutive models for each of these materials are briefly described in the following sections.

3.1.1 Reinforcing fibres

In the present work, a simple transversely isotropic, linear-elastic constitutive model is used to simulate the individual reinforcing carbon fibres. Following Melro et al. [87], the diameter of the individual carbon fibres is considered constant along the entire RVE. Table 3.1 presents the material properties of the standard carbon fibres used in the present micro-mechanical approach [15; 16].

Table 3.1: Fibre diameter, fibre volume fraction and properties of the carbon fibres [15; 16].

Material Property	Units	Value
Fibre diameter		
D_f	mm	0.0052
Fibre volume fraction		
V_f	%	56.27
***Young's* moduli**		
E_1	MPa	276000
E_2		15000
***Poisson's* ratio**		
ν_{12}	-	0.2
Shear moduli		
G_{12}	MPa	15000
G_{23}		7000
Coefficients of thermal expansion		
α_{11}	$^{\circ}\mathrm{C}^{-1}$	-0.5×10^{-6}
α_{22}		15×10^{-6}
Mass density		
ρ	$\mathrm{t\,mm}^{-3}$	1.78×10^{-9}

3.1.2 Epoxy matrix

The epoxy matrix is modelled using the pressure dependent, elasto-plastic thermodinamically consistent damage model proposed by Melro et al. [104], implemented as a VUMAT user subroutine [92; 93; 105] of the FE commercial software ABAQUS® [106]. According to this model, the initial elastic behaviour is defined by a linear relation between the stress tensor and the elastic strain. A paraboloidal yield criterion, based on Ref. [107], defined

as a function of the stress tensor and of the compressive and tensile yield strengths, is used together with a non-associative flow rule, which allows for a correct definition of the volumetric deformation in plasticity. The tensile and compressive hardening functions are provided by two piecewise functions of the equivalent plastic strain. Since it is fully differentiable, the paraboloidal yield function is integrated by means of a general return mapping algorithm.

Damage in the epoxy matrix is modelled by a single damage variable that affects only the *Young's* modulus of the material once activated. This isotropic damage model is defined in a thermodynamically consistent way, ensuring irreversibility of the damage process.

Damage onset is defined by a damage activation function similar to the paraboloidal yield criterion, but using the final compressive and tensile strengths of the epoxy matrix instead of the yield strengths, and the concept of effective stress tensor, i.e., the stress tensor calculated using the undamaged stiffness tensor [104]. To avoid damage localisation (mesh size dependency), Bažant and Oh's crack band model [108], which makes use of the characteristic length of the FE and the fracture toughness of the epoxy matrix to regularise the computed dissipated energy, is implemented along with the definition of the damage evolution law [104]. The chosen damage evolution law forces damage localisation and strain softening on the material under tensile load, but under compressive load the influence of the hydrostatic pressure causes a different evolution of the damage variable. The progression of damage is softer than in the tensile case, which suggests a slower propagation of damage [104]. For a comprehensive explanation of the constitutive model used for the epoxy matrix, the reader is referred to Ref. [104].

Fiedler et al. [109] experimentally characterised the stress-strain behaviour of a typical epoxy matrix material (Toho # 113) under tension, compression and shear. The relevant elastic and strength properties needed to model the material behaviour of the epoxy matrix were extracted from those experimental results, as well as the hardening laws for tension and compression. The plastic Poisson's ratio, ν_p, has been determined by Guild et al. [110], which is considered a standard value for epoxy resins, and the critical ERR, $\mathcal{G}_c$, used in this numerical approach is a mean value of the values reported in the literature [87].

Table 3.2 presents the properties of the epoxy matrix [15; 16]. The tensile and compressive hardening laws are shown in Figure 3.2 [15; 16].

3.1.3 Fibre-matrix interface

The interfaces between fibres and matrix are modelled using the cohesive element formulation available in the FE commercial software ABAQUS® [106]. The cohesive element behaviour is linear elastic up to damage onset and defined by a bilinear traction-separation law. The onset of damage in the cohesive element is mode dependent, and it is defined by the corresponding strengths in mode I (τ_3^0) and mode II ($\tau_1^0 = \tau_2^0$). The rate of damage progression is controlled by the critical ERR of the cohesive elements under mode I, mode II, or mixed-mode, following the BK law [111].

Table 3.3 presents the properties of the fibre-matrix interface [15; 16]. The initial stiffness, K, of the cohesive element is set to maintain continuity of the stress and strain fields between fibre and matrix [87]. The low values of the interface fracture energies,

Table 3.2: Properties of the epoxy matrix [15; 16].

Material Property	Units	Value
***Young's* modulus**		
E	MPa	3760
***Poisson's* ratio**		
ν	-	0.39
Coefficient of thermal expansion		
α	$^{\circ}\mathrm{C}^{-1}$	58×10^{-6}
Stress free temperature		
T_0	°C	155
Plastic *Poisson's* ratio		
ν_p	-	0.3
Critical ERR		
$\mathcal{G}_c$	$\mathrm{N\,mm}^{-1}$	0.277
Tensile strength		
X_T	MPa	93
Compressive strength		
X_C	MPa	350
Mass density		
ρ	$\mathrm{t\,mm}^{-3}$	1.3×10^{-9}

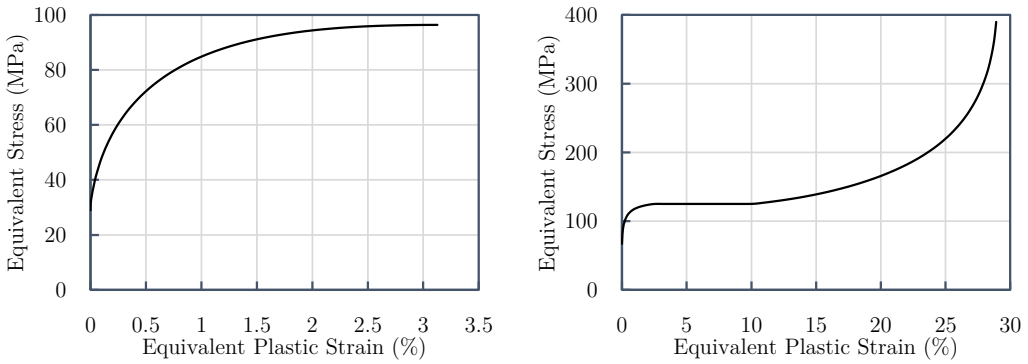

(a) Tensile hardening curve (b) Compressive hardening curve

Figure 3.2: Yield curves given in Equivalent Stress vs. Equivalent Plastic Strain

$\mathcal{G}_{\mathrm{I}c}$ and $\mathcal{G}_{\mathrm{II}c}$, are justified not only by the experimental work performed by Varna et al. [112], but also from previous micro-mechanical numerical analyses [87; 100], which have demonstrated that the brittle behaviour in transverse tension typical of composites is only captured for such low values of interfacial toughness [15; 16; 87].

3.1.4 Homogenised outer plies

The outer plies are modelled assuming a linear-elastic transversely isotropic constitutive behaviour. Since the homogenised outer plies are only introduced in the present micro-mechanical model to assess the effect of the stiffness of the adjacent plies in the mechanical

Table 3.3: Fibre-matrix interface properties [15; 16].

Material Property	Units	Value
Interface Stiffness		
K	$\mathrm{N\,mm^{-3}}$	10^8
Interface maximum strengths		
τ_1^0		75
τ_2^0	MPa	75
τ_3^0		50
Interface critical ERRs		
$\mathcal{G}_{\mathrm{I}c}$		0.002
$\mathcal{G}_{\mathrm{II}c}$	$\mathrm{N\,mm^{-1}}$	0.006
$\mathcal{G}_{\mathrm{III}c}$		0.006
Mixed-mode interaction parameter (BK law [111])		
η	-	1.45

response and damage evolution of the intermediate 90° lamina, no nonlinear or fracture behaviour is considered.

The IM7/8552 carbon/epoxy composite system is used to model the outer plies of the proposed RVE, as the corresponding material properties are available in several publications [113–115]. Table 3.4 presents the relevant material properties for the homogenised plies [15; 16].

Table 3.4: Properties of the homogenised outer plies (IM7/8552) [15; 16].

Material Property	Units	Value
***Young's* moduli**		
E_1	MPa	171420
E_2		9080
***Poisson's* ratio**		
ν_{12}	-	0.32
Shear moduli		
G_{12}	MPa	5290
G_{23}		3920
Coefficients of thermal expansion		
α_{11}	$^\circ\mathrm{C}^{-1}$	-5.5×10^{-6}
α_{22}		25.8×10^{-6}
Mass density		
ρ	$\mathrm{t\,mm^{-3}}$	1.57×10^{-9}

3.1.5 Plies interface

The interfaces between the intermediate 90° lamina and the adjacent homogenised plies are modelled using the cohesive element formulation existent in the FE commercial software ABAQUS® [106]. Similarly to the fibre-matrix interface, the cohesive element constitutive behaviour is linear elastic up to damage onset and defined by a mode dependent bilinear traction-separation law. The rate of damage progression is controlled by the critical ERR of the cohesive element under mode I, mode II, or mixed-mode according to the BK law [111].

The interlaminar properties of the IM7/8552 carbon/epoxy composite system [113] are used to model the interfaces between the intermediate 90° lamina and the adjacent homogenised plies. The main reason for this consideration is the use of the IM7/8552 elastic and physical properties to model the constitutive behaviour of the homogenised outer plies. Table 3.5 presents the corresponding material properties [15; 16].

Table 3.5: Interlaminar interface properties of the IM7/8552 carbon/epoxy composite system [15; 16].

Material Property	Units	Value
Interface stiffness		
K	$\mathrm{N\,mm^{-3}}$	10^8
Interface maximum strengths		
τ_1^0		93
τ_2^0	MPa	93
τ_3^0		71
Interface critical ERRs		
$\mathcal{G}_{\mathrm{I}c}$		0.277
$\mathcal{G}_{\mathrm{II}c}$	$\mathrm{N\,mm^{-1}}$	0.788
$\mathcal{G}_{\mathrm{III}c}$		0.788
Mixed-mode interaction parameter (BK law [111])		
η	-	1.634

3.2 Finite element modelling

3.2.1 Introduction

The present CMM model imposes severe non-linearities on the respective numerical analyses due to the constitutive inelastic behaviour of the matrix material, which lead to convergence difficulties in implicit integration FE solvers. Here, an explicit numerical scheme is used to avoid such difficulties and obtain meaningful numerical predictions within an acceptable CPU time. Accordingly, the CMM analyses are performed using ABAQUS®/Explicit as explicit dynamic analyses.

3.2.2 Finite element discretisation

Figure 3.3 shows a schematic view of the thin-ply sublaminate RVE, where b is the thickness of the intermediate 90° lamina (z-direction), t_{out} is the thickness of each individual outer

ply, which is equal to 0.075 mm, and remains constant throughout the analyses, a is the width of the RVE (y-direction), defined to ensure the representativeness of the different RVEs analysed in the present research — see Table 3.6, c is the length of the RVE (x-direction), and θ is the orientation of the outer plies, here fixed at 0° throughout the analyses.

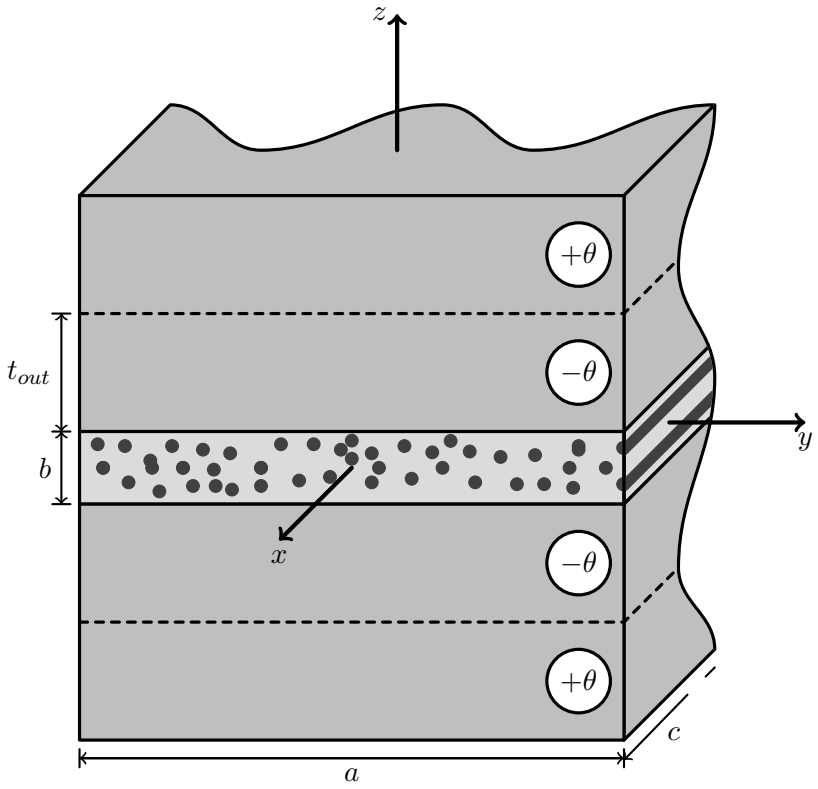

Figure 3.3: Schematic of the RVE of a thin-ply sublaminate (adapted from Arteiro et al. [15]).

In order to further understand the effect of the embedded 90° ply thickness on ply damage, several 90° ply thicknesses are studied, spanning from the ultra-thin 0.020 mm to more conventional 0.140 mm. For some ply thicknesses, different random fibre distributions are analysed to assess the effect of microstructural randomness — see Table 3.6.

The width of the RVEs of the thin-ply sublaminates along the y-direction is 0.200 mm. The reason for such definition is the need to ensure that any diffuse damage, which might occur before a transverse crack has grown entirely through the thickness of the ply, can be captured [15; 16]. In a compromise between the computational cost of the proposed models and the results obtained, it was observed by Arteiro et al. [15; 16] that an RVE width of 0.200 mm was adequate to capture the diffuse damage occuring in the thinner transverse plies under transverse tensile and compressive loading scenarios. However, due to the enormous computational cost of the present models, the RVEs of the sublaminates with transverse ply thicknesses above or equal to 0.100 mm were modelled to accommodate approximately a single transverse crack, reducing the total width of the RVEs to 0.120 mm. Nevertheless, Arteiro et al. [15; 16] observed that, for such transverse ply thicknesses, diffuse damage before transverse cracking was very limited. Therefore, defining the width of the RVE such that a single transverse crack could be captured was sufficient to study

Table 3.6: Dimensions of the thin-ply sublaminate RVE and random fibre distributions.

RVE thickness (mm)	**Fibre distributions**	**RVE width** (mm)
0.020	DIST01 DIST02 DIST03 DIST04	0.200
0.040	DIST01 DIST02 DIST03	0.200
0.060	DIST01 DIST02 DIST03	0.200
0.080	DIST01	0.200
0.100	DIST01	0.120
0.120	DIST01 DIST02 DIST03	0.120
0.140	DIST01 DIST02 DIST03	0.120

the damage morphology and predict failure of the thicker transverse plies. Reducing the RVE width from 0.200 mm to 0.120 mm for transverse ply thicknesses above 0.100 mm was enough to capture transverse cracking and keep the computational cost of the models within reasonable values.

First order hexaedral FEs with reduced integration (ABAQUS® C3D8R) are choosen following Melro et al. [87] to generate the mesh of both matrix and fibres of the transverse ply RVE. However, due to the randomness of the distribution of reinforcements and consequent difficulty to mesh such geometry, a few linear wedge elements with reduced integration (ABAQUS® C3D6R) had to be included in the mesh. According to Melro et al. [87], these wedge elements have no influence on the global response of the composite system. The mesh of the homogenised outer plies is generated employing also ABAQUS® C3D8R elements. Concerning the interface between fibres and matrix of the intermediate 90° ply and the interface between the mid-90° ply and the adjacent homogenised plies, 8-node cohesive elements (ABAQUS® COH3D8) are used to generate the mesh. Figure 3.4 shows a schematic representation of an FE discretisation of part of an RVE with a 0.040 mm thick transverse ply.

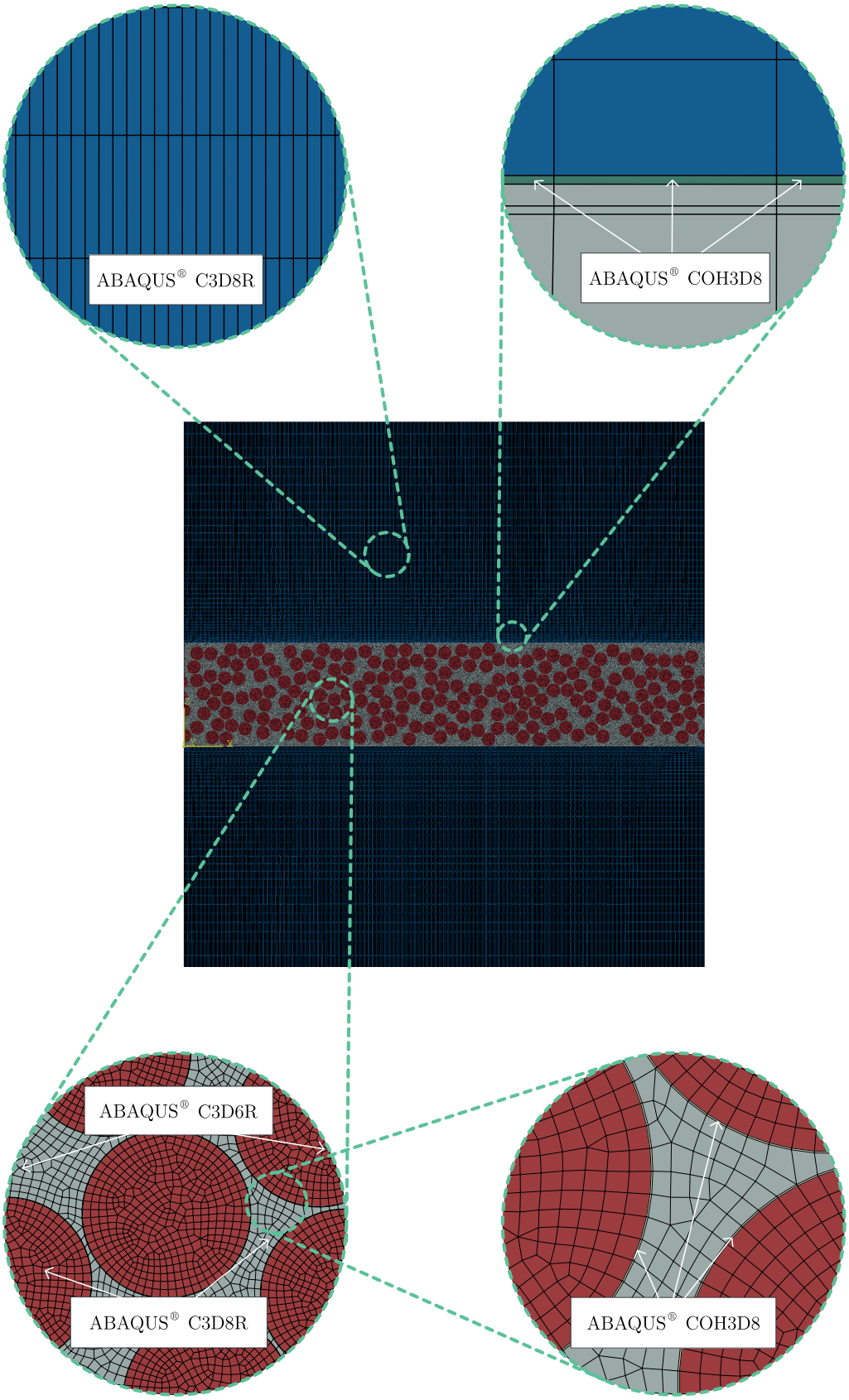

Figure 3.4: Schematic representation of an FE discretisation of part of an RVE with a 0.040 mm thick transverse ply.

3.2.3 Loading and boundary conditions

In a CMM analysis, apart from the selection of the RVE size, which must be sufficient to capture the stress-strain response and failure mechanisms of the composite, the applied boundary conditions play a key role on the assessment of the homogenised properties [116].

In FE studies of RVEs, PBCs are generally used to represent the boundary conditions of a small volume of material surrounded by identical material, representing the overall material volume. The RVE size is typically a very small portion of the material being considered. PBCs ensure compatibility of deformation and correct computation of stress and strain. These boundary conditions can be incorporated in a FE analysis by using linear multi-point constraints. These are kinematic constraints imposed by a set of equations on the degrees of freedom of each pair of nodes belonging to opposite faces, edges or vertices of the RVE. These equations include the corresponding degrees of freedom, as well as the far-field applied strains [87; 117; 118]. In its essence, this method requires the mesh to be periodic, in such a way that every node on each RVE boundary has its homologous node on the respective opposite (periodic) boundary, although enhancements, based on polynomial interpolation [119; 120] and Lagrange multipliers [121], have been proposed in order to avoid the need of matching the mesh topology on opposite RVE boundaries.

The traditional PBC approach is quite appropriate for implicit integration FE solvers but the fulfilment of the periodicity equations in dynamic explicit integration FE solvers tends to lead to spurious displacement oscillations that compromise the numerical solution [116]. Furthermore, there is a limited number of multi-point constraints allowed in ABAQUS®/Explicit [106], thus in the current micro-mechanical analyses PBCs could not be used.

In the literature, several authors [122–124] concluded that microstructural RVEs can be solved with sufficient accuracy without the imposition of PBCs, as long as the RVE is sufficiently large. In addition, several researchers have been trying to circumvent the use of PBCs in their micro-mechanical analyses, either due to the existent limitations on multi-point constraints in ABAQUS®/Explicit [21; 88; 116; 125; 126], or the unsuitability of imposing PBCs in their analyses [127], and thus employing alternative techniques.

Sádaba et al. [116] proposed an approach based on the implementation of a user-defined element, which enforces the periodicity between periodic nodes through a spring-mass-dashpot system. This reformulation of the elements solved the issue of spurious oscillations resulting from the application of the traditional PBCs in the explicit FE method, overcomed limitations in the number of constraint relations and allowed gains in computational efficiency.

Varandas et al. [126] performed CMM analyses in order to obtain the mechanical properties of the fibre tows for any given fibre volume fraction. These CMM analyses were performed using ABAQUS®/Explicit, and different RVEs were subjected to PBCs. In these FE analyses, PBCs were incorporated by using linear multi-point constrains, but using small 3D RVEs or imposing 2D PBCs [106].

Sebaey et al. [88], in a CMM analysis to assess the effect of fibre misalignment on the longitudinal compression and shear properties of UD fibre-reinforced plastics, implemented

a different set of displacement boundary conditions applied to the corresponding faces of the RVE, being the remaining faces considered traction free and un-restrained. This assumption affected the quantitive predictions, but the predicted trends were representative of the composite system behaviour, even without the imposition of PBCs. A similar strategy concerning displacement relations to the boundary conditions was implemented by Soni et al. [127] in their study of damage localisation in composite laminates.

Kohler et al. [21] implemented a multi-scale FE model consisting of an "embedded cell" modelling approach. The RVE was embedded in a larger continuum model of the laminate, where the total model length was at least three times the embedded cell length to simulate damage events in the bulk of the material due to transverse tension. The boundary conditions applied enforced a plane strain state, namely a symmetry on the front side of the model and a planarity constraint on all the nodes of the back face. The transverse tensile tension was implemented by a displacement relation imposed at the boundaries of the model, while the opposite boundaries were simply supported.

Strategy adopted

The strategy adopted in this work concerning the transverse shear analysis is schematized in Figure 3.5. Since this is an explicit dynamic analysis, the transverse shear load was applied through a velocity in the z-direction along the entire left face of the RVE, with a smooth step amplitude throughout the step time [106]. The smooth step amplitude is used to avoid initial dynamic phenomena.

Concerning the general boundary conditions, in order to simulate a pure transverse shear stress state on the micromechanical model (see Figure 3.6), the right face of the RVE is simply supported (along the y-direction) and the opposite face is clamped — see Figure 3.5.

Since long-fibre-reinforced composites are being considered here, a plane strain state is assumed along the x-direction. This condition was approximated by simply supporting (along the x-direction) the front and back faces of the RVE.

This simplified strategy is adopted instead of PBCs due to the intrinsic limitations of ABAQUS®/Explicit. To assess the effect of RVE size, following Kohler et al. [21], homogenised material was added to the present micro-mechanical model to ensure remote loading on the RVE ("embedded cell" approach). The homogenised material is added by expanding the homogenised outer plies along the y-direction by a certain dimension, h, and by including a homogenised 90° thin lamina material of the same size, h — see Figure 3.5. A parametric study was performed to assess the effect of the dimension of homogenised material, h, on the remote loading of the RVE.

As a reference, the analyses performed using ABAQUS®/Explicit, which employ the loading and boundary conditions described before, are compared with an analysis performed on ABAQUS®/Standard (implicit solver) with PBCs implemented using multi-point constraints on the micro-mechanical model — see Table 3.7. All analyses considered the same distribution of the reinforcements and the same embedded 90° ply thickness.

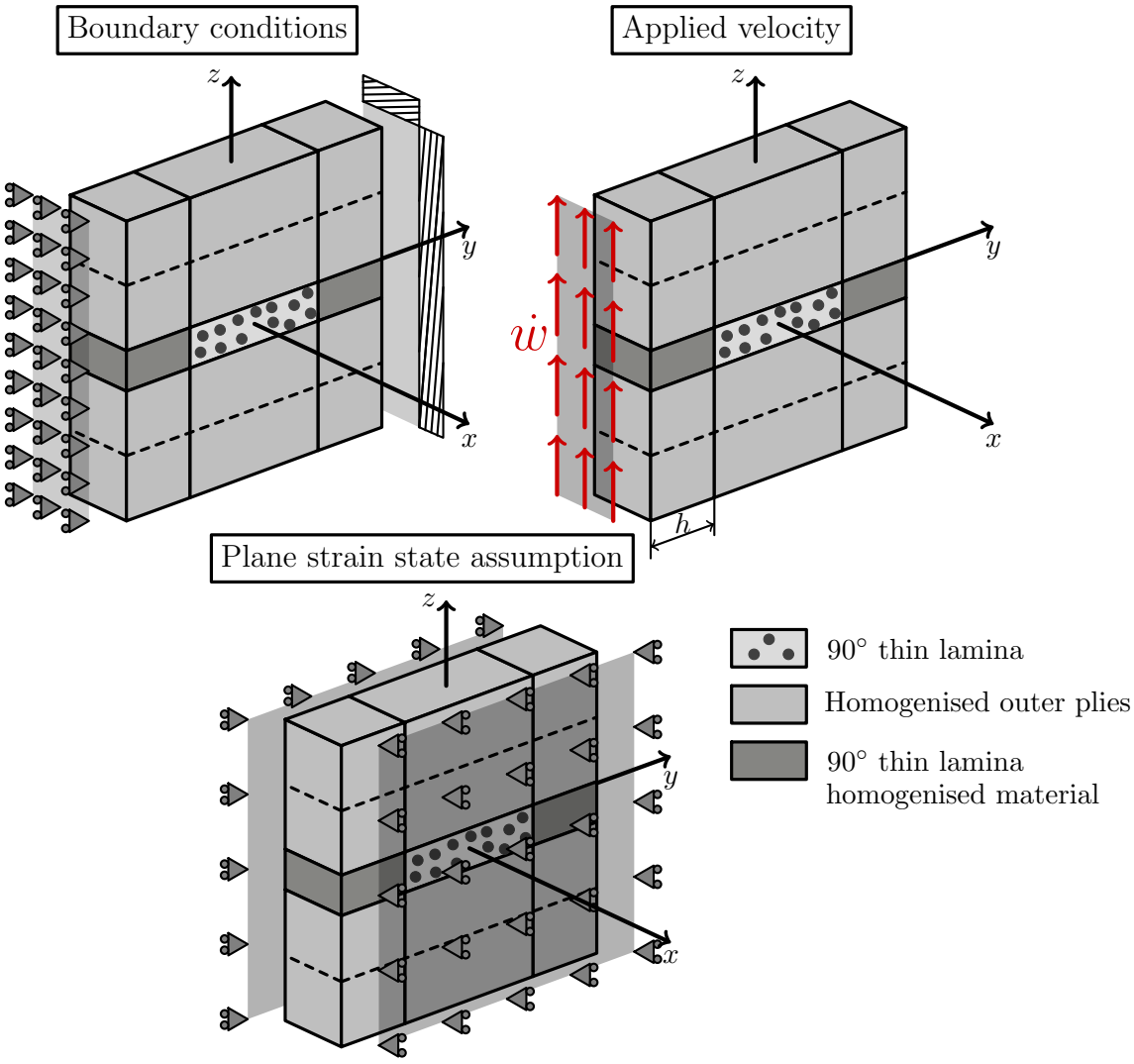

Figure 3.5: Schematic representation of the loading and boundary conditions applied to the micromechanical model for the transverse shear analysis (for simplicity, the loading and boundary conditions are represented separately here, but applied simultaneously in the FE model).

For each model, the homogenised stress-strain curve in the 90° thin lamina RVE was obtained after performing a first-order volumetric homogenisation [87]:

$$\tau_{23}^0 = \frac{1}{V}\int_V \tau_{23}\, dV = \frac{1}{V}\sum_{k=1}^{N_p} \tau_{23}^k V^k \tag{3.1}$$

$$\gamma_{23}^0 = \frac{1}{V}\int_V \gamma_{23}\, dV = \frac{1}{V}\sum_{k=1}^{N_p} \gamma_{23}^k V^k \tag{3.2}$$

where τ_{23}^0 and γ_{23}^0 represent, respectively, the homogenised stress and strain components of the 90° thin lamina RVE, τ_{23}^k and γ_{23}^k are, respectively, the stress and strain components determined at integration point k, V^k is the associated volume of the integration point, $V = \sum_{k=1}^{N_p} V^k$ is the volume of the RVE, and N_p represents the total number of integration

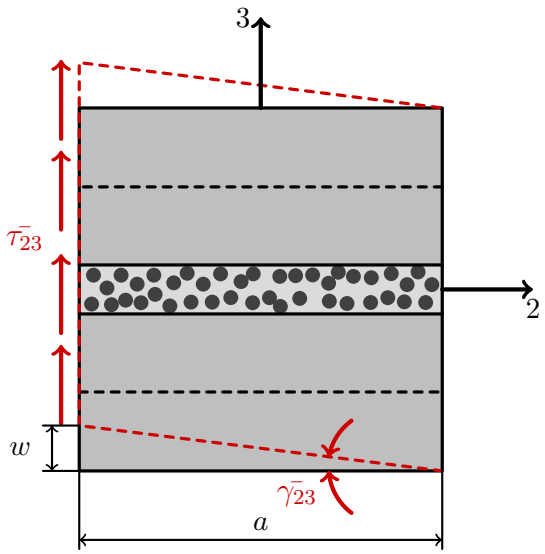

Figure 3.6: Schematic representation of a pure transverse shear stress state applied to the micro-mechanical model.

Table 3.7: Different models to assess remote loading on the RVE.

Model	**Embedding homogenised material size** (h)		**ABAQUS® FE Solver**
	Units	**Value**	
EXP00		0	Explicit
EXP01		0.1	Explicit
EXP02	mm	0.2	Explicit
EXP04		0.4	Explicit
EXP08		0.8	Explicit
IMP		-	Standard

points in the RVE. From this volumetric homogenisation, it is possible to quantify the strain evolution on the RVE for the different models, and to compare with the model with PBCs.

Figure 3.7 shows the homogenised stress-strain curves for each model considered in this parametric study. It should be noted that, after damage initiation (represented with a triangular marker), the homogenisation procedure becomes ill-posed, due to the stress softening resulting from damage localisation. Hence, the stress-strain diagrams are interrupted shortly after damage localisation (the softening part of the curve is still plotted in dashed line for reference). The circular marker corresponds to the penetration of the first matrix crack through the thickness of the 90° lamina and serves also as a reference. The unfilled triangular marker refers to the model with imposition of PBCs and it corresponds to fiber-matrix debonding initiation, which in this model precedes damage initiation in the matrix.

As observed, the homogenised stress-strain response of the RVE does not follow any particular trend, and, therefore, it can be considered independent of the size of the RVE

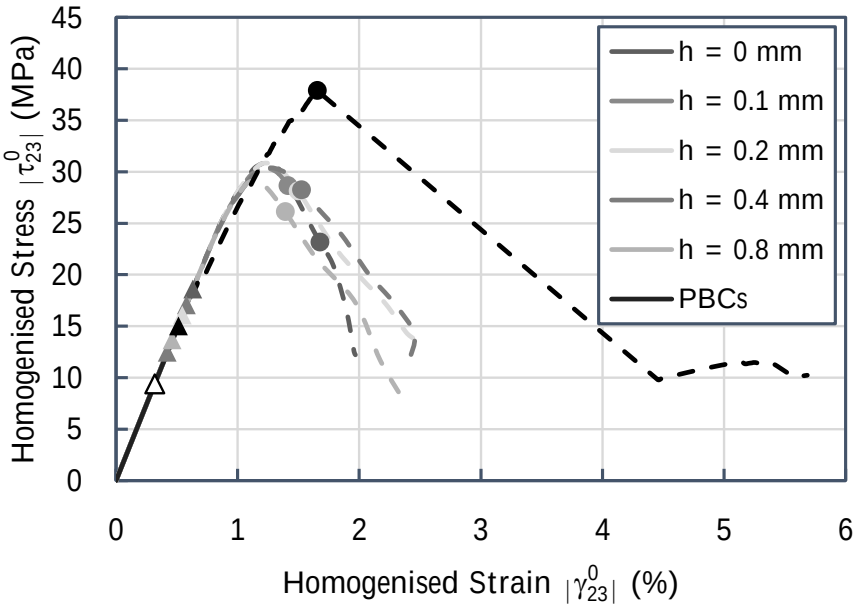

Figure 3.7: Homogenised stress-strain curves obtained after performing a first-order volumetric homogenisation.

for the current embedded cell size (a) of 0.200 mm. Hence, for the sake of computational efficiency, in the following micro-mechanical analyses (Chapter 4), it is opted to not include homogenised parts attached to the embedded RVE (i.e. $h = 0$ mm).

3.2.4 Transverse shear deformation in the RVE

With the imposition of PBCs, it is possible to quantify the remote strain applied to the RVE [87; 128]. To determine the applied transverse shear strain applied to the RVE using the present loading and boundary conditions, the applied vertical (along the z-direction) displacement (w) can be used, considering the dimensions of the RVE (see Figure 3.6), as:

$$\bar{\gamma_{23}} = \tan^{-1}\left(\frac{w}{a+2h}\right) \approx \frac{w}{a+2h} \tag{3.3}$$

Figure 3.8 shows the comparison between the homogenised transverse shear strain, γ^0_{23}, obtained using Equation 3.2, and the applied transverse shear deformation obtained from the vertical displacement applied to the RVE — Equation 3.3 — for the dynamic models (ABAQUS®/Explicit) presented in Table 3.7. Firstly, it can be observed that, as it had been concluded before, the mechanical response of the RVE is independent of its size for the current embedded cell size (a) of 0.200 mm. However, it should be also pointed that this numerical comparison is only valid for the linear-elastic response of the RVE, i.e., before damage initiation occurs, which, again is represented with a triangular marker for reference. Furthermore, it can be also concluded that the transverse shear strain obtained from the vertical displacement applied to the micro-mechanical model does not represent correctly the homogenised transverse shear strain, γ^0_{23}, in the 90° RVE, even in the elastic regime, and independently of the size of the model.

Hence, for a more representative measure of the applied transverse shear strain, at least in the elastic regime, it is opted here to follow a different strategy.

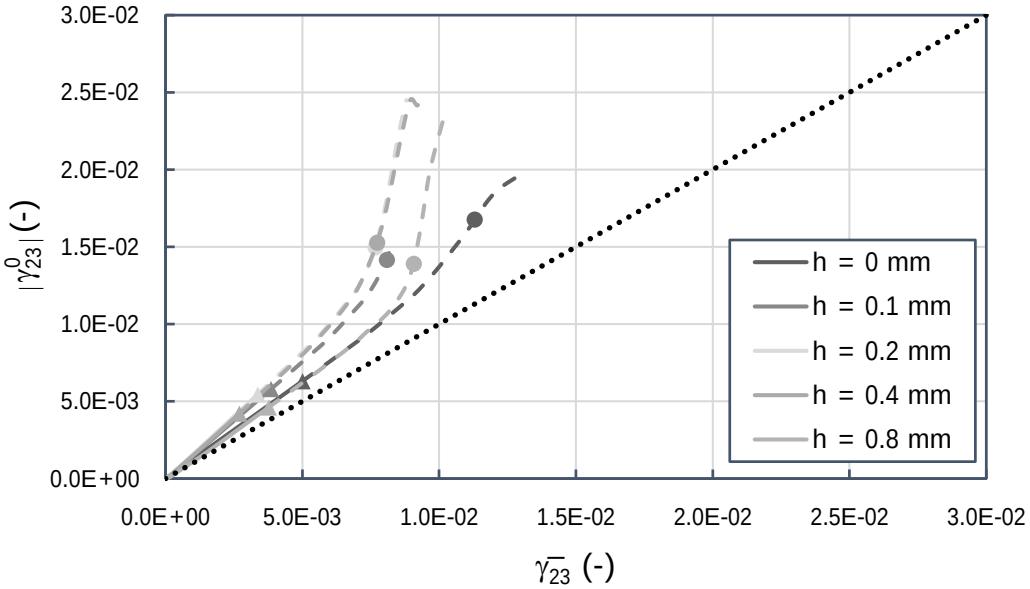

Figure 3.8: Comparison between the homogenised transverse shear strain ($|\gamma_{23}^{0}|$) and the applied transverse shear strain ($\bar{\gamma_{23}}$).

As mentioned before, the transverse shear loading was applied on the RVE through a vertical (along the z-direction) velocity with a smooth step amplitude throughout the step time. This smooth step amplitude is based on a fifth-order polynomial equation [106], thus the evolution of the vertical displacement applied to the micro-mechanical model through the step time can be approximated by a sixth-order polynomial fitting. The same holds for the applied transverse shear strain on the RVE.

To validate this numerical approach, a numerical comparison throughout the step time between the evolution of the homogenised transverse shear strain, γ_{23}^{0}, and the evolution of an equivalent applied transverse shear strain, $\gamma_{23}^{0,\mathrm{Eq}}$, obtained by curve fitting with a sixth-order polynomial equation of the homogenised transverse shear strain obtained before damage onset, is performed. Figure 3.9 shows this comparison. As can be observed, fitting by a sixth-order polynomial equation correctly represents the applied transverse shear strain prior to damage onset (valid domain for volumetric homogenisation) — see Figure 3.10.

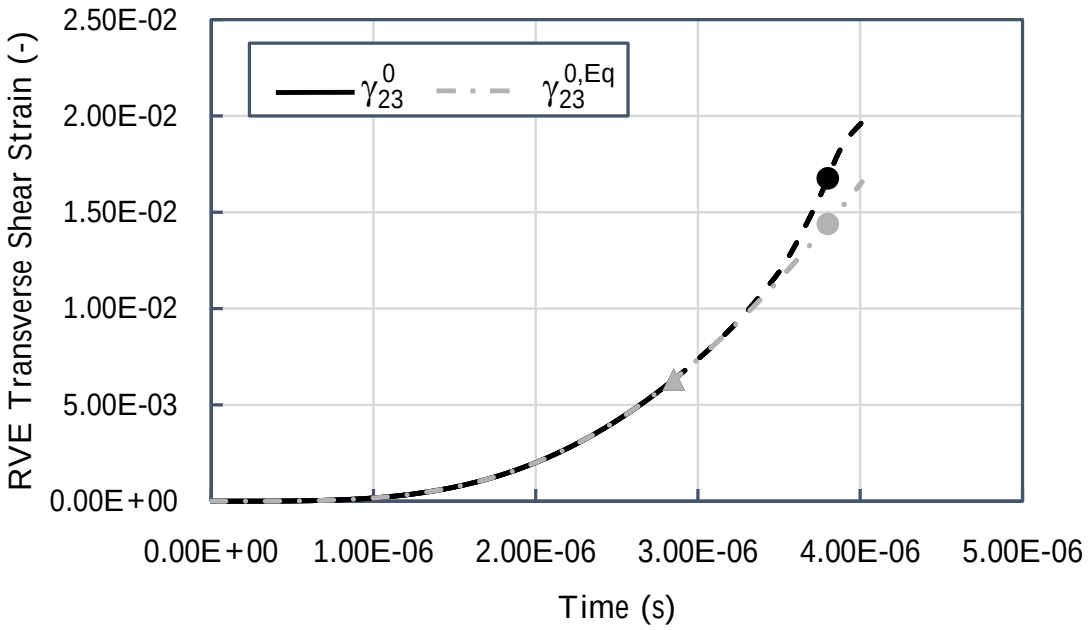

Figure 3.9: Comparison between the evolutions of γ_{23}^{0} and $\gamma_{23}^{0,Eq}$ throughout the step time for a representative analysis. Curve fitting (gray interrupted line) is performed just on the region of γ_{23}^{0} prior to damage onset (full black line).

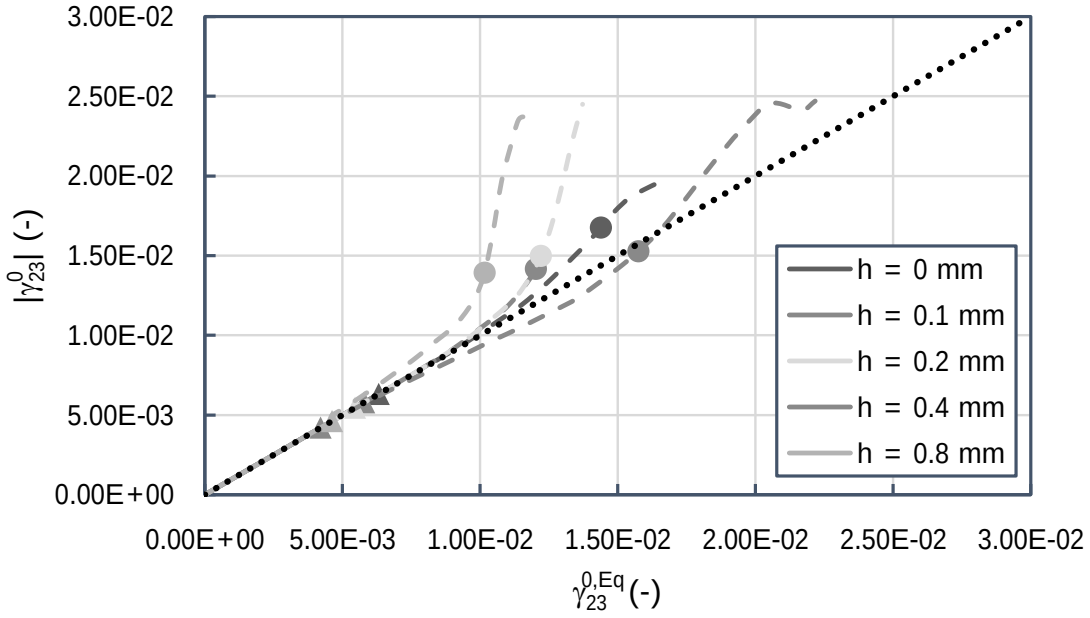

Figure 3.10: Comparison between the equivalent transverse shear strain ($\gamma_{23}^{0,Eq}$) and the homogenised transverse shear strain ($|\gamma_{23}^{0}|$). The triangular markers represent damage initiation, while the circular markers represent complete damage penetration through the thickness.

3.3 Model execution definitions

3.3.1 Introduction

The purpose of simulating a quasi-static response of a composite material through an explicit dynamic analysis performed in ABAQUS®/Explicit requires special considerations and model execution definitions. These special considerations are briefly described in the next sections.

3.3.2 Quasi-static analysis with ABAQUS®/Explicit

The explicit solution method is a true dynamic procedure originally developed to model high-speed impact phenomenona in which inertia plays a dominant role in the solution. Out-of-balance forces are propagated as stress waves between neighboring elements while solving for a state of dynamic equilibrium. Since the minimum stable time increment is usually quite small, most problems require a large number of increments [106].

Because a static solution is, by definition, a stationary solution, it is often computationally impractical to simulate an event in its natural time scale, as this would require an excessive number of small time increments. In order to obtain a computationally economical solution, the event must be accelerated in some way. The problem is that as the event is accelerated, the state of static equilibrium evolves into a state of dynamic equilibrium in which inertial forces become more dominant, thus it is not considered a quasi-static analysis. The goal is to model the process in the shortest time period in which inertial forces remain negligible.

3.3.3 Energy balance

The most effective means of evaluating whether or not a simulation is producing an appropriate quasi-static response involves studying the various model energies. The energy balance equation in ABAQUS®/Explicit can be written as [106]:

$$E_I + E_V + E_{FD} + E_{KE} + E_{IHE} - E_W - E_{PW} - E_{CW} - E_{MW} - E_{HF} = E_{total} \quad (3.4)$$

where E_I is the internal energy, E_V is the viscous energy dissipated, E_{FD} is the frictional energy dissipated, E_{KE} is the kinetic energy, E_{IHE} is the internal heat energy, E_W is the work done by the externally applied loads, and E_{PW}, E_{CW}, and E_{MW} are the work done by contact penalties, by constraint penalties, and by propelling added masses, respectively. E_{HF} is the external heat energy through external fluxes. The sum of those energy components is E_{total}, which should remain constant throughout the analysis.

If a simulation is quasi-static, the work applied by the external forces is nearly equal to the internal energy of the system, which is directly related with the deformation component of the model considered. The viscously dissipated energy is generally small unless viscoelastic materials, discrete dashpots, or material damping are used, which is not the case of the present FE models. By a proper definition of the model parameters, in terms of step time and velocity applied, the inertial forces should remain negligible in a quasi-static analysis. The corollary to both of these conditions is that the kinetic energy, which reflects the dynamic component of the model considered, is also small [106]. Thus, in a linear-elastic regime of the composite material, a possible way to identify a quasi-static

response from the FE model is to compare the kinetic energy of the deforming material with the internal energy, and ensure that the first is at least one order of magnitude lower than the second throughout most of the process [106].

Therefore, during the definition of the current FE model, a specific choice of the step time and velocity is employed to ensure a quasi-static response of the composite material.

Figure 3.11 shows the internal and kinetic energy evolutions throughout a representative analysis. As in the homogenised stress-strain curves (see Figure 3.7), after damage initiation, the curves are plotted in dashed line. These curves are plotted only until damage has penetrated completely through the thickness of the 90° layer. As observed, the kinetic energy is at least one order of magnitude lower than the internal energy. This means that, throughout this representative analysis, the inertial forces and dynamic phenomena remain negligible, leading to a quasi-static simulation. This energy balance between the kinetic and internal energies was verified in all micro-mechanical analyses performed in this work.

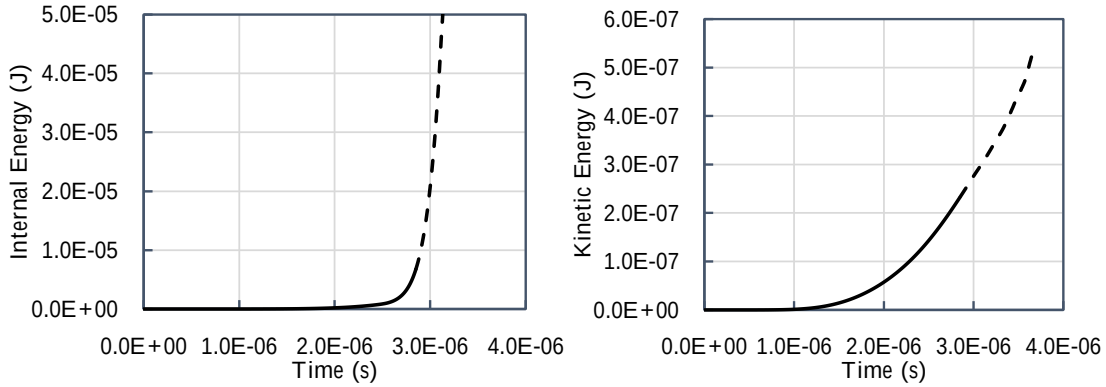

(a) Internal energy (b) Kinetic energy

Figure 3.11: Internal and kinetic energies of a representative FE analysis.

3.3.4 Mass scaling

Introduction

For dynamic analyses, time integration can be carried out in explicit or implicit methods. Explicit time integration in FE analysis is particularly suitable for simulations involving complex nonlinear phenomena that cause severe convergence problems. To numerically implement a formally explicit integration, one must use a diagonal lumped mass matrix in which the equations of motion are decoupled, and integrated using the explicit central-difference integration rule [106; 129; 130]. This integration method leads to lower required memory and minimal time per step time increment because the size of the step time increment needed to solve the transients is often of the same order of magnitude as the critical step time increment imposed by the conditional stability of the explicit central-difference integration rule [129; 130]. The drawback is that this integration method is only conditionally stable, thus the step time increment adopted must be smaller than the so-called critical threshold step time increment, in order to avoid numerical instabilities [106; 129–133]. Therefore, runtime on a transient dynamic model is not only function of the model size but also of the step time.

In ABAQUS®/Explicit the step time increment is internally calculated to provide a stable solution and to accurately predict the propagation of the highest frequency waves along the model. Accordingly, in the explicit central-difference time integration approach, the stability limit for the operator in an undamped case is given, in terms of the highest frequency of the system, as [106; 129; 130; 134]:

$$\Delta t \leq \frac{2}{\omega_{max}} \tag{3.5}$$

where ω_{max} is the maximum eigenfrequency of the assembled mesh. One can also show that [106; 134]:

$$\omega_{max} \leq \omega_{max}^{e} \tag{3.6}$$

where ω_{max}^{e} is the highest eigenfrequency of an individual element in the mesh. A physical interpretation of the stability limit can be obtained from the Courant, Friedrichs and Lewy condition, which denotes that the step time increment must be smaller than the time required by a dilatational stress wave to traverse the smallest element of the mesh, i.e. [106; 134]:

$$\Delta t \leq \frac{L_{min}}{c_d} \tag{3.7}$$

where L_{min} is the element smallest geometric dimension (element characteristic length), and c_d is the dilatational wave speed in the element, which can be written as [106; 134]:

$$c_d = \sqrt{\frac{\lambda + 2\mu}{\rho}} \tag{3.8}$$

where λ and μ are the Lamé constants and ρ is the mass density, both quantities function of the material considered [106; 134].

One approach commonly used in the literature [106; 131–135] to ensure reasonable simulation time in explicit dynamic analyses is to increase the critical step time increment in a heuristic manner called mass scaling. This technique can improve the computational efficiency of explicit dynamic analyses by adjusting (increasing) the mass density to reach higher stable time increments, which is reflected on the CPU time [106; 135]. However, mass scaling is not recommended for models representing high-speed phenomena as, in those cases, inertial forces play a significant role. Because the purpose of the present work is to simulate a quasi-static response of the composite material, the only restriction when applying this technique is related to ensuring the kinetic and internal energy balance described in Section 3.3.3.

Implementation

In the literature [106; 131–134], two different methods can be found to apply mass scaling on a FE model in ABAQUS®/Explicit. The simplest mass scaling approach consists of a uniform increase of the material density, which means that this technique is not mass-conservative. Furthermore, this increase equally affects all structural eigenmodes and therefore leads to unacceptable inaccuracies in most cases. This method is designated as fixed mass scaling, and has been reported as satisfactory for relatively slow forming processes. However, more accurate approaches can be pursued considering that individual

FEs contribute to the lowest structural eigenmodes mainly with the inertia associated to their rigid body modes [134].

A more accurate approach is to add to the mass matrix a non-diagonal matrix with net zero mass. This method is mass-conservative and selectively reduces the highest structural eigenfrequencies, with little or zero modifications of the lowest ones, keeping the eigenmodes unchanged [131–134]. Due to the fact that this method affects mainly the higher eigenfrequency, it is more suitable for dynamic analyses.

Since the critical step time increment is limited by the highest eigenfrequency of the system, it would be preferable to target the mass scaling to the upper eigenfrequency domain which generally only contains small accounts of kinetic energy. The lower eigenfrequency domain should remain as unaffected as possible [131; 133]. This method is designated as selective mass scaling, as it only increases the density in the smallest elements which control the critical step time increment. Within the selective mass scaling method, there are two ways to scaling the mass, uniformly, in which all the elements specified are scaled uniformly by a single mass scaling factor automatically defined by ABAQUS®/Explicit, or user selective, i.e., elements are mass scaled element by element, by a certain stable time increment below a user-specified value. The latter is the most appropriate for quasi-static simulations [106].

Because in this work the CMM analyses are performed as explicit dynamic analyses, the most suitable method to apply mass scaling in the present FE model is to apply the method referred as selective mass scaling. Accordingly, variable mass scaling was applied element by element, by defining a minimum stable time increment of 1×10^{-12} s.

Discussion

Figure 3.12 shows the internal and kinetic energy evolutions throughout a representative analysis, after implementing mass scaling on the FE model. Again, after damage initiation, the curves are plotted in dashed line and limited to the period until penetration of the first matrix crack. It can be noted that, after implementing mass scaling in the FE model, the kinetic energy remained, at least, one order of magnitude lower than the internal energy. Thus, mass scaling did not affect the energy balance, leading to a quasi-static response of the composite material. Furthermore, in all micro-mechanical analyses performed in this work, the maximum value of mass percentage changed registered was 4.95%, which had no effect on the present micro-mechanical model.

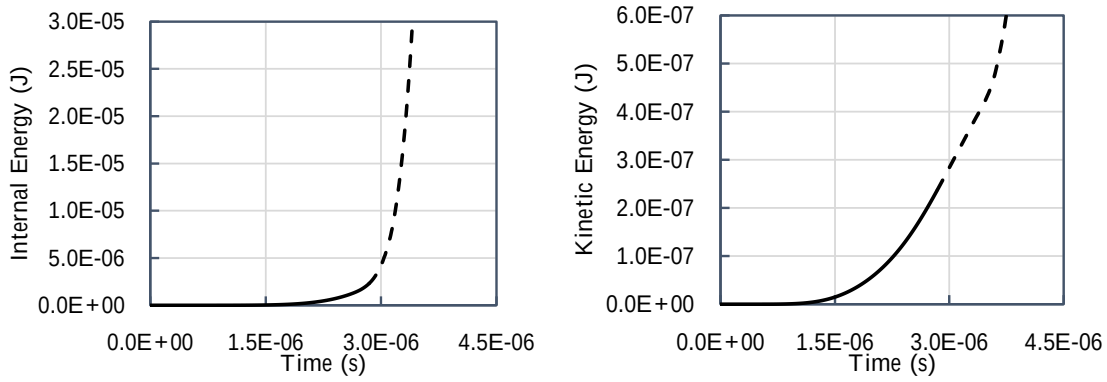

(a) Internal energy

(b) Kinetic energy

Figure 3.12: Internal and kinetic energies after implementing mass scaling on a representative analysis.

Chapter 4

Micro-mechanical analysis of ply damage under transverse shear stress. Numerical results

In this chapter, the numerical results concerning the micro-mechanical analyses performed in this research are presented. The 3D CMM framework is able to accurately represent the micro-mechanical response of ultra-thin plies, including (i) the mechanics of transverse shear cracking onset and propagation, (ii) a consistent orientation of the fracture plane of the 90° lamina, (iii) the constraining effect observed in the laminae embedded in multidirectional laminates, (iv) the gradual, slow stress relaxation and progressive transverse cracking observed in very thin plies, and consequent increase of the crack density, and (v) an *in-situ* effect.

4.1 Mechanics of transverse shear cracking

Figures 4.1 to 4.5 show the contour plots of the matrix damage variable (SDV3) on representative RVEs of 90° laminae with thicknesses ranging between 0.020 mm to 0.140 mm for different values of $\gamma_{23}^{0,\mathrm{El}}$. Only sublaminates with 0° outer plies are considered. Although only one random distribution of fibres is presented for each case, it is representative of other random distributions in terms of damage localisation and propagation.

Similarly to what was observed experimentally from *in-situ* observations [51], and reported from an analytical perspective [48], the mechanics of transverse shear cracking can be describred as follows:

- Apparently, damage localisation does not occur for the same instant of applied $\gamma_{23}^{0,\mathrm{El}}$. Figures 4.1a to 4.5a reflect this fact, as the instant of applied $\gamma_{23}^{0,\mathrm{El}}$ varies for the different 90° laminae thicknesses. This becomes even more apparent observing the numerical results presented as RVE homogenised stress-strain response (please refer to Section 4.4).

- Damage starts in the narrower portions of matrix between the closest adjacent fibres, whose center is not aligned with the loading direction. Damage onset is identified by the emmergence of matrix micro-cracks oriented at approximately 45° with the thickness of the RVE (z-direction), i.e., as Olson et al. [48] proposed, in multidirectional laminates, matrix transverse shear micro-cracks typically appear as inclined mode I transverse shear cusps — see Figures 4.1b to 4.5b.

- Following damage onset, these matrix transverse shear micro-cracks grow, and join with multiple shear micro-cracks present within the ply, propagating throughout the ply thickness along an oblique pattern — see Figures 4.1c to 4.5c. In Section 4.2, this oblique pattern of crack propagation is numerically quantified by a comprehensive analysis concerning the orientation of the fracture plane of the RVE corresponding to the embedded 90° lamina.

- The propagation of matrix cracks through the ply thickness, leads to crack penetration through the ply — see Figures 4.1d to 4.5d.

- Lastly, the propagation of matrix cracks through the ply thickness causes delaminations, following the experimental *in-situ* observations performed by García-Rodriguez et al. [51] and the analytical scenario proposed by Olsson [48]. Due to the randomness of reinforcements in the RVE, these delaminations are not symmetric — see Figures 4.1e to 4.5e.

Arteiro et al. [15], in their CMM analyses of the *in-situ* effect under transverse tensile loading observed that, for the thicker 90° plies, once a transverse crack is formed, it rapidly penetrates through the thickness. This fact was also observed in the present simulations, as shown in Figures 4.4 and 4.5 for more conventional transverse ply thicknesses. However, it should be noted that due to the enormous computational cost of these models, the sublaminate RVEs with transverse ply thicknesses (z-direction) above or equal to 0.100 mm were modelled to accommodate at least a single transverse crack, with a reduction of the total width (y-direction) of the RVEs when compared to the thin-ply sublaminate RVEs. Though, from the present micro-mechanical analyses, it can be concluded that the width of the sublaminate RVEs for the conventional transverse ply thicknesses adopted in the present CMM model was not enough to accomodate at least a single transvere shear crack, because its oblique pattern leads to a transverse shear crack larger than the width (y-direction) of the RVE — see Figures 4.4e and 4.5e. Nevertheless, even though the models for the thicker RVEs shown in Figures 4.4 and 4.5 may not be completely representative in terms of damage progression after full extension of the first transverse shear crack, they are useful in showing the differences between the thin-ply and conventional ply sublaminates in terms of damage evolution in a first stage of the transverse shear crack propagation.

(a) $\gamma_{23}^{0,\mathrm{Eq}}$ of 0.63%.

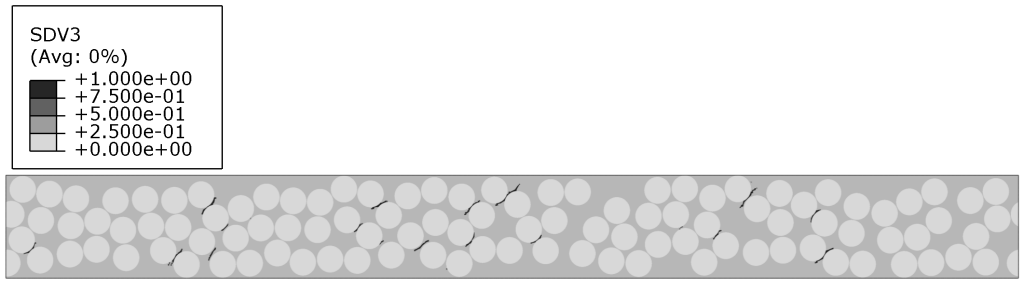

(b) $\gamma_{23}^{0,\mathrm{Eq}}$ of 1.02%.

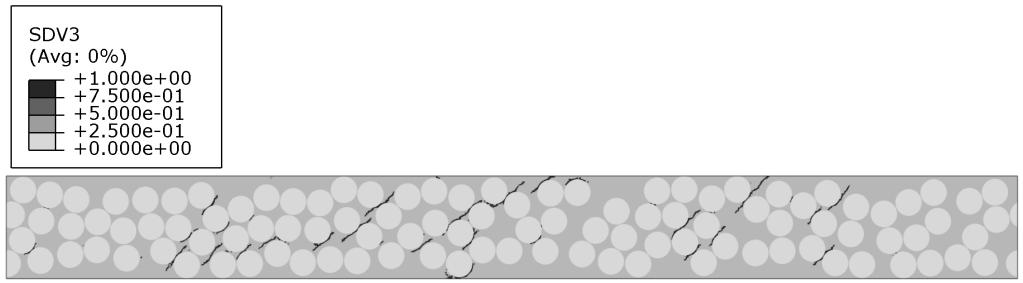

(c) $\gamma_{23}^{0,\mathrm{Eq}}$ of 1.20%.

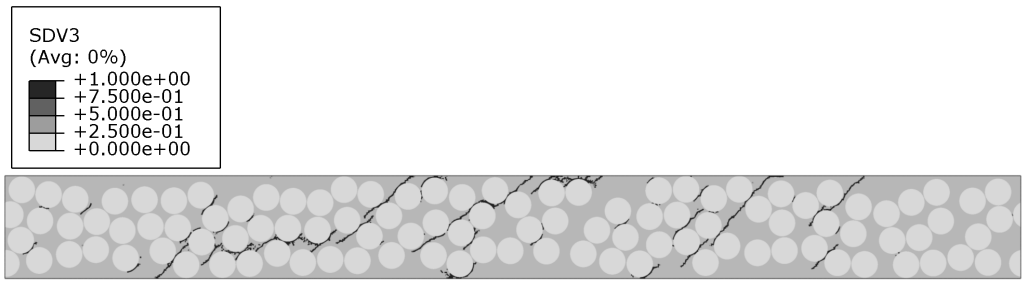

(d) $\gamma_{23}^{0,\mathrm{Eq}}$ of 1.29%.

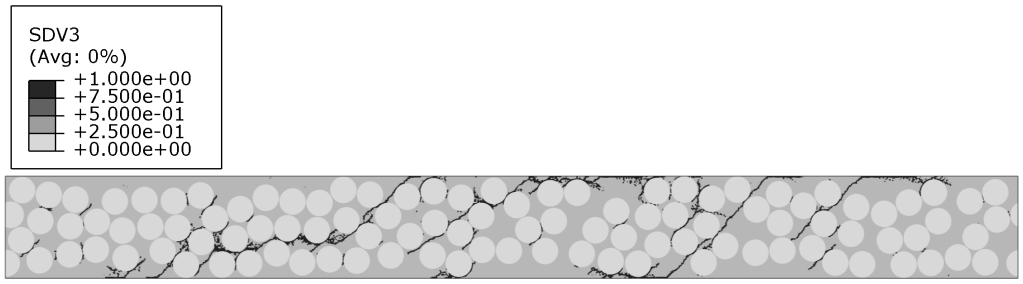

(e) $\gamma_{23}^{0,\mathrm{Eq}}$ of 1.49%.

Figure 4.1: Contour plots of the matrix damage variable (SDV3) on an RVE of a 0.020 mm thick 90° lamina of a sublaminate with 0° outer plies (only the 90° lamina is presented).

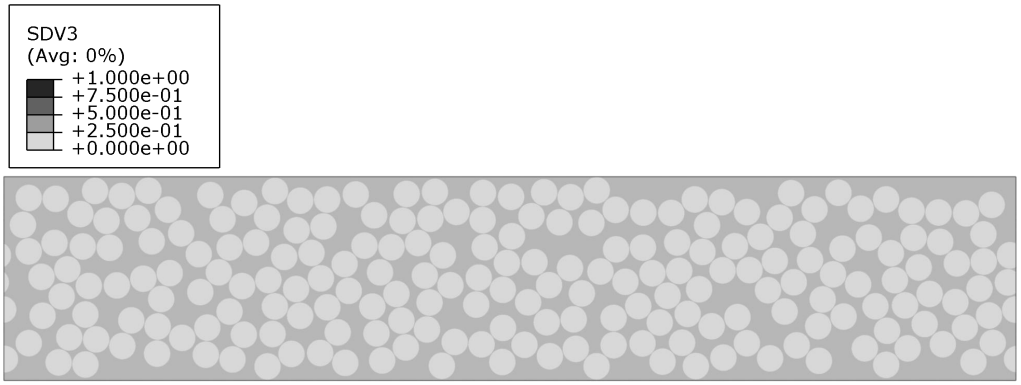

(a) $\gamma_{23}^{0,\mathrm{Eq}}$ of 0.52%.

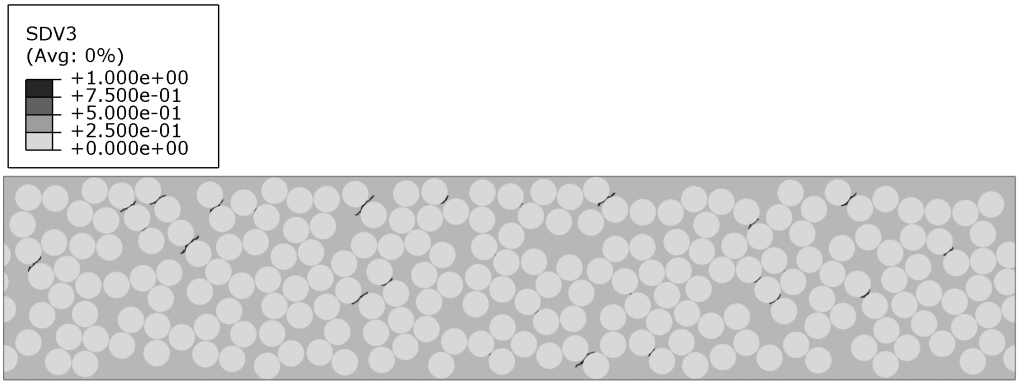

(b) $\gamma_{23}^{0,\mathrm{Eq}}$ of 0.92%.

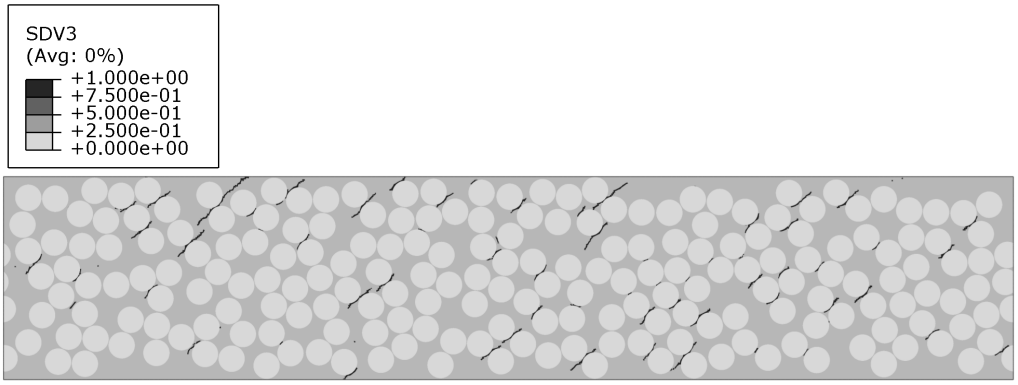

(c) $\gamma_{23}^{0,\mathrm{Eq}}$ of 1.12%.

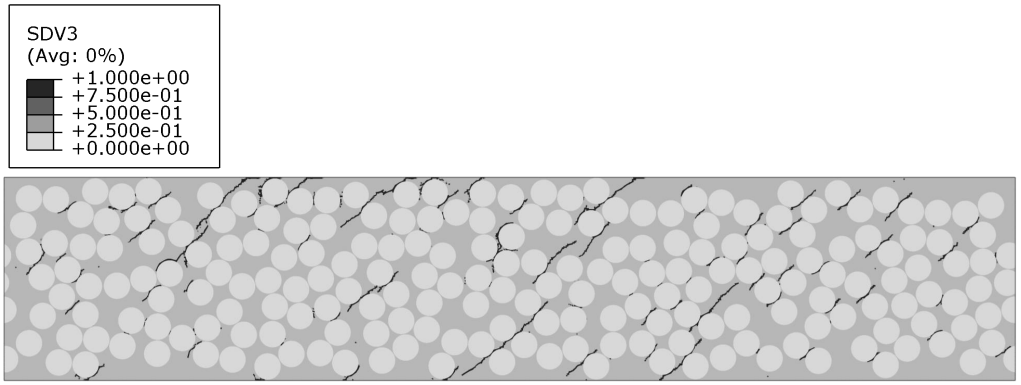

(d) $\gamma_{23}^{0,\mathrm{Eq}}$ of 1.25%.

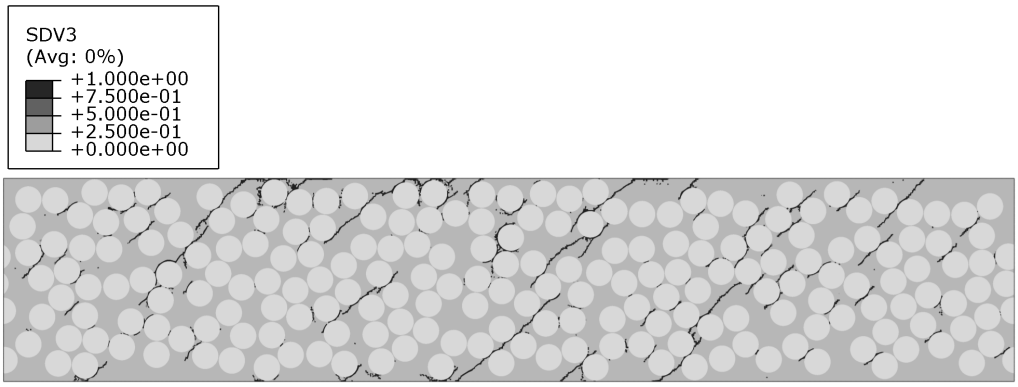

(e) $\gamma_{23}^{0,\mathrm{Eq}}$ of 1.33%.

Figure 4.2: Contour plots of the matrix damage variable (SDV3) on an RVE of a 0.040 mm thick 90° lamina of a sublaminate with 0° outer plies (only the 90° lamina is presented).

(a) $\gamma_{23}^{0,\mathrm{Eq}}$ of 0.44%.

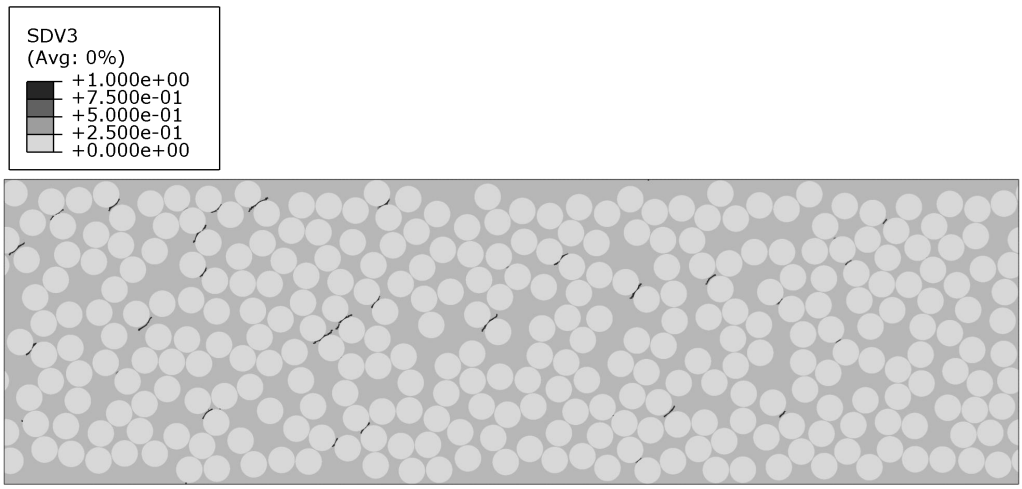

(b) $\gamma_{23}^{0,\mathrm{Eq}}$ of 0.92%.

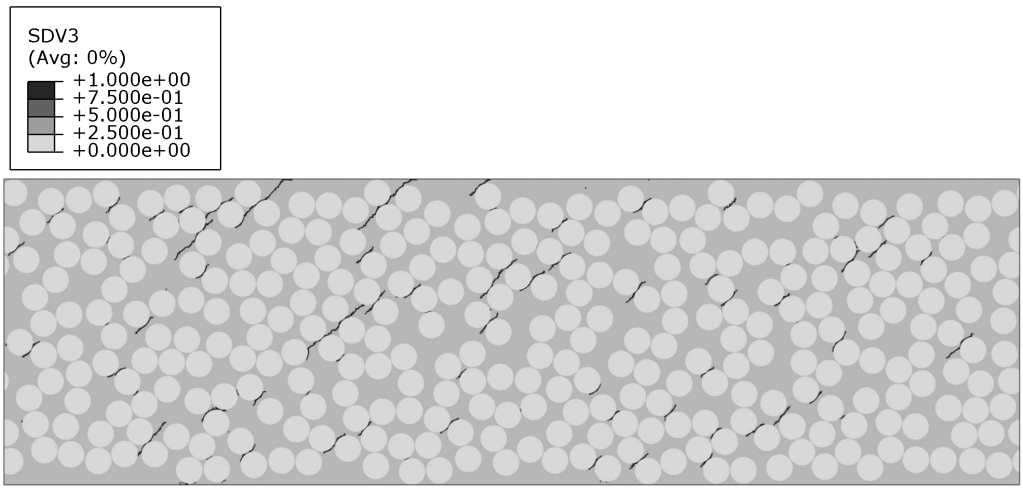

(c) $\gamma_{23}^{0,\mathrm{Eq}}$ of 1.08%.

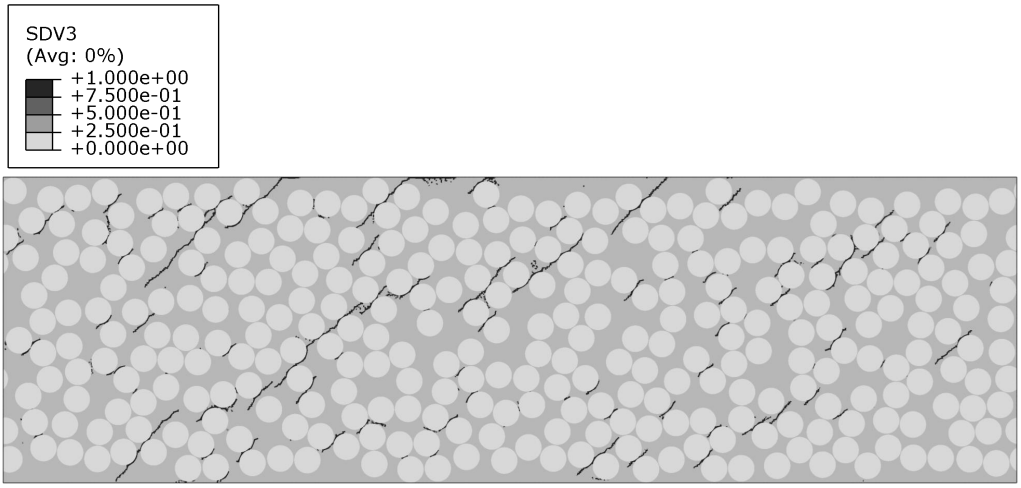

(d) $\gamma_{23}^{0,\mathrm{Eq}}$ of 1.24%.

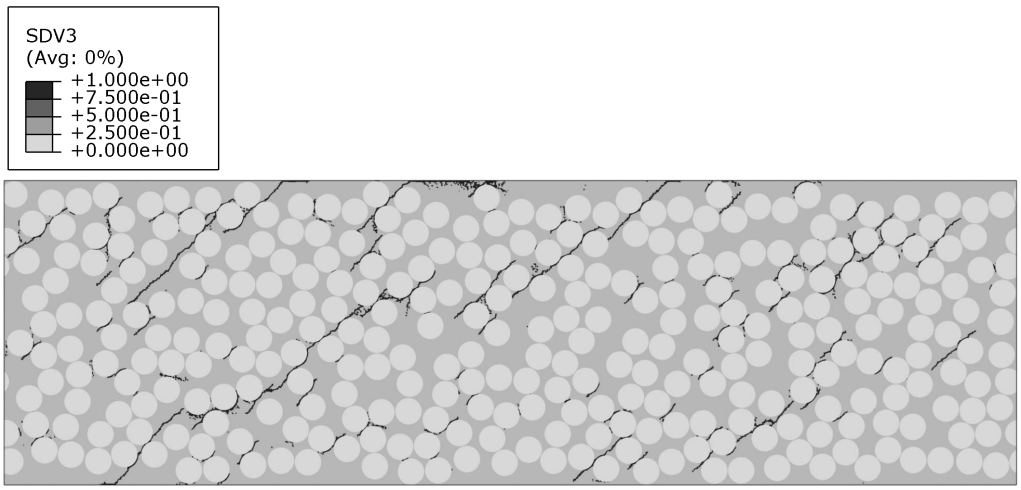

(e) $\gamma_{23}^{0,\mathrm{Eq}}$ of 1.28%.

Figure 4.3: Contour plots of the matrix damage variable (SDV3) on an RVE of a 0.060 mm thick 90° lamina of a sublaminate with 0° outer plies (only the 90° lamina is presented).

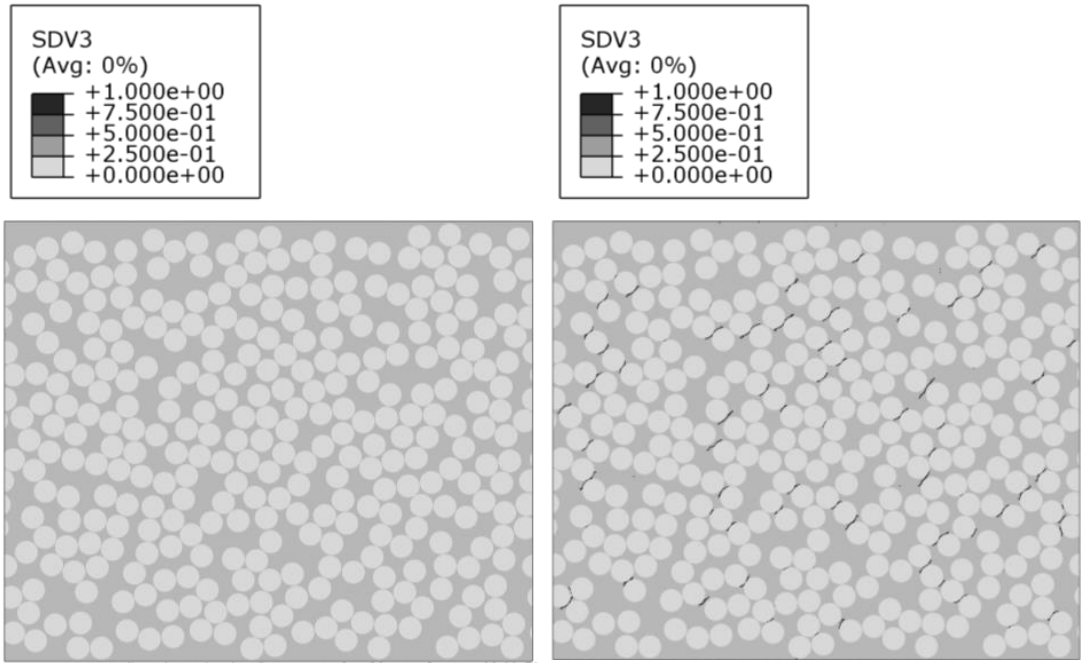

(a) $\gamma_{23}^{0,\mathrm{Eq}}$ of 0.58%. (b) $\gamma_{23}^{0,\mathrm{Eq}}$ of 0.88%.

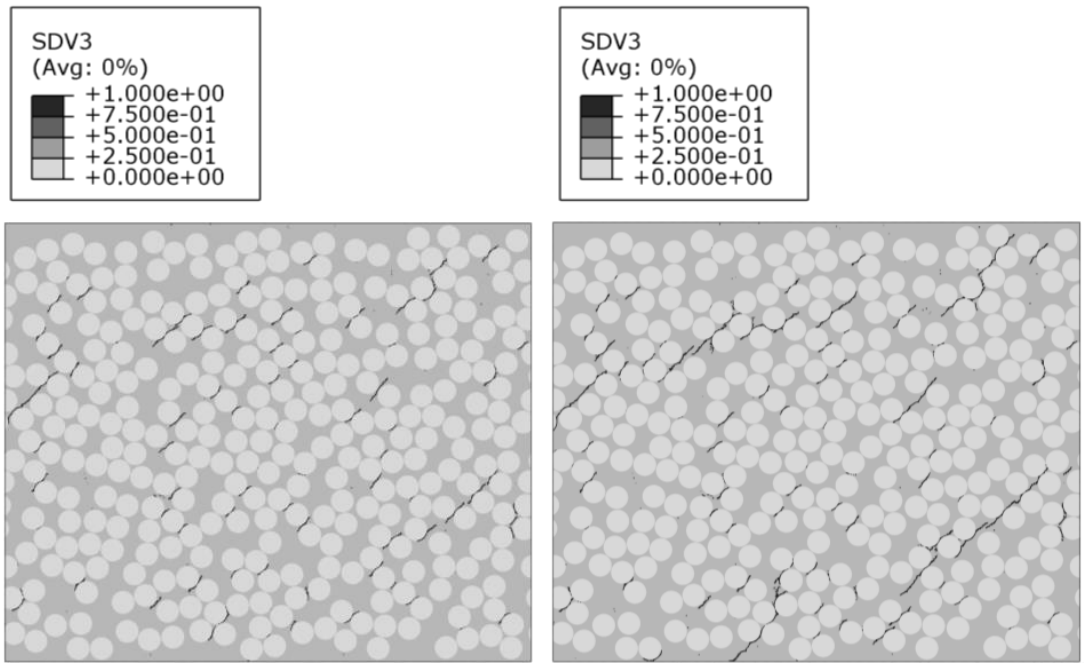

(c) $\gamma_{23}^{0,\mathrm{Eq}}$ of 0.95%. (d) $\gamma_{23}^{0,\mathrm{Eq}}$ of 1.02%.

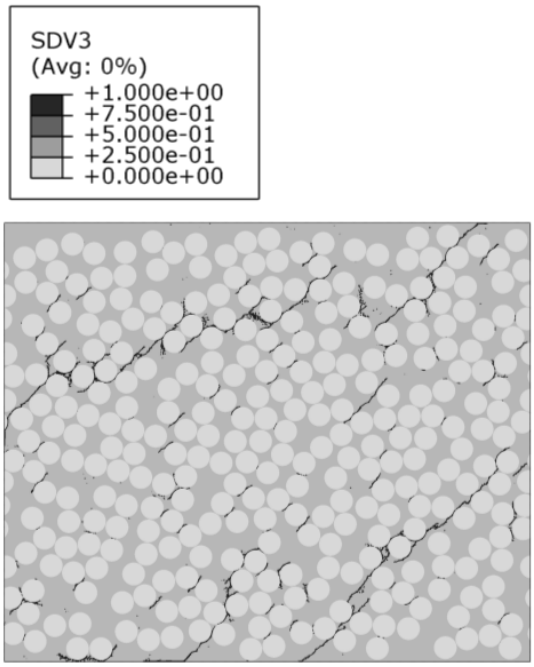

(e) $\gamma_{23}^{0,\mathrm{Eq}}$ of 1.18%.

Figure 4.4: Contour plots of the matrix damage variable (SDV3) on an RVE of a 0.100 mm thick 90° lamina of a sublaminate with 0° outer plies (only the 90° lamina is presented).

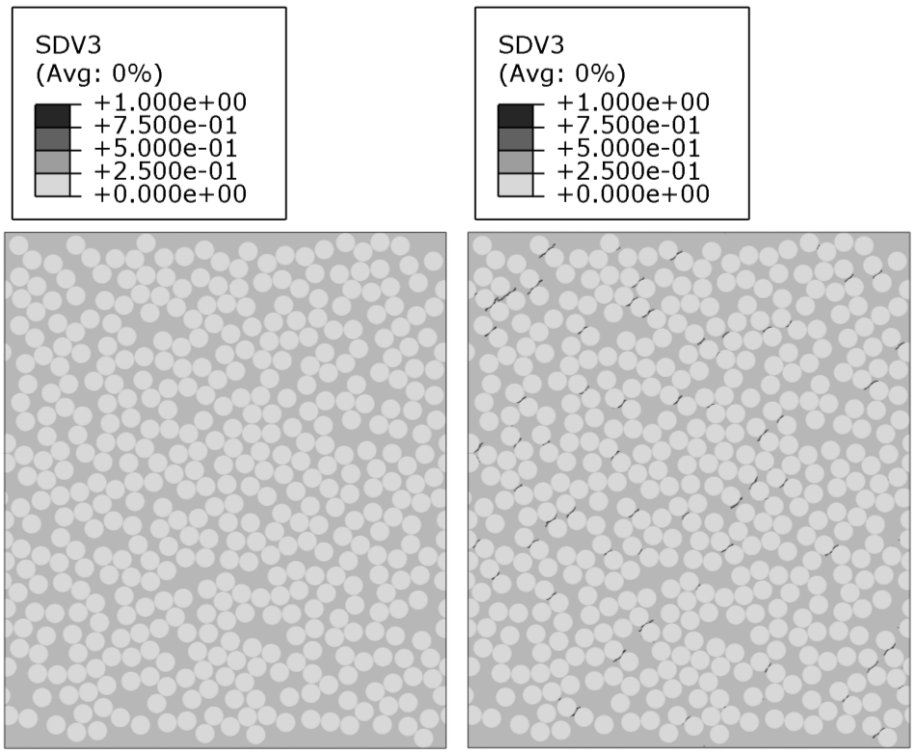

(a) $\gamma_{23}^{0,\mathrm{El}}$ of 0.52%.

(b) $\gamma_{23}^{0,\mathrm{Eq}}$ of 0.74%.

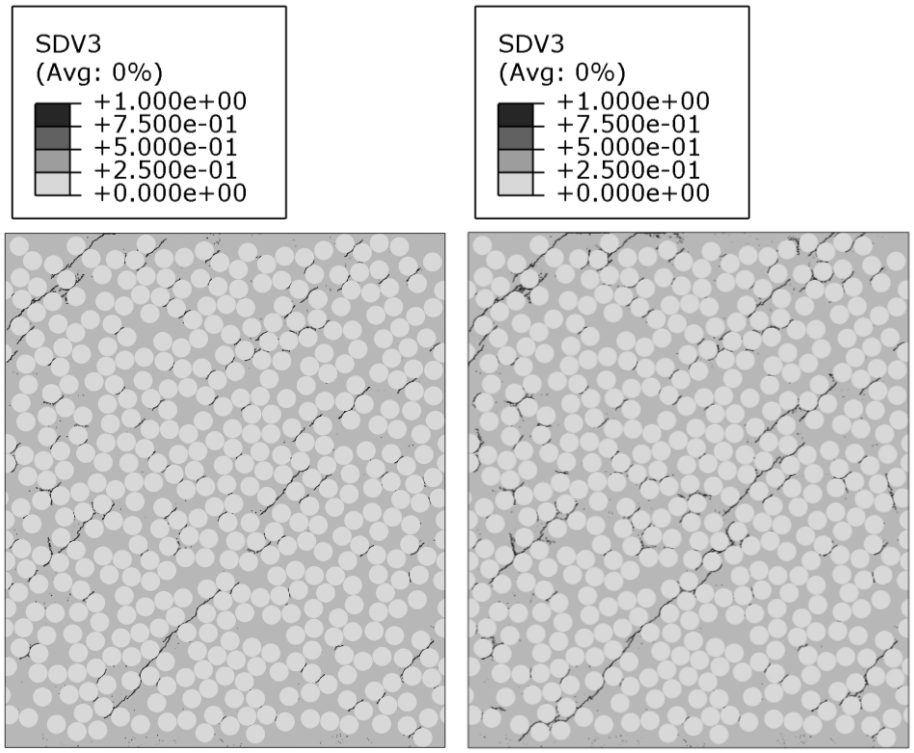

(c) $\gamma_{23}^{0,\mathrm{Eq}}$ of 0.87%. (d) $\gamma_{23}^{0,\mathrm{Eq}}$ of 0.94%.

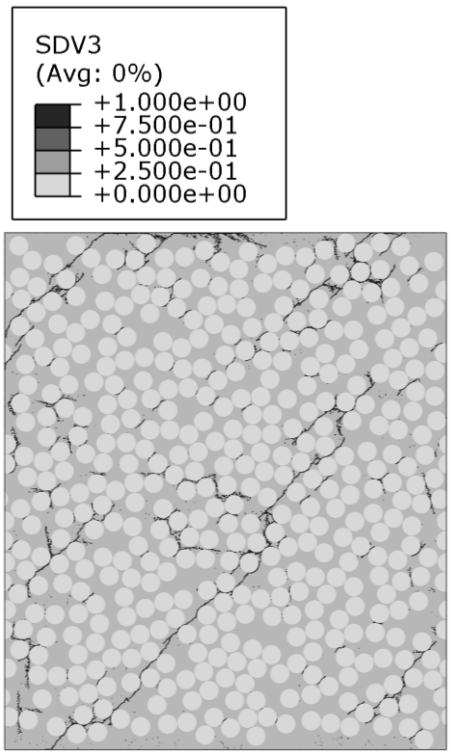

(e) $\gamma_{23}^{0,\mathrm{Eq}}$ of 1.08%.

Figure 4.5: Contour plots of the matrix damage variable (SDV3) on an RVE of a 0.140 mm thick 90° lamina of a sublaminate with 0° outer plies (only the 90° lamina is presented).

Another interesting numerical result of the CMM analyses performed by Arteiro et al. [15] was the reportedly slower crack extension with increasing applied remote strain on the sublaminate RVEs for the case of thinner transverse plies. In the numerical simulations performed in this work, the same trend is observed (compare, for example, Figures 4.1 and 4.4). This trend becomes even more clear observing the predicted normalised crack height (please refer to Section 4.3).

Naya et al. [89], in their micro-mechanical analyses of the transverse and in-plane shear behaviour of UD fibre reinforced polymers including environmental effects, reported that, apart of the environental effects, the damage process of a UD composite lamina, when subjected to a shear stress state (transverse or in-plane), is controlled by fiber-matrix interface debonding. The authors stated that after failure of the fibre-matrix interface, the matrix holds progressively shear loads and plastic band deformations are formed accumulating damage until the ultimate failure of the matrix ligaments. Particularly, when comparing the case of in-plane shear stress state with the case of transverse shear stress state, applied to the RVE, the deformation pattern after matrix yielding is different. In the latter, once interface debonding initiates, fibre rotation starts, resulting in a gradually stiffer response of the composite material. The final failure of the RVE is reproduced by the development of a transverse crack perpendicular to the loading axis [89].

In contrast to what was observed by Naya et al. [89] in their micro-mechanical analyses of an UD composite lamina subjected to a transverse shear load, from the present micro-mechanical analyses, it can be reported that, for a multidirectional composite laminate subjected to a transverse shear load, the damage sequence events are different, damage process is not controlled by fibre-matrix interface debonding. Figure 4.6 reflects this fact, and although only one thin-ply sublaminate RVE is presented, it is representative of other thin and conventional ply sublaminate RVEs employed in this research in terms of damage sequence events. By observing the damage variable (SDEG) of the cohesive elements representing the interface between fibre and matrix, it can be concluded that, although some initial fibre-matrix decohesions started to emerge, these damage event is preceded by matrix cracking, thus, it can be stated that such fibre-matrix decohesions are a result of the already existent damage in the lamina — compare Figures 4.6a and 4.6b. In a later instant further growth of fibre-matrix interface debonding is observed — see Figure 4.6c.

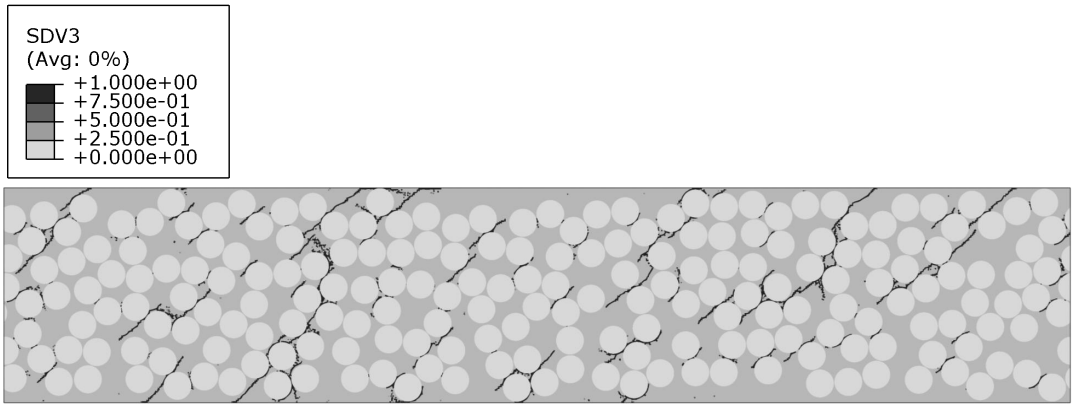

(a) Contour plot of the matrix damage variable (SDV3) in an RVE of a 0.040 mm thick 90° lamina of a sublaminate with 0° outer plies at an $\gamma_{23}^{0,\mathrm{Eq}}$ of 1.44%.

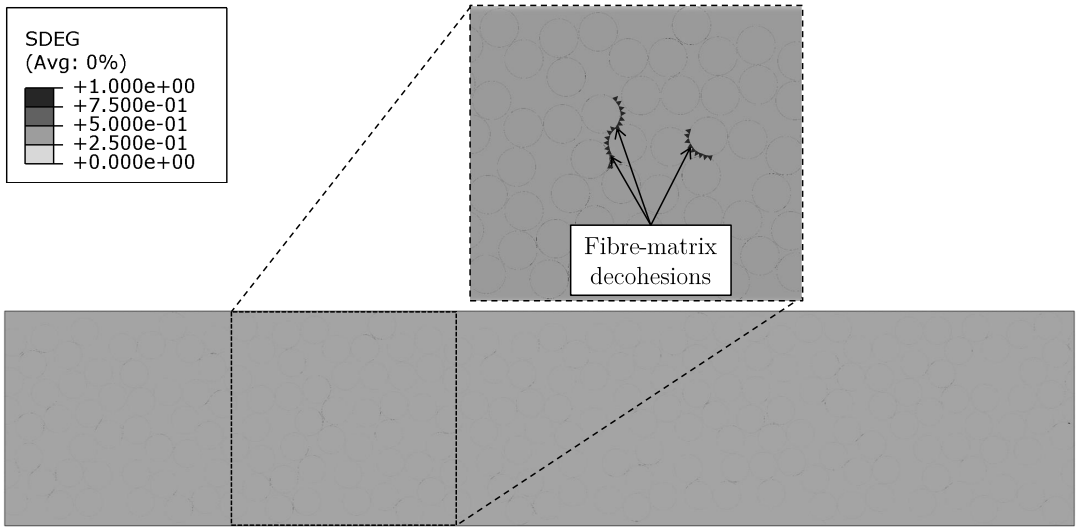

(b) Contour plot of the damage variable (SDEG) of the cohesive elements representing the interface between fibre and matrix in an RVE of a 0.040 mm thick 90° lamina of a sublaminate with 0° outer plies at an $\gamma_{23}^{0,\mathrm{Eq}}$ of 1.44%.

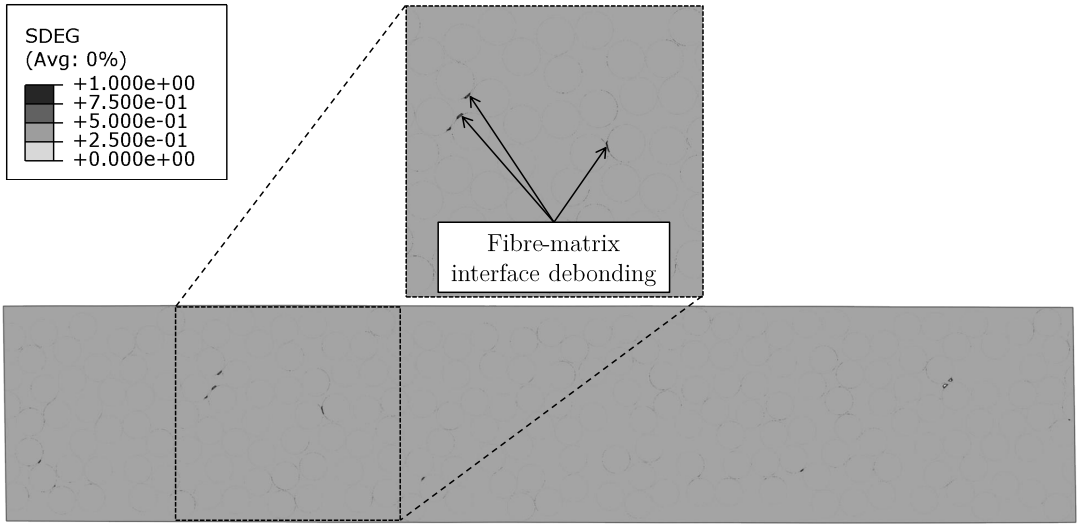

(c) Contour plot of the damage variable (SDEG) of the cohesive elements representing the interface between fibre and matrix in an RVE of a 0.040 mm thick 90° lamina of a sublaminate with 0° outer plies at an $\gamma_{23}^{0,\mathrm{Eq}}$ of 1.78%.

Figure 4.6: Schematic explanation of the sequence damage events leading to fibre-matrix interface debonding, for an RVE of a 0.040 mm thick 90° lamina of a sublaminate with 0° outer plies (only the 90° lamina is presented).

4.2 Fracture plane orientation

Another interesting finding observed from the present micro-mechanical analyses is a consistency of the orientation of the fracture plane of the embedded 90° thin lamina. As stressed before, the sublaminate RVEs with the thicker transverse plies, due to the reduced size of the RVE (along the y-direction) justified by limitations in computational power, were not completely representative in terms of damage progression until full extension of the first transverse shear crack, reason why the fracture plane orientation analysis was not conducted for those cases. The orientation of the fracture plane is determined from the first transverse shear crack that penetrates completely through the thickness of the ply.

Melro et al. [87] also performed micro-mechanical analyses of polymer composites reinforced by UD fibres, submitting different RVEs to a transverse shear stress state through the application of PBCs. The authors reported a band of localised damage along a diagonal direction, whose orientation was difficult to judge, given the observed constant swerving around the fibres. Nevertheless, it was possible to conclude that failure in the matrix occured in a plane roughly perpendicular to the maximum principal macro-stress, i.e., at approximately 45°.

In fact, the present micro-mechanical analyses confirm that failure in the matrix occurs in a plane perpendicular to the maximum principal macro-stress, at approximately 45°, as Melro et al. [87] proposed. Figures 4.7 to 4.10 show that the orientation of the fracture plane ranges between 40° and 52° for the different fibre distributions and ply thicknesses considered. Figure 4.11, which sumarises the observed results concerning the orientation of the fracture plane for the different ply thicknesses, shows that there is not an influence of the ply thickness on the orientation of the fracture plane of the embedded 90° thin lamina, and that the mean value of the observed results is 45°, in agreement with Melro et al. [87] and Camanho et al. [47].

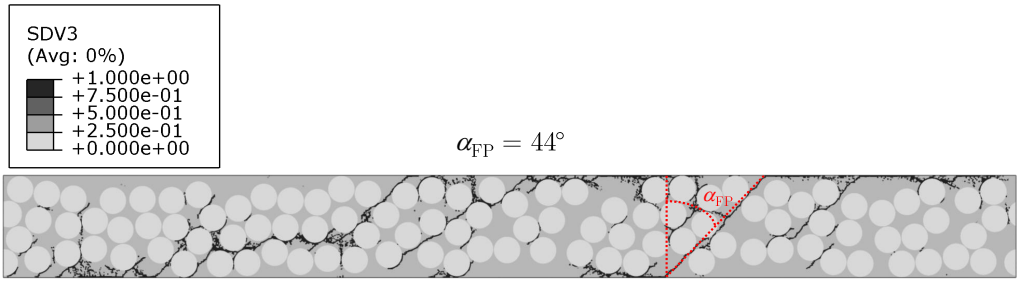

(a) DIST01

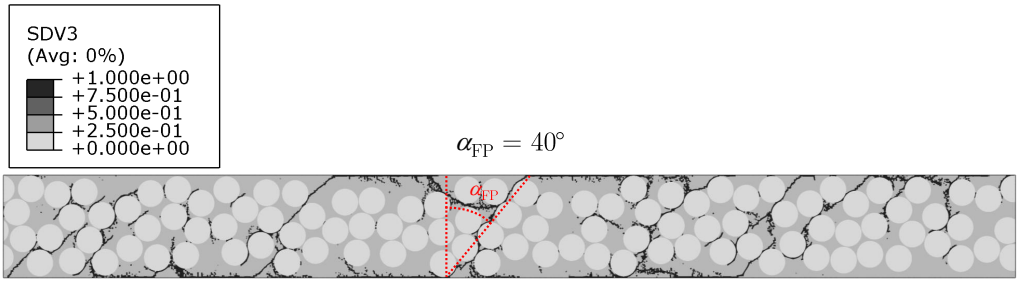

(b) DIST02

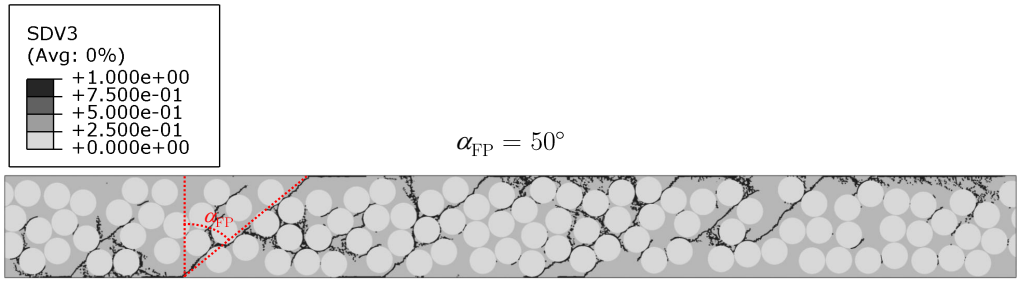

(c) DIST03

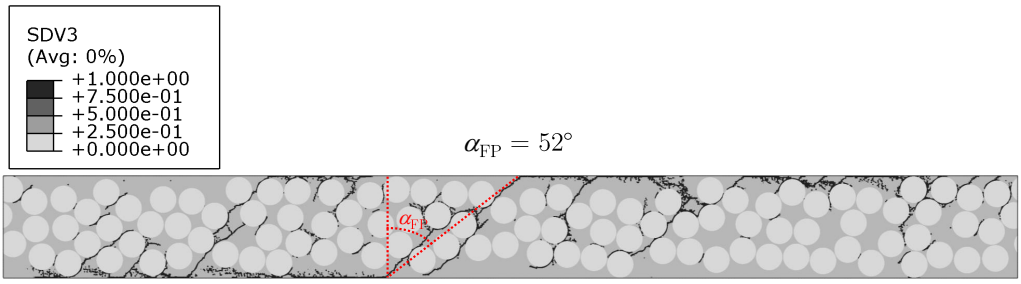

(d) DIST04

Figure 4.7: Contour plots of the matrix damage variable (SDV3) in the RVE of 0.020 mm thick 90° laminae of sublaminates with 0° outer plies (only the 90° lamina is presented), and the corresponding orientations of the fracture plane (α_{FP}) for the different fibre distributions.

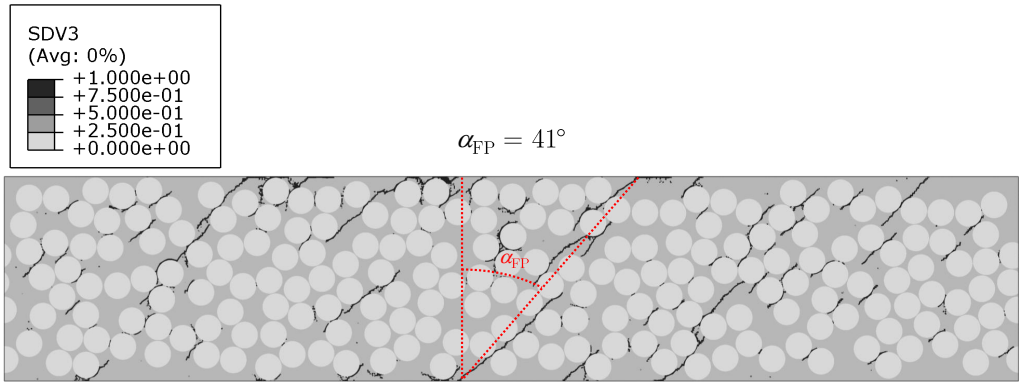

(a) DIST01

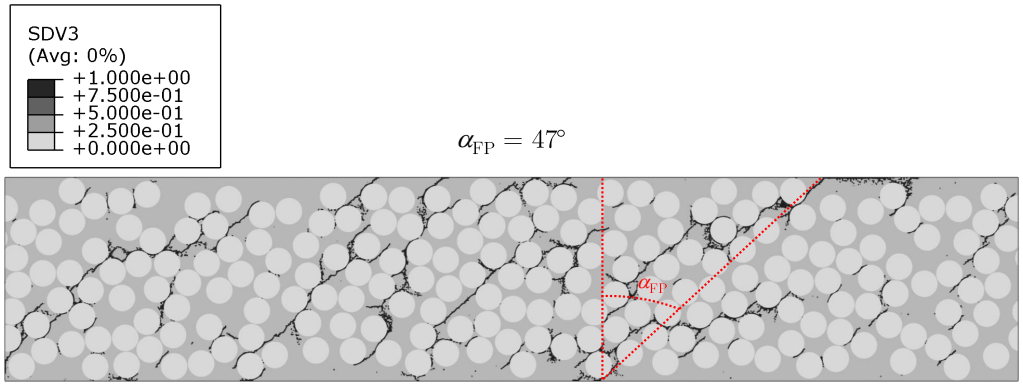

(b) DIST02

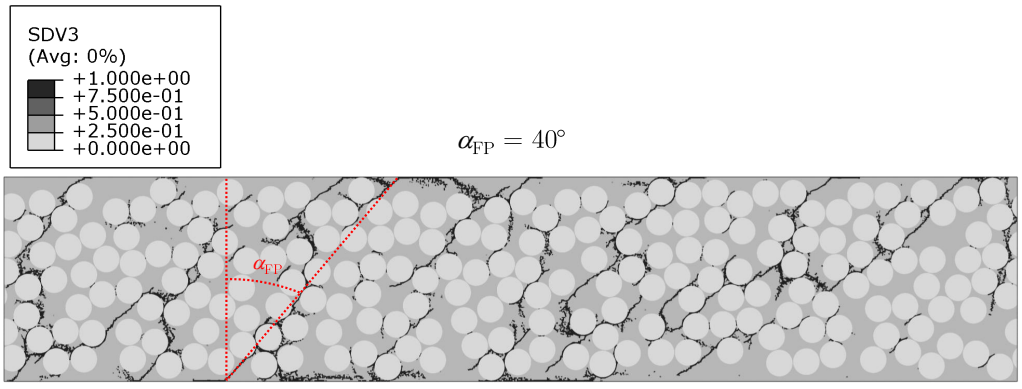

(c) DIST03

Figure 4.8: Contour plots of the matrix damage variable (SDV3) in the RVE of 0.040 mm thick 90° laminae of sublaminates with 0° outer plies (only the 90° lamina is presented), and the corresponding orientations of the fracture plane (α_{FP}) for the different fibre distributions.

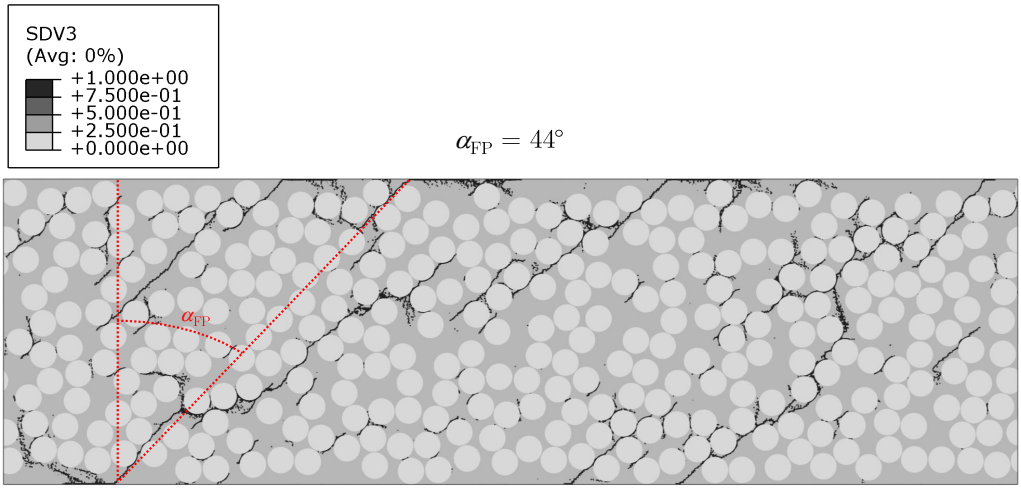

(a) DIST01

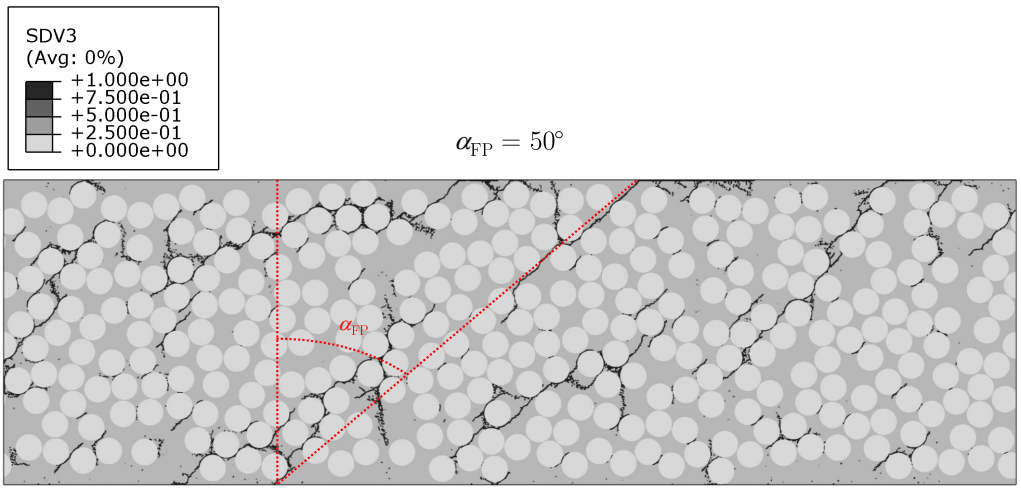

(b) DIST02

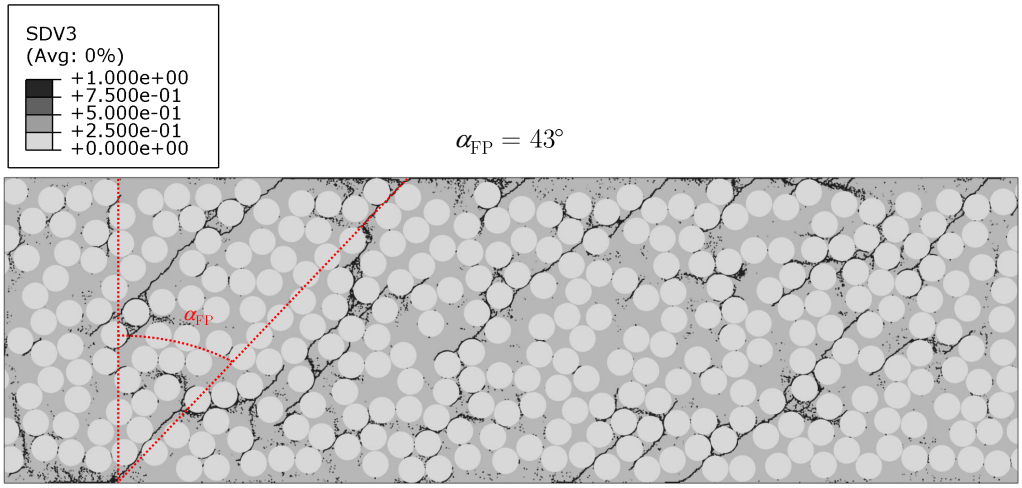

(c) DIST03

Figure 4.9: Contour plots of the matrix damage variable (SDV3) in the RVE of 0.060 mm thick 90° laminae of sublaminates with 0° outer plies (only the 90° lamina is presented), and the corresponding orientations of the fracture plane (α_{FP}) for the different fibre distributions.

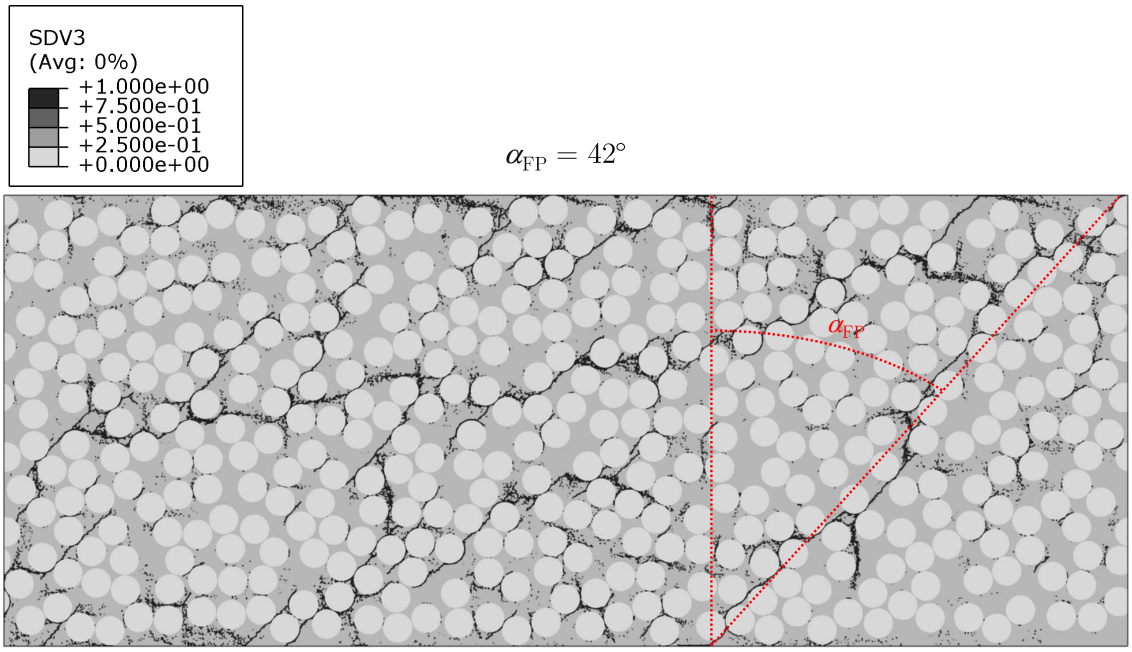

(a) DIST01

Figure 4.10: Contour plot of the matrix damage variable (SDV3) in an RVE of 0.080 mm thick 90° lamina of a sublaminate with 0° outer plies (only the 90° lamina is presented), and the corresponding orientation of the fracture plane (α_{FP}).

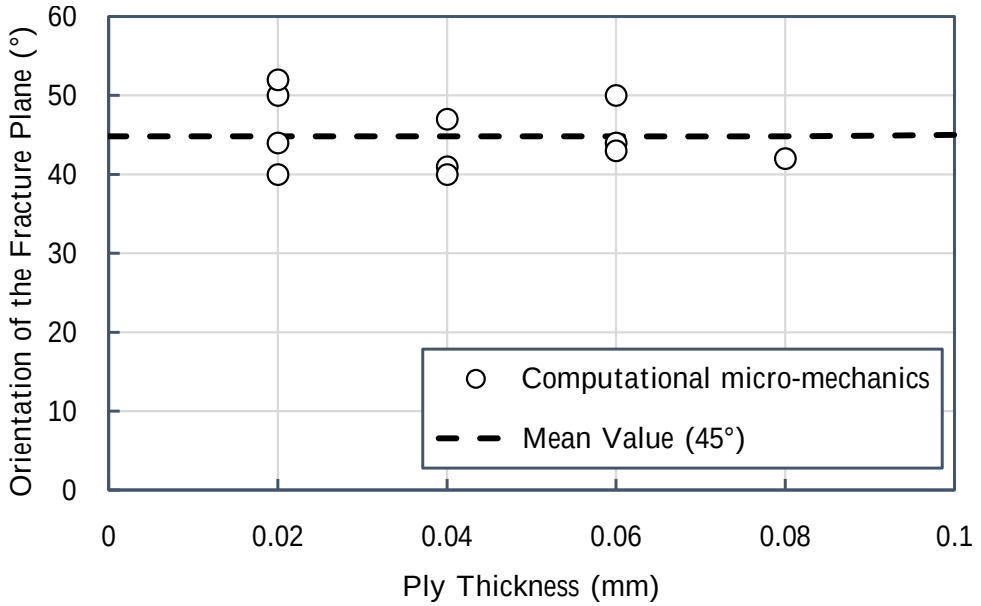

Figure 4.11: Orientation of the fracture plane (α_{FP}) as a function of the ply thickness.

4.3 Normalised crack height

To assess the effect of ply thickness on the transverse shear crack suppression, a normalised crack height was determined by the quotient between the height of the transverse crack, h_c, and thickness of the 90° ply, b, for increasing $\gamma_{23}^{0,\mathrm{Eq}}$. The height of the transverse crack, h_c, was obtained by the deformed distance (along the z-direction) between the nodes in the tips of the longer transverse crack in the RVE, as Figure 4.12 indicates. To further assess the effect of the 90° ply thickness on crack extension, the different fibre distributions of the RVEs with 0.020 mm, 0.060 mm, 0.100 mm, and 0.120 mm thick transverse plies are considered in this numerical analysis.

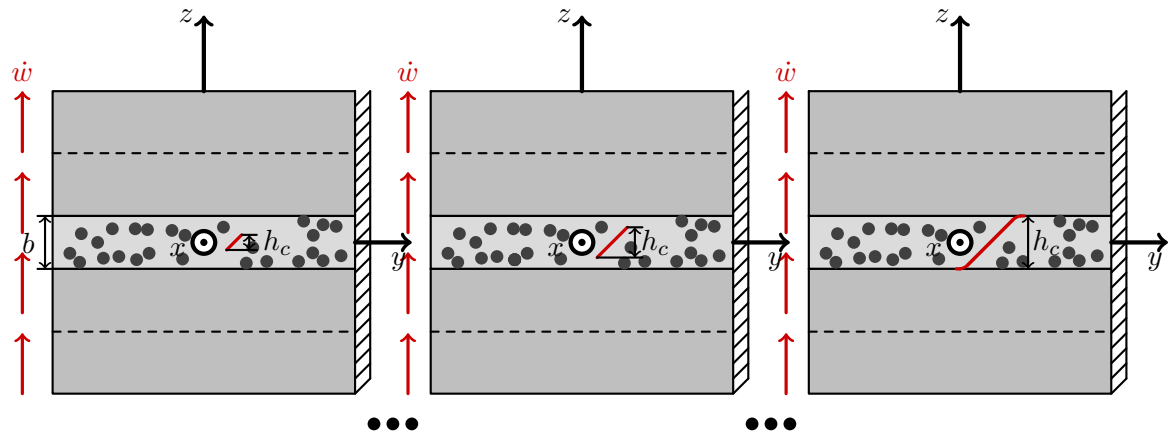

Figure 4.12: Schematic explanation of the normalised crack height definition.

Figure 4.13 shows the numerical results concerning the normalised crack height as a function of $\gamma_{23}^{0,\mathrm{Eq}}$ for the different sublaminates analysed. As can be observed, in the case

of the thinner transverse plies (0.020 mm and 0.060 mm), damage initiation and through-thickness crack penetration, occurs at a lower rate. In the case of the conventional transverse plies (0.100 mm and 0.120 mm), crack extension is much faster. By the observation of this behaviour, it is possible to conclude that, as the ply thickness decreases, crack extension reportedly slows down with increasing $\gamma_{23}^{0,Eq}$. This result is similar to what was observed previously by Arteiro et al. [15] in the case of transverse tensile loading. These results also confirm the existence of a constraining effect on the 90° laminae embedded in multidirectional laminates. This constraining effect can be attributed to the existence of an *in-situ* effect in transverse shear.

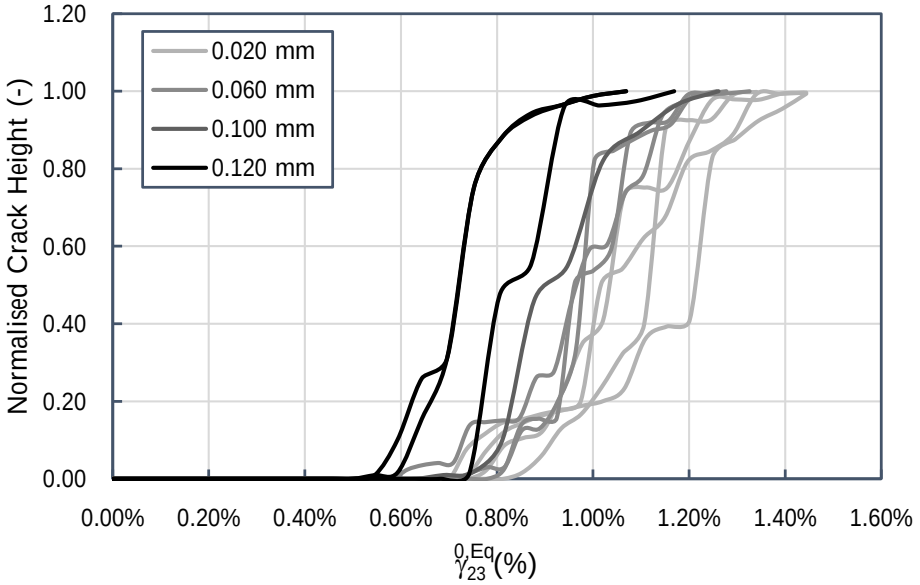

Figure 4.13: Normalised crack height as a function of $\gamma_{23}^{0,Eq}$ for sublaminate RVEs with 0.020 mm, 0.060 mm, 0.100 mm and 0.120 mm thick transverse plies.

4.4 Homogenised stress-strain response

As described in Section 2.3.3, different researchers [15; 17; 18], based on CMM analyses, observed that, as suggested by Saito et al. [13], sudden matrix crack extension in the thickest transverse laminae leads to strong stress relaxation, whereas the thinner transverse laminae show a gradual extension of the tranverse cracks, causing more gradual stress relaxation. The homogenised stress-strain evolution of the embedded 90° laminae can provide some hints on the level of stress relaxation, as suggested in Ref. [15].

To obtain the homogenised stress-strain evolutions of the embedded 90° ply, a first-order volumetric homogenisation is performed following the numerical procedures prescribed on Equations 3.1 and 3.2 (please refer to Chapter 3). Figure 4.14 show the homogenised stress-strain curves obtained for the different embedded 90° ply RVEs corresponding to sublaminates with 0° outer plies (the circular marker corresponds to the penetration of the first matrix crack through the thickness of the 90° lamina). From the observation of these numerical results, it can be concluded that:

- For the different embedded 90° ply RVEs here considered, damage onset (represented with a triangular marker for reference) shows some variability, occurring at a different $\gamma_{23}^{0,\mathrm{Eq}}$.

- After damage localisation occurs, the corresponding softening region (represented in dashed line for reference) is more gradual for the thinner transverse plies (compare Figures 4.14a and 4.14b).

- Lastly, although for more conventional ply thicknesses, for the sake of computational efficiency, the total width (y-direction) of the RVEs is reduced when compared to the thin-ply sublaminate RVEs, a similar softening behaviour is observed (compare Figures 4.14e and 4.14g).

As a final remark, it can be concluded that, as in the transverse tensile loading scenario [13; 15; 17; 18], sudden matrix crack extension due to transverse shear loading leads to stress relaxation for the thickest transverse laminae, whereas the thinner transverse laminae show a gradual extension of the transverse cracks, thus stress relaxation is fairly less pronounced in this case.

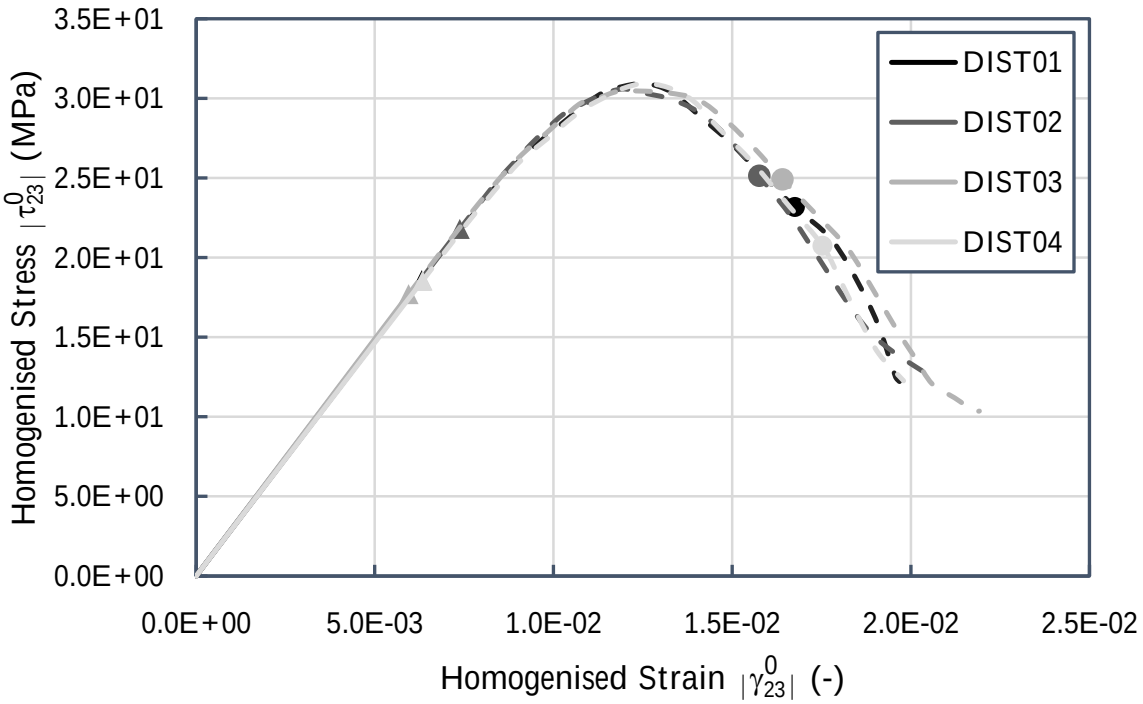

(a) RVE of a 0.020 mm thick 90° lamina

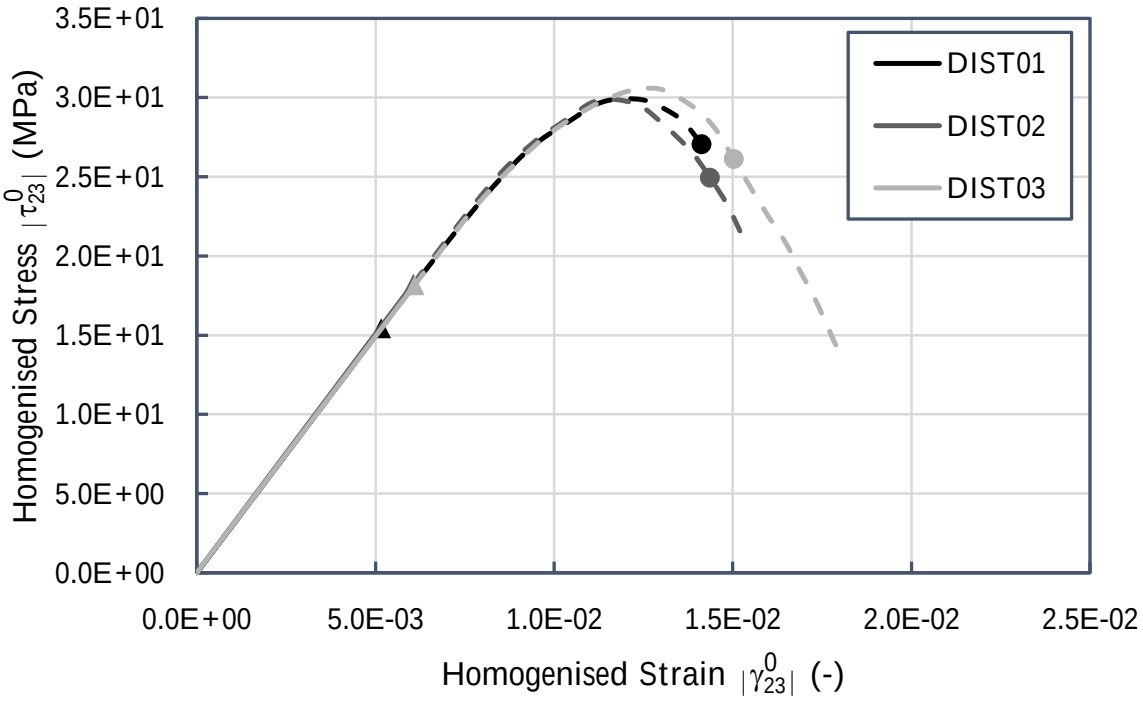

(b) RVE of a 0.040 mm thick 90° lamina

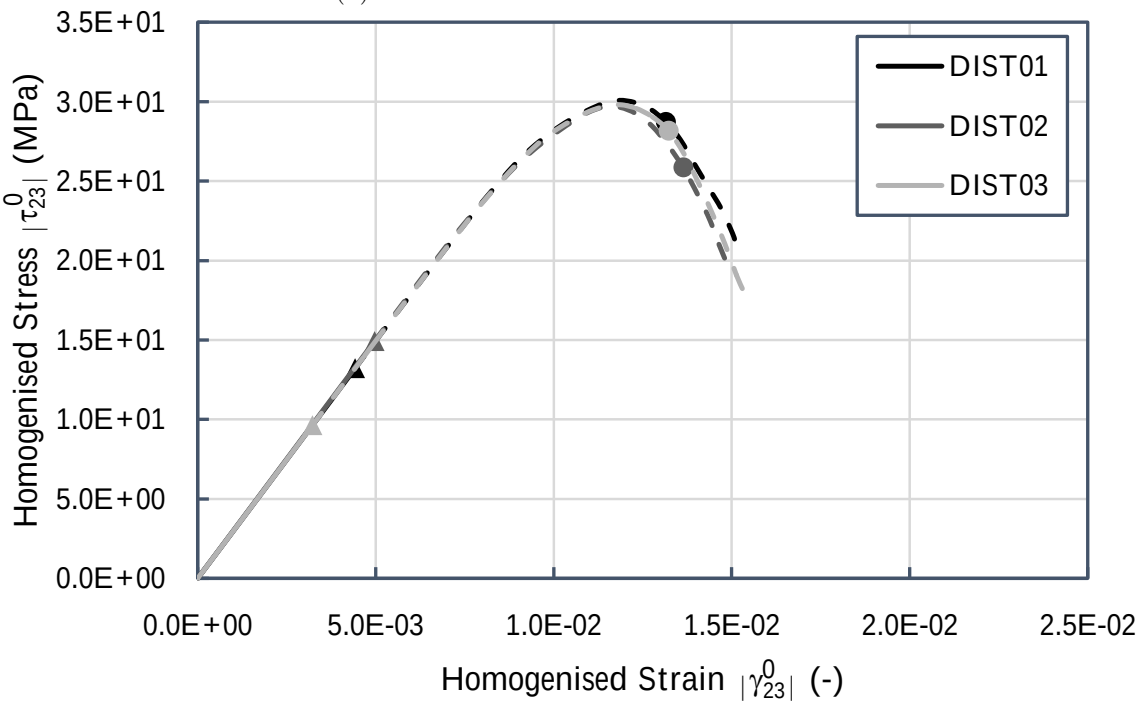

(c) RVE of a 0.060 mm thick 90° lamina

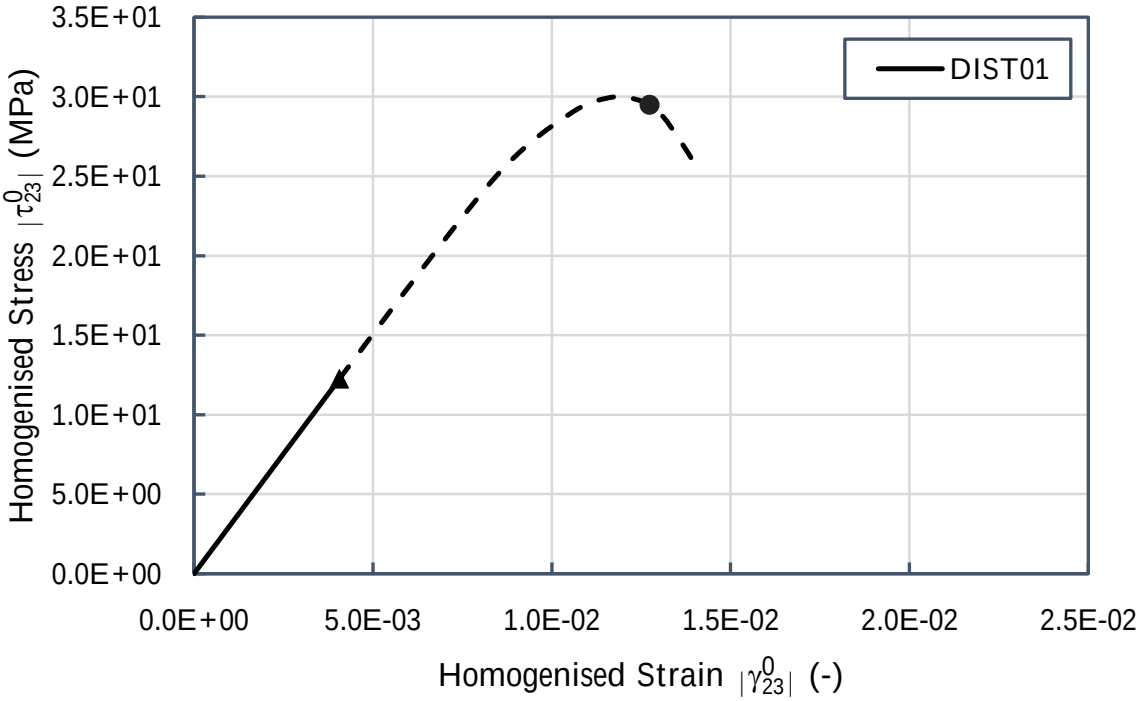

(d) RVE of a 0.080 mm thick 90° lamina

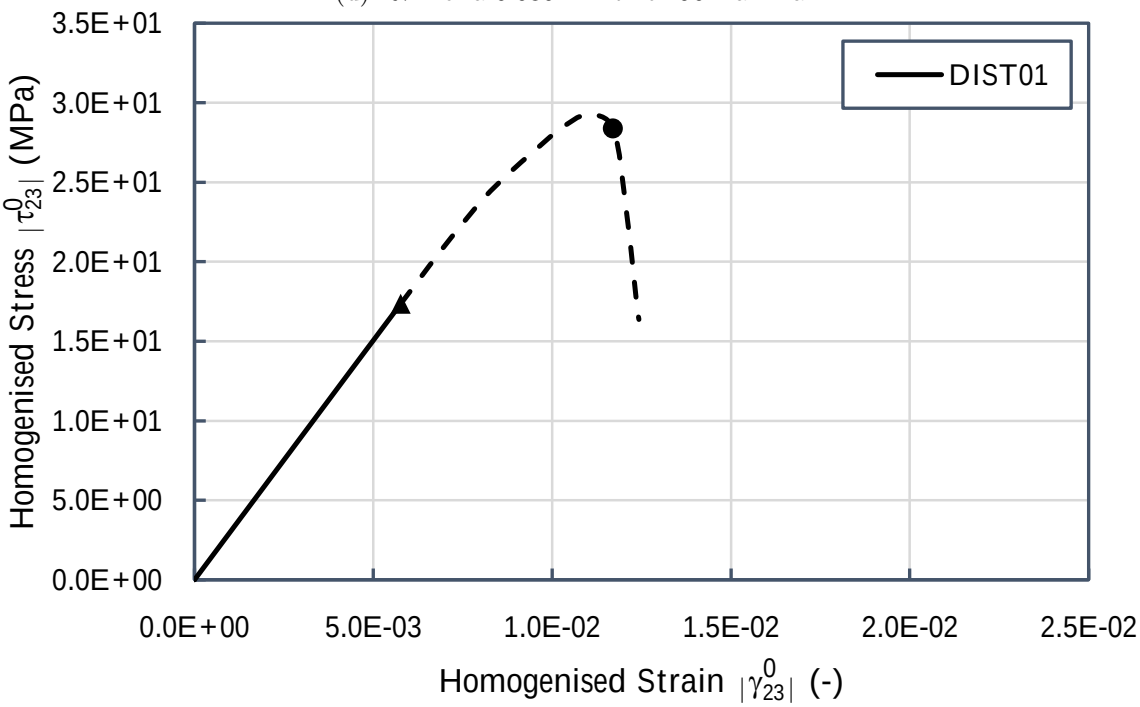

(e) RVE of a 0.100 mm thick 90° lamina

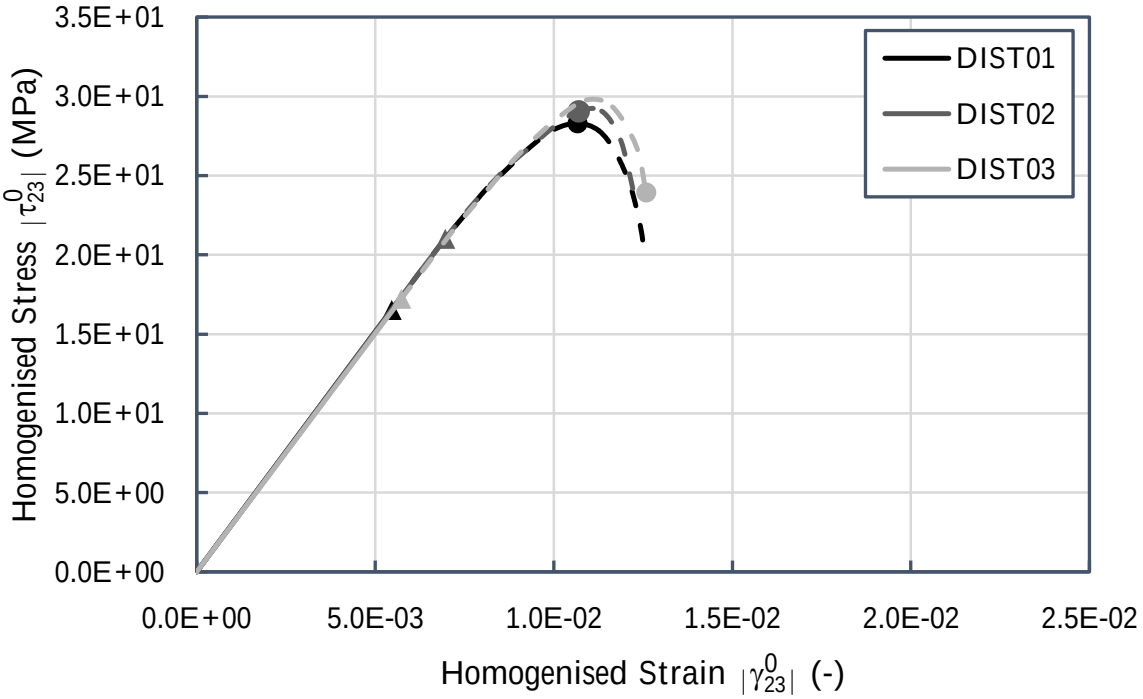

(f) RVE of a 0.120 mm thick 90° lamina

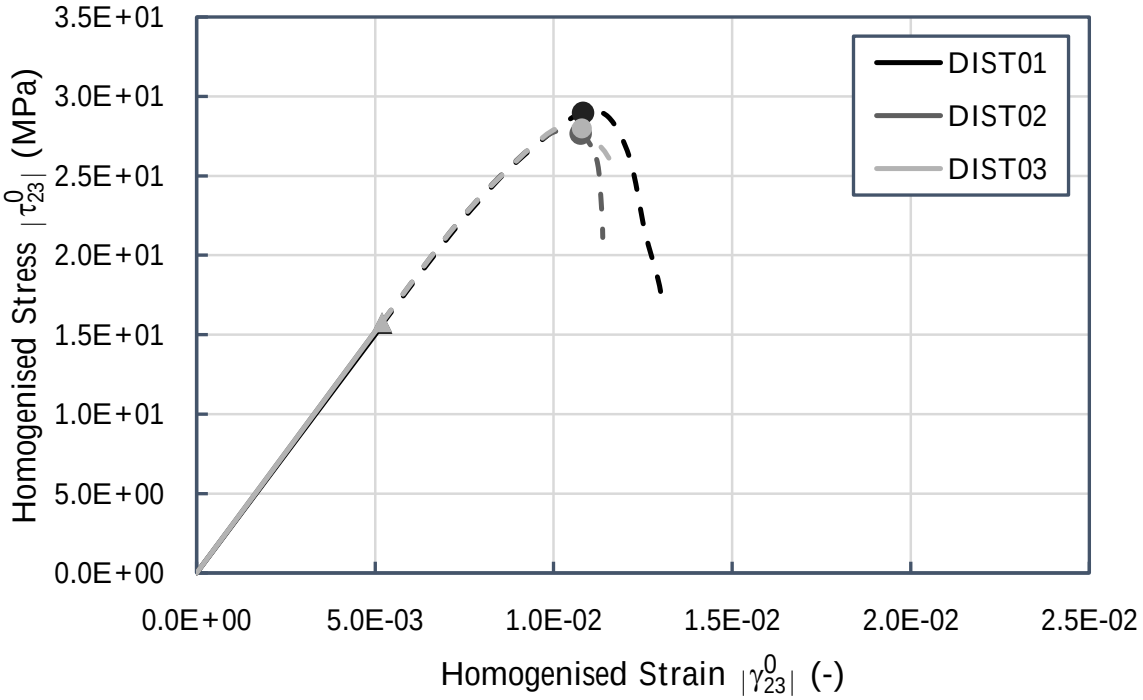

(g) RVE of a 0.140 mm thick 90° lamina

Figure 4.14: Homogenised stress-strain curves of the RVEs with an embedded 90° ply for sublaminates with 0° outer plies.

4.5 *In-situ* effect

Figure 4.15 shows the $\gamma_{23}^{0,Eq}$ values of at failure, corresponding to the development of a damage localisation zone, in terms of matrix cracking (for a value of the matrix damage variable, SDV3, equal to 1), through the thickness of the 90° ply, and consequent development of a secondary failure mechanism, which also occurs, as mentioned in Section 4.1, the delaminations.

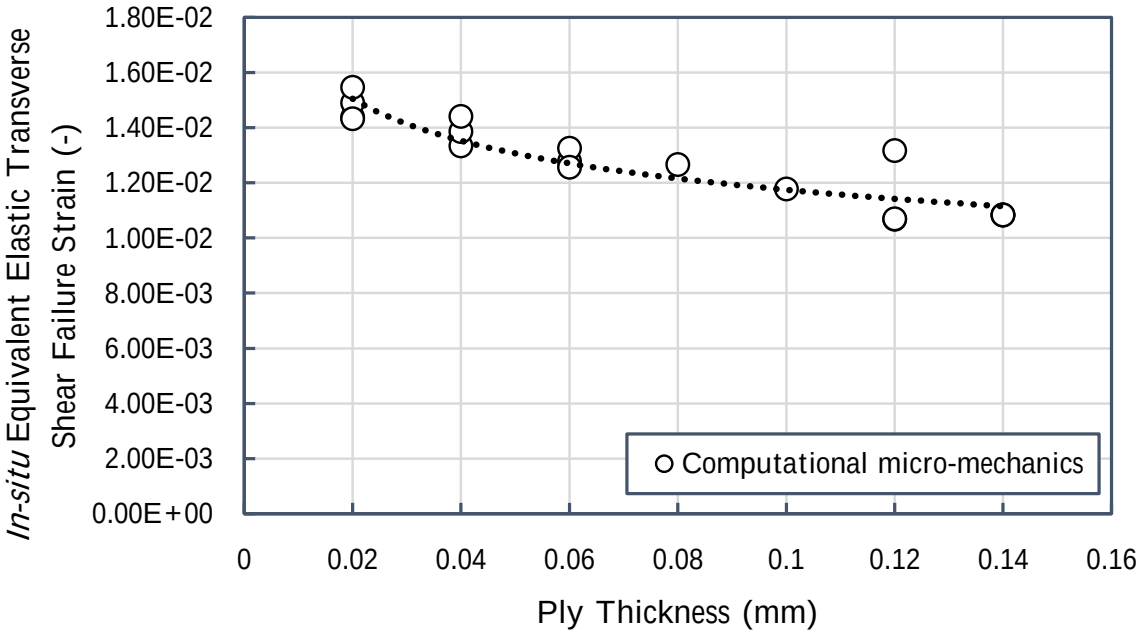

Figure 4.15: *In-situ* equivalent elastic transverse shear strain at failure as a function of ply thickness (the dotted line is a trendline fitted to the numerical results).

As can be observed, although there is some variability, which can be attributed to the different fibre distributions, it is clear that reducing the ply thickness leads to higher equivalent elastic transverse shear failure strain of the different embedded 90° laminae. This is a clear evidence of an *in-situ* effect in transverse shear. Furthermore, the fact that this trend is also observed for RVEs with ply thicknesses above 0.100 mm, shows that the 0.120 mm wide RVEs could capture this *in-situ* relation and the underlying mechanisms of transverse cracking for such ply thicknesses.

Chapter 5

Conclusion

In this dissertation, the structural integrity, in terms of matrix cracking and delamination, of thin-ply composite laminates, was assessed by a 3D CMM framework. The effect of ply thickness on the micro-mechanical response of embedded UD laminae subjected to a transverse shear stress state, was studied, thus further elucidating about the ply damage behaviour. In this chapter, the main conclusions of this thesis are discussed. Because it is recognised that this thesis is just a first step towards the understanding of the structural integrity of thin-ply composite laminates subjected to shear loading scenarios, in terms of matrix cracking and *in-situ* effect, the future work that needs to be carried out in order to further characterise this deterministic size effect is also proposed.

5.1 Conclusions

A 3D CMM framework [15; 16] was used in this dissertation to assess the effect of ply thickness on the micro-mechanical response of embedded UD laminae subjected to a transverse shear stress state. In an analogy with the only experimental study available in the literature for a similar case [51], with an analytical scenario [48], and with similar micro-mechanical analyses assessing the *in-situ* effect, considering transverse, tensile [15; 17–21] and compressive [16] stress states, it was observed that the proposed framework is able to accurately represent the micro-mechanical response of ultra-thin plies subjected to transverse shear loading, including:

- **The mechanics of transverse shear cracking onset and propagation**
  When comparing the results of the CMM framework with the experimental campaign performed by García-Rodríguez et al. [51] and with the analytical scenario proposed by Olsson et al. [48], similar damage events, concerning the mechanics of transverse shear cracking, were observed, emphasising the validity of both the CMM, the experimental campaign [51] and the analytical scenario prediction [48].

- **A consistent orientation of the fracture plane**
  A consistent orientation of the fracture plane of the embedded transverse laminae was observed, in agreement with the results observed by Melro et al. [87] for UD polymer composites subjected to a transverse shear stress state.

- **The constraining effect observed in the laminae embedded in multidirectional laminates**
  As in the micro-mechanical analysis performed by Arteiro et al. [15], a constraining effect was also observed in the present work for transverse laminae embedded in multidirectional laminates. This constraining effect can be attributed to the presence of an *in-situ* effect on transverse shear.

- **The gradual, slow stress relaxation and progressive transverse shear cracking observed in very thin plies, and consequent increase of the crack density**
  In the first experimental studies concerning matrix cracking of thin plies it was reported by Saito et al. [13] that for the thickest transverse laminae, the sudden matrix crack extension leads to stronger stress relaxation, whereas the thinner tranverse laminae show a gradual extension of the transverse cracks, making stress relaxation less pronounced. This fact had already been confirmed numerically by a few researchers considering a transverse tensile loading scenario [15; 17; 18]. Through the observation of a similar trend from the present micro-mechanical analyses, the same is concluded for transverse shear loading.

- **An *in-situ* effect**
  This numerical result is the most clear evidence of an *in-situ* effect for transverse shear.

This research is seen as a sequel of the previous micro-mechanical analyses performed by Arteiro et al [15; 16], extending the analysis to transverse shear scenarios, thus further understanding the ply damage behaviour.

Based on the main conclusions reported above, and as a final remark, the present CMM model and corresponding FE strategy proved to be fairly suitable to assess the effect of ply thickness on the micro-mechanical response of embedded UD laminae subjected to transverse shear stress states.

5.2 Future Work

Notwithstanding the efforts made previously to characterise the mechanical behaviour and the structural integrity of thin-ply composite laminates, in terms of matrix cracking and the *in-situ* effect, there is still a lot of work that can be done to complement the results obtained during this dissertation, and to improve the present CMM model. Amongst many possible suggestions, a few are here presented:

- Adapt the present CMM model, considering again an explicit numerical FE solver on ABAQUS®, but subjecting the embedded UD laminae to an in-plane shear stress state, implementing an alternative strategy concerning the loading and the boundary conditions of the FE model (a possible suggestion is presented in Appendix A), as an alternative to PBCs.

- Adapt the present CMM model, considering again an explicit numerical FE solver on ABAQUS® and shear loading scenarios, but imposing the traditional PBCs on the micro-mechanical analyses, following the technique used by Varandas et al. [126],

i.e., imposing PBCs by using linear constraint equations in the FE commercial software ABAQUS® [106].

- Once quantified the transverse shear remote strain applied to the RVE, (for instance, by imposing PBCs), numerically quantify the *in-situ* transverse shear strength, and compare with the analytical predictions [46–48] presented in Chapter 2). The same is valid to a future micro-mechanical analysis considering an in-plane shear stress state.

- The presence of defects resulting from the manufacturing of FRPs is inevitable, and they greatly influence the mechanical response, properties and the process of damage initiation and propagation of composite materials [94; 136]. Voids are assumed the most common defects found, that result from virtually any manufacturing process, whether autoclave curing, liquid compression moulding, or resin transfer moulding [136]. The effect of voids on the mechanical behaviour of composite materials has been a topic of increasing interest in recent years [94; 136; 137]. Besides the reduction of the elastic properties [137], voids can have significant effects on the microdamage mechanisms of composite laminates [94; 138]. For instance, voids can be the cause of crack initiation [94; 138], which can lead to crack growth to the fiber surface resulting in debonding of the fiber-matrix interface [136; 138], thus significantly affecting the mechanics of transverse cracking. Thereby, incorporating voids in the CMM model would be of great interest to reflect on an even more realistic micro-mechanical analysis.

- FRPs in its most varied structural applications within the aeronautical, automotive, and marine industries, are currently exposed, during service life, to the effects of hostile environments of various kinds, and, in particular to great variations of temperature and environmental humidity [139]. Particularly, the atmospheric humidity easily permeates epoxy resins, and the diffusion processes controlling movement of moisture through a composite material are substantially modified by the arrangement of the reinforcements [139]. Therefore, incorporating those hostile environmental effects, following the technique used by Naya et al. [89], in the present CMM model would as is also reflect on an even more realistic micro-mechanical analysis.

References

[1] Gay D., Hoa S.V., and Tsai S.W. *Composite Materials: Design and Applications*. Boca Raton: CRC Press, 2002.

[2] I.M. Daniel and Ishai O. *Engineering Mechanics of Composite Materials*. New York: Oxford University Press, 2006.

[3] Reddy J.N. *Mechanics of Laminated Composite Plates and Shells: Theory and Analysis*. Boca Raton: CRC Press, 2003.

[4] Laurin F., Charrier J.S., Lévêque D., Maire J.F., Mavel A., and Nuñez P. Determination of the properties of composite materials thanks to digital image correlation measurements. *Procedia IUTAM*, 4:106–115, 2012.

[5] Cousigné O., Moncayo D., Coutellier D., Camanho P., and Naceur H. Numerical modeling of nonlinearity, plasticity and damage in CFRP-woven composites for crash simulations. *Composite Structures*, 115:75–88, 2014.

[6] Behrens B.A., Rolfes R., Vucetic M., Reinoso J., Vogler M., and Grbic N. Material modelling of short fiber reinforced thermoplastic for the FEA of a clinching test. *Procedia CIRP*, 18:250–255, 2014.

[7] Baley C., Davies P., Grohens Y., and Dolto G. Application of interlaminar tests to marine composites. A literature review. *Applied Composite Materials*, 11:99–126, 2004.

[8] Camanho P.P. and Matthews F.L. A progressive damage model for mechanically fastened joints in composite laminates. *Journal of Composite Materials*, 33(24): 2248–2280, 1999.

[9] Sihn S., Kim R.Y., Kawabe K., and Tsai S.W. Experimental studies of thin-ply laminated composites. *Composites Science and Technology*, 67(6):996–1008, 2007.

[10] Kawabe K., Matsuo T., and Maekawa Z. New technology for opening various reinforcing fiber tows. *Journal of the Society of Materials Science, Japan*, 47(7):727–734, 1998. In Japanese.

[11] Kawabe K. New spreading technology for carbon fiber tow and its application to composite materials. *Sen-i Gakkaishi*, 64(8):262–267, 2008. In Japanese.

[12] Tao J. and Sun C.T. Influence of ply orientation on delamination in composite laminates. *Journal of Composite Materials*, 32(21):1933–1947, 1998.

[13] Saito H., Takeuchi H., and Kimpara I. Experimental evaluation of the damage growth restraining in 90° layer of thin-ply CFRP cross-ply laminates. *Advanced Composite Materials*, 21(1):57–66, 2012.

[14] Saito H., Takeuchi H., and Kimpara I. A study of crack suppression mechanism of thin-ply carbon-fiber-reinforced polymer laminate with mesoscopic numerical simulation. *Journal of Composite Materials*, 48(1):2085–2096, 2014.

[15] Arteiro A., Catalanotti G., Melro A.R., Linde P., and Camanho P. Micro-mechanical analysis of the in situ effect in polymer composite laminates. *Composite Structures*, 116:827–840, 2014.

[16] Arteiro A., Catalanotti G., Melro A.R., Linde P., and Camanho P. Micro-mechanical analysis of the effect of ply thickness on the transverse compressive strength of polymer composites. *Composites Part A: Applied Science and Manufacturing*, 79: 127–137, 2015.

[17] Naderi M. and Iyyer N. Micromechanical analysis of damage mechanisms under tension of 0°–90° thin-ply composite laminates. *Composites Structures*, 234:111659, 2020.

[18] Fu C. and Wang X. Micro-mechanical analysis of matrix crack-induced delamination in cross-ply laminates in tension. *Composite Structures*, 243:112202, 2020.

[19] Leopold C., Harder S., Buggisch C., Liebig W.V., and Fiedler B. Influence of 90°–layer thickness on damage initiation and propagation in CFRP cross-ply laminates. In *Proceedings of ECCM17*, Munich, 2016.

[20] Guillén-Hernández T., Quintana-Corominas A., García I.G., Reinoso J., Paggi M., and Turón A. In-situ strength effects in long fibre reinforced composites: A micromechanical analysis using the phase field approach of fracture. *Theoretical and Applied Fracture Mechanics*, page 102621, 2020.

[21] Kohler S., Cugnoni J., Amacher R., and Botsis J. Transverse cracking in the bulk and at the free edge of thin-ply composites: Experiments and multiscale modelling. *Composites Part A: Applied Science and Manufacturing*, 124:105468, 2019.

[22] Furtado C. Optimal use of ultra-thin plies in composite structures. Master's thesis, University of Porto, Oporto, 2015.

[23] Arteiro A., Furtado C., Catalanotti G., Linde P., and Camanho P.P. Thin-ply polymer composite materials: A review. *Composites Part A: Applied Science and Manufacturing*, 132:105777, 2020.

[24] Fernberg P. and Joffe R. Thin-ply effects on lon-term thermal stability of high temperature polyimide composites. In *Proceedings of ICCM-22*, pages 1–2, Melbourne, 2019.

[25] Tsai S.W. *Strength and life of composites. Composites Design Group, Department of Aeronautics and Astronautics.* Stanford University, 2008.

[26] Mencattelli L. and Pinho S.T. Realising bio-inspired impact damage-tolerant thin-ply CFRP Bouligand structures via promoting diffused sub-critical helicoidal damage. *Composites Science and Technology*, 182:107684, 2019.

[27] Galos J. Thin-ply composite laminates: A review. *Composite Structures*, 236:111920, 2020.

[28] Sebaey T.A., Costa J., Maimí P., Batista Y., Blanco N., and Mayugo J.A. Measurement of the *in situ* transverse tensile strength of composite plies by means of the real time monitoring of microcracking. *Composites Part B: Engineering*, 65:40–46, 2014.

[29] Yokozeki T., Aoki T., Ogasawara T., and Ishikawa T. Effects of layup angle and ply thickness on matrix crack interaction in contiguous plies of composite laminates. *Composites Part A: Applied Science and Manufacturing*, 36(9):1229–1235, 2005.

[30] Quaresimin M. and Carraro P.A. On the investigation of the biaxial fatigue behaviour of unidirectional composites. *Composites Part B: Engineering*, 54:200–208, 2013.

[31] Flaggs D.L. and Kural M.H. Experimental determination of the in situ transverse lamina strength in graphite/epoxy laminates. *Journal of Composite Materials*, 16 (2):103–116, 1982.

[32] Dvorak G.J. and Laws N. Analysis of progressive matrix cracking in composite laminates ii. First ply failure. *Journal of Composite Materials*, 21(4):309–329, 1987.

[33] Camanho P.P., Dávila C.G., Pinho S.T., Iannucci L., and Robinson P. Prediction of in situ strengths and matrix cracking in composites under transverse tension and in-plane shear. *Composites Part A: Applied Science and Manufacturing*, 37(2):165–176, 2006.

[34] Berthelot J.M. Transverse cracking and delamination in cross-ply glass-fiber and carbon-fiber reinforced plastic laminates: Static and fatigue loading. *Applied Mechanics Reviews*, 56:111–147, 2013.

[35] Adolfsson E. and Gudmundson P. Matrix crack initiation and progression in composite laminates subjected to bending and extension. *International Journal of Solids and Structures*, 36(21):3131–3169, 1999.

[36] Andersons J., Joffe R., Spārniņš E., and Rubenis O. Progressive cracking master-curves of the transverse ply in a laminate. *Polymer Composites*, 30(8):1175–1182, 2009.

[37] Amacher R., Cugnoni J., Botsis J., Sorensen L., Smith W., and Dransfeld C. Thin ply composites: Experimental characterization and modeling of size-effects. *Composites Science and Technology*, 101:121–132, 2014.

[38] Chang F.K. and Chen M.H. The in situ ply shear strength distributions in graphite/epoxy laminated composites. *Journal of Composite Materials*, 21:708–733, 1987.

[39] Catalanotti G. Prediction of in situ strengths in composites: Some considerations. *Composite Structures*, 207:889–893, 2019.

[40] Garrett K.W. and Bailey J.E. Multiple transverse fracture in 90° cross-ply laminates of a glass fibre-reinforced polyester. *Journal of Materials Science*, 12:157–168, 1977.

[41] Parvizi A., Garrett K.W., and Bailey J.E. Constrained cracking in glass fibre-reinforced epoxy cross-ply laminates. *Journal of Materials Science*, 13:195–201, 1978.

[42] Parvizi A. and Bailey J.E. On multiple transverse cracking in glass fibre epoxy cross-ply laminates. *Journal of Materials Science*, 13:2131–2136, 1978.

[43] Boniface L., Smith P.A., and Bader M.G. Transverse ply cracking in cross-ply CFRP laminates—initiation or propagation controlled? *Journal of Composite Materials*, 31(11):1080–1112, 1997.

[44] Herakovich C.T. Influence of layer thickness on the strength of angle-ply laminates. *Journal of Composite Materials*, 16(3):216–227, 1982.

[45] Erçin G.H., Camanho P.P., Xavier J., Catalanotti G., Mahdi S., and Linde P. Size effects on the tensile and compressive failure of notched composite laminates. *Composite Structures*, 96:736–744, 2013.

[46] Catalanotti G., Camanho P.P., and Marques A.T. Three-dimensional failure criteria for fiber-reinforced laminates. *Composite Structures*, 95:63–79, 2013.

[47] Camanho P.P., Arteiro A., Melro A.R., Catalanotti G., and Vogler M. Three-dimensional invariant-based failure criteria for transversely isotropic fibre-reinforced composites. In Camanho P.P. and Hallet S.R., editors, *Numerical Modelling of Failure in Advanced Composite Materials*, chapter 5, pages 111–150. Woodhead Publishing, Cambridge, 2015.

[48] Olsson R. Analytical prediction of damage due to large mass impact on thin ply composites. *Composites Part A: Applied Science and Manufacturing*, 72:184–191, 2015.

[49] Kalfon-Cohen E., Kopp R., Furtado C., Ni X., Arteiro A., Borstnar G., Mavrogordato M.N., Sinclair I., Spearing S.M., Camanho P.P., and Wardle B.L. Synergetic effects of thin plies and aligned carbon nanotube interlaminar reinforcement in composite laminates. *Composites Science and Technology*, 166:160–168, 2018.

[50] Bhudolia S.K., Joshi S.C., and Boon Y.D. Experimental and microscopic investigation on mechanical performance of textile spread-tow thin ply composites. *Fibers and Polymers*, 20(5):1036–1045, 2019.

[51] García-Rodríguez S.M., Costa J., Maimí P., Singery V., Cózar I.R., Quintanas-Corominas A., and Sasikumar A. Experimental demonstration of the *in-situ* effect under transverse shear. *Composites Part A: Applied Science and Manufacturing*, page 106047, 2020.

[52] Fuller J.D. and Wisnom M.R. Pseudo-ductility and damage suppression in thin ply CFRP angle-ply laminates. *Composites Part A: Applied Science and Manufacturing*, 69:64–71, 2015.

[53] Laws N. A note on interaction energies associated with cracks in anisotropic solids. *The Philosophical Magazine: A Journal of Theoretical Experimental and Applied Physics*, 36(2):367–372, 1977.

[54] Chang K.Y., Liu S., and Chang F.K. Damage tolerance of laminated composites containing an open hole and subjected to tensile loadings. *Journal of Composite Materials*, 25(3):274–301, 1991.

[55] Lavoie J.A., Soutis C., and Morton J. Apparent strength scaling in continuous fiber composite laminates. *Composites Science and Technology*, 60(2):283 – 299, 2000.

[56] Lavoie J.A. and Adolfsson E. Stitch cracks in constraint plies adjacent to a cracked ply. *Journal of Composite Materials*, 35(23):2077–2097, 2001.

[57] Huchette C. *Sur la complémentarité des approches expérimentales et numériques pour la modélisation des mécanismes d'endommagement des composites stratifiés*. PhD thesis, Université Paris 6, Paris, 2005. In French.

[58] Pierron F., Green B., and Wisnom M.R. Full-field assessment of the damage process of laminated composite open-hole tensile specimens. Part I: Methodology. *Composites Part A: Applied Science and Manufacturing*, 38(11):2307–2320, 2007.

[59] Pierron F., Green B., Wisnom M.R., and Hallett S.R. Full-field assessment of the damage process of laminated composite open-hole tensile specimens. Part II: Experimental results. *Composites Part A: Applied Science and Manufacturing*, 38(11): 2321–2332, 2007.

[60] O'Higgins R.M., McCarthy M.A., and McCarthy C.T. Comparison of open hole tension characteristics of high strength glass and carbon fibre-reinforced composite materials. *Composites Science and Technology*, 68(13):2770–2778, 2008.

[61] Laurin F., Carrere N., Huchette C., and Maire J.F. A multiscale hybrid approach for damage and final failure predictions of composite structures. *Journal of Composite Materials*, 47(20-21):2713–2747, 2013.

[62] Ho Y.C., Sasayama H., and Yanagimoto J. Mechanical properties and drawing process of multilayer carbon-fiber-reinforced plastic sheets with various prepreg thicknesses. *Advances in Mechanical Engineering*, 9(3):1687814017692695, 2017.

[63] Sasayama H., Kawabe K., Tomoda S., and Ohsawa I. Effect of lamina thickness on first ply failure in multidirectionally laminated composites. *Journal of the Japan Society for Composite Materials*, 30(1):142–148, 2004.

[64] Takagi K. and Nakatani H. Effect of ply thickness on mechanical property of CFRP symmetric angle-ply laminate. In *Proceedings of ICCM-18*, pages 1–4, Jeju Island, 2011.

[65] Ogihara S. and Nakatani H. Effect of ply thickness on mechanical properties in CFRP angle-ply laminate. In *Proceedings of ECCM15*, pages 1–6, Venice, 2012.

[66] Guillamet G., Turon A., Costa J., Renart J., Linde P., and Mayugo J.A. Damage occurrence at edges of non-crimp-fabric thin-ply laminates under off-axis uniaxial loading. *Composites Science and Technology*, 98:44–50, 2014.

[67] Arteiro A., Catalanotti G., Xavier J., Linde P., and Camanho P.P. Effect of tow thickness on the structural response of aerospace-grade spread-tow fabrics. *Composite Structures*, 179:208–223, 2017.

[68] Chang F.K., Scott R.A., and Springer G.S. The effect of laminate configuration on characteristic lengths and rail shear strength. *Journal of Composite Materials*, 18: 290–296, 1984.

[69] Liu H., Falzon B., and Catalanotti G. Studies on the effects of lamina thickness and orientation on the shear response of composite laminates. In *Proceedings of ICCM-21*, pages 1–10, Xi'an, 2017.

[70] Puck A. and Schürmann H. Failure analysis of FRP laminates by means of physically based phenomenological models. *Composites Science and Technology*, 58(7):1045–1067, 1998.

[71] Puck A. and Schürmann H. Failure analysis of FRP laminates by means of physically based phenomenological models. *Composites Science and Technology*, 62(12):1633–1662, 2002.

[72] Vogler M., Ernst G., and Rolfes R. Invariant based transversely-isotropic material and failure mode for fiber-reinforced polymers. *Computers, Materials and Continua*, 16(1):25–49, 2010.

[73] Vogler M., Rolfes R., and Camanho P.P. Modeling the inelastic deformation and fracture of polymer composites – Part i: Plasticity model. *Mechanics of Materials*, 59:50–64, 2013.

[74] Kawebe K., Sasayama H., Kageyama K., and Ogata N. Effect of ply thickness on compressive properties in multidirectionally laminated composites. *Journal of the Japan Society for Composite Materials*, 34:173–181, 2008. In Japanese.

[75] Arteiro A., Catalanotti G., Xavier J., and Camanho P.P. Notched response of non-crimp fabric thin-ply laminates. *Composites Science and Technology*, 79:97–114, 2013.

[76] De Borst R. and Remmers J.J.C. Computational Methods for Debonding in Composites. In Camanho P.P., Dávila C.G., Pinho S.T., and Remmers J.J.C., editors, *Mechanical Response of Composites*, volume 10 of *Computational Methods in Applied Sciences*, chapter 1, pages 1–25. Springer, Dordrecht, 2008.

[77] Dávila C.G., Rose C.A., and Iarve E.V. Modeling Fracture and Complex Crack Networks in Laminated Composites. In Mantič V., editor, *Mathematical Methods and Models in Composites*, volume 5 of *Computational and Experimental Methods in Structures*, chapter 8, pages 297–347. Imperial College Press, London, 2014.

[78] Melro A.R. *Analytical and numerical modelling of damage and fracture of advanced composites*. PhD thesis, University of Porto, Oporto, 2011.

[79] Ladevèze P., Lubineau G., Violeau D., and Marsal D. A computational damage micromodel for laminate composites. In Sadowski T., editor, *IUTAM Symposium on Multiscale Modelling of Damage and Fracture Processes in Composite Materials*, pages 1–12. Springer, 2006.

[80] Soden P.D., Kaddour A.S., and Hinton M.J. Recommendations for designers and researchers resulting from the world-wide failure exercise. *Composites Science and Technology*, 64:589–604, 2004.

[81] Arteiro A., Catalanotti G., Reinoso J., Linde P., and Camanho P.P. Simulation of the mechanical response of thin-ply composites: From computational micro-mechanics to structural analysis. *Archives of Computational Methods in Engineering*, 26:1445–1487, 2019.

[82] Tessitore N. and Riccio A. A novel FEM model for biaxial non-crimp fabric composite materials under tension. *Computers and Structures*, 84(19):1200–1207, 2006.

[83] Petriccione A., Annicchiarico D., Antonucci V., Giordano M., Riccio A., and Scaramuzzino F. A stiffness volume averaging based approach to model non-crimp fabric reinforced composites. *Composites Science and Technology*, 72(2):360–369, 2012.

[84] González C. and Llorca J. Mechanical behavior of unidirectional fiber-reinforced polymers under transverse compression: Microscopic mechanisms and modeling. *Composites Science and Technology*, 67(13):2795–2806, 2007.

[85] Melro A.R., Camanho P.P., and Pinho S.T. Generation of random distribution of fibres in long-fibre reinforced composites. *Composites Science and Technology*, 68 (9):2092–2102, 2008.

[86] Trias D., Costa J., Turon A., and Hurtado J.E. Determination of the critical size of a statistical representative volume element (SRVE) for carbon reinforced polymers. *Acta Materialia*, 54(13):3471–3484, 2006.

[87] Melro A.R., Camanho P.P., Pires F.M.A., and Pinho S.T. Micromechanical analysis of polymer composites reinforced by unidirectional fibres: Part II – Micromechanical analyses. *International Journal of Solids and Structures*, 50:1906–1915, 2013.

[88] Sebaey T.A., Catalanotti G., Lopes C.S., and O'Dowd N. Computational micromechanics of the effect of fibre misalignment on the longitudinal compression and shear properties of ud fibre-reinforced plastics. *Composite Structures*, 248:112487, 2020.

[89] Naya F., González C., Lopes C.S., Van der Veen S., and Pons F. Computational micromechanics of the transverse and shear behavior of unidirectional fiber reinforced polymers including environmental effects. *Composites Part A: Applied Science and Manufacturing*, 92:146–157, 2017.

[90] Varandas L.F., Catalanotti G., Melro A.R., Tavares R.P., and Falzon B.G. Micromechanical modelling of the longitudinal compressive and tensile failure of unidirectional composites: The effect of fibre misalignment introduced via a stochastic process. *International Journal of Solids and Structures*, 203:157–176, 2020.

[91] Bednarcyk B.A., Aboudi J., and Arnold S.M. The effect of general statistical fiber misalignment on predicted damage initiation in composites. *Composites Part B: Engineering*, 66:97–108, 2014.

[92] Varandas L.F., Arteiro A., Catalanotti G., and Falzon B.G. Micromechanical analysis of interlaminar crack propagation between angled plies in mode I tests. *Composite Structures*, 220:827–841, 2019.

[93] Varandas L.F., Arteiro A., Bessa M.A., Melro A.R., and Catalanotti G. The effect of through-thickness compressive stress on mode II interlaminar crack propagation: A computational micromechanics approach. *Composite Structures*, 182:326–334, 2017.

[94] Mehdikhani M., Petrov N.A., Straumit I., Melro A.R., S.V. Lomov, and Gorbatikh L. The effect of voids on matrix cracking in composite laminates as revealed by combined computations at the micro- and meso-scales. *Composites Part A: Applied Science and Manufacturing*, 117:180–192, 2019.

[95] Li S. General unit cells for micromechanical analyses of unidirectional composites. *Composites Part A: Applied Science and Manufacturing*, 32(6):815–826, 2001.

[96] Romanowicz M. A numerical approach for predicting the failure locus of fiber reinforced composites under combined transverse compression and axial tension. *Computational Materials Science*, 51(1):7–12, 2012.

[97] Hobbiebrunken T., Fiedler B., Hojo M., Ochiai S., and Schulte K. Microscopic yielding of CF/epoxy composites and the effect on the formation of thermal residual stresses. *Composites Science and Technology*, 65(10):1626–1635, 2005.

[98] Trias D., Costa J., Mayugo J.A., and Hurtado J.E. Random models versus periodic models for fibre reinforced composites. *Computational Materials Science*, 38(2): 316–324, 2006.

[99] Vaughan T.J. and McCarthy C.T. A combined experimental–numerical approach for generating statistically equivalent fibre distributions for high strength laminated composite materials. *Composites Science and Technology*, 70(2):291–297, 2010.

[100] Vaughan T.J. and McCarthy C.T. Micromechanical modelling of the transverse damage behaviour in fibre reinforced composites. *Composites Science and Technology*, 71(3):388–396, 2011.

[101] Totry E., Molina-Aldareguía J.M., González C., and LLorca J. Effect of fiber, matrix and interface properties on the in-plane shear deformation of carbon-fiber reinforced composites. *Composites Science and Technology*, 70(6):970–980, 2010.

[102] Canal L.P., González C., Segurado J., and LLorca J. Intraply fracture of fiber-reinforced composites: Microscopic mechanisms and modeling. *Composites Science and Technology*, 72(11):1223–1232, 2012.

[103] Ghorbel E. A viscoplastic constitutive model for polymeric materials. *International Journal of Plasticity*, 24(11):2032–2058, 2008.

[104] Melro A.R., Camanho P.P., Pires F.M.A., and Pinho S.T. Micromechanical analysis of polymer composites reinforced by unidirectional fibres: Part I – Constitutive modelling. *International Journal of Solids and Structures*, 50:1897–1905, 2013.

[105] Bai X., M.A. Bessa, Camanho P.P., Guo L., and W.K. Liu. High-fidelity micro-scale modeling of the thermo-visco-plastic behavior of carbon fiber polymer matrix composites. *Composite Structures*, 134:132–141, 2015.

[106] *ABAQUS 6.12 Documentation.* Dassault Systèmes Simulia Corp., Providence, RI, USA, 2012.

[107] Tschoegl N. W. Failure surfaces in principal stress space. *Journal of Polymer Science Part C: Polymer Symposia*, 32:239–267, 2007.

[108] Bažant Z.P. and Oh B.H. Crack band theory for fracture of concrete. *Matériaux et Constructions*, 16(93):155–177, 1983.

[109] Fiedler B., Hojo M., Ochiai S., Schulte K., and Ando M. Failure behavior of an epoxy matrix under different kinds of static loading. *Composites Science and Technology*, 61(11):1615–1624, 2001.

[110] Guild F.J., Potter K.D., Heinrich J., Adams R.D., and Wisnom M.R. Understanding and control of adhesive crack propagation in bonded joints between carbon fibre composite adherends II. Finite element analysis. *International Journal of Adhesion and Adhesives*, 21(6):445–453, 2001.

[111] Benzeggagh M.L. and Kenane M. Measurement of mixed-mode delamination fracture toughness of unidirectional glass/epoxy composites with mixed-mode bending apparatus. *Composites Science and Technology*, 56(4):439–449, 1996.

[112] Varna J., Berglund L.A., and Ericson M.L. Transverse single-fibre test for interfacial debonding in composites: 2. Modelling. *Composites Part A: Applied Science and Manufacturing*, 28(4):317–326, 1997.

[113] Camanho P.P. and Lambert M. A design methodology for mechanically fastened joints in laminated composite materials. *Composites Science and Technology*, 66 (15):3004–3020, 2006.

[114] Wisnom M.R., Khan B., and Hallett S.R. Size effects in unnotched tensile strength of unidirectional and quasi-isotropic carbon/epoxy composites. *Composite Structures*, 84(1):21–28, 2008.

[115] Koerber H., Xavier J., and Camanho P.P. High strain rate characterisation of unidirectional carbon-epoxy IM7-8552 in transverse compression and in-plane shear using digital image correlation. *Mechanics of Materials*, 42(11):1004–1019, 2010.

[116] Sádaba S., Herráez M., Naya F., González C., Llorca J., and Lopes C.S. Special-purpose elements to impose Periodic Boundary Conditions for multiscale computational homogenization of composite materials with the explicit Finite Element Method. *Composite Structures*, 208:434–441, 2019.

[117] Barbero E.J., Cosso F.A., and Campo F.A. Benchmark solution for degradation of elastic properties due to transverse matrix cracking in laminated composites. *Composite Structures*, 98:242–252, 2013.

[118] Okereke M.I. and Akpoyomare A.I. A virtual framework for prediction of full-field elastic response of unidirectional composites. *Computational Materials Science*, 70: 82–99, 2013.

[119] Nguyen V.D., Béchet E., Geuzaine C., and Noels L. Imposing periodic boundary condition on arbitrary meshes by polynomial interpolation. *Computational Materials Science*, 55:390–406, 2012.

[120] Tyrus J.M., Gosz M., and DeSantiago E. A local finite element implementation for imposing periodic boundary conditions on composite micromechanical models. *International Journal of Solids and Structures*, 44(9):2972–2989, 2007.

[121] Reis F.J.P. and F.M. Andrade Pires. A mortar based approach for the enforcement of periodic boundary conditions on arbitrarily generated meshes. *Computer Methods in Applied Mechanics and Engineering*, 274:168–191, 2014.

[122] Kanit T., Forest S., Galliet I., Mounoury V., and Jeulin D. Determination of the size of the representative volume element for random composites: Statistical and numerical approach. *International Journal of Solids and Structures*, 40(13):3647–3679, 2003.

[123] Kanit T., N'Guyen F., Forest S., Jeulin D., Reed M., and Singleton S. Apparent and effective physical properties of heterogeneous materials: Representativity of samples of two materials from food industry. *Computer Methods in Applied Mechanics and Engineering*, 195(33):3960–3982, 2006.

[124] Chen G., Ozden U.A., Bezold A., and Broeckmann C. A statistics based numerical investigation on the prediction of elasto-plastic behavior of WC–Co hard metal. *Computational Materials Science*, 80:96–103, 2013.

[125] Garoz D., Gilabert F.A., Sevenois R.D.B., Spronk S.W.F., and Van Paepegem W. Consistent application of periodic boundary conditions in implicit and explicit finite element simulations of damage in composites. *Composites Part B: Engineering*, 168: 254–266, 2019.

[126] Varandas L.F., Catalanotti G., Melro A.R., and Falzon B.G. On the importance of nesting considerations for accurate computational damage modelling in 2D woven composite materials. *Computational Materials Science*, 172:109323, 2020.

[127] Soni G., Gupta S., Singh R., Mitra M., Yan W., and Falzon B.G. Study of localized damage in composite laminates using micro–macro approach. *Composite Structures*, 113:1–11, 2014.

[128] Barbero E.J. *Finite element analysis of composite materials*. CRC Press, 2008.

[129] Bathe K.J. *Finite element procedures in engineering analysis*. New Jersey: Prentice Hall, Pearson Education, Inc., 1982.

[130] Biggs J.M. *Introduction to structural dynamics*. McGraw-Hill, Inc., 1964.

[131] Olovsson L., Simonsson K., and Unosson M. Selective mass scaling for explicit finite element analyses. *International Journal for Numerical Methods in Engineering*, 63 (10):1436–1445, 2005.

[132] Askes H., Nguyen D.C., and Tyas A. Increasing the critical time step: Micro-inertia, inertia penalties and mass scaling. *Computational Mechanics*, 47(06):657–667, 2011.

[133] Olovsson L. and Simonsson K. Iterative solution technique in selective mass scaling. *Communications in Numerical Methods in Engineering*, 22(1):77–82, 2006.

[134] Cocchetti G., Pagani M., and Perego U. Selective mass scaling and critical time-step estimate for explicit dynamics analyses with solid-shell elements. *Computers & Structures*, 127:39–52, 2013.

[135] N. B. Hamid, J. Dennis, K. Mehdi, Sprengers A., S.P. Emin, V.d.B. Ton, and V. Nico. A comparison between dynamic implicit and explicit finite element simulations of the native knee joint. *Medical Engineering & Physics*, 38(10):1123–1130, 2016.

[136] Chowdhury K., Talreja R., and Benzerga A. Effects of manufacturing-induced voids on local failure in polymer-based composites. *Journal of Engineering Materials and Technology*, 130(2):021010, 2008.

[137] Huang H. and Talreja R. Effects of void geometry on elastic properties of unidirectional fiber reinforced composites. *Composites Science and Technology*, 65(13): 1964–1981, 2005.

[138] Varna J., Joffe R., Berglund L.A., and Lundström T.S. Effect of voids on failure mechanisms in RTM laminates. *Composites Science and Technology*, 53(2):241–249, 1995.

[139] Jones C.J., Dickson R.F., Adam T., Reiter H., and Harris B. Environmental fatigue of reinforced plastics. *Composites*, 14(3):288–293, 1983.

Appendix A

Analysis of ply damage using computational micro-mechanics - In-plane shear failure mechanisms

A.1 Introduction

The present appendix intends to present a suggestion to perform a similar micro-mechanical analysis to further assess the effect of ply thickness on the in-plane shear response of UD laminae embedded in multidirectional laminates. Similarly, this suggestion consists of performing CMM analyses using ABAQUS®/Explicit as explicit dynamic analyses, considering the CMM model used in this dissertation.

A.2 Finite element modelling

Concerning the FE modelling, the model discretisation could remain unaltered, except for the length (x-direction) of the RVE, c, which should be defined to capture in-plane shear load damage growth parallel to the fibres direction.

A.2.1 Loading and Boundary Conditions

A possible strategy to perform a micro-mechanical analysis considering an in-plane shear load is schematized in Figure A.1. Similarly, as in the transverse shear analyses performed in this dissertation, the in-plane shear load could be applied through a velocity in the x-direction (see Figure A.1) along the left face of the RVE, as a smooth step amplitude throughout the step time [106]. Again, the smooth step amplitude is used to avoid initial dynamic phenomena, thus simulating a quasi-static response of the composite material.

Concerning the general boundary conditions, in order to simulate a pure in-plane shear stress state in the micromechanical model, the right face of the RVE could be simply supported (fixed only along the y-direction) and the opposite face could be clamped — see Figure A.1.

However, following this alternative strategy of loading and boundary conditions, to accurately capture in-plane shear load damage, the length (x-direction) of the RVE , c, should be increased, thus the primary task to perform such micro-mechanical analysis should be a parametric study to assess the required RVE length, c, that accurately captures the in-plane damage mechanisms, including crack tunneling.

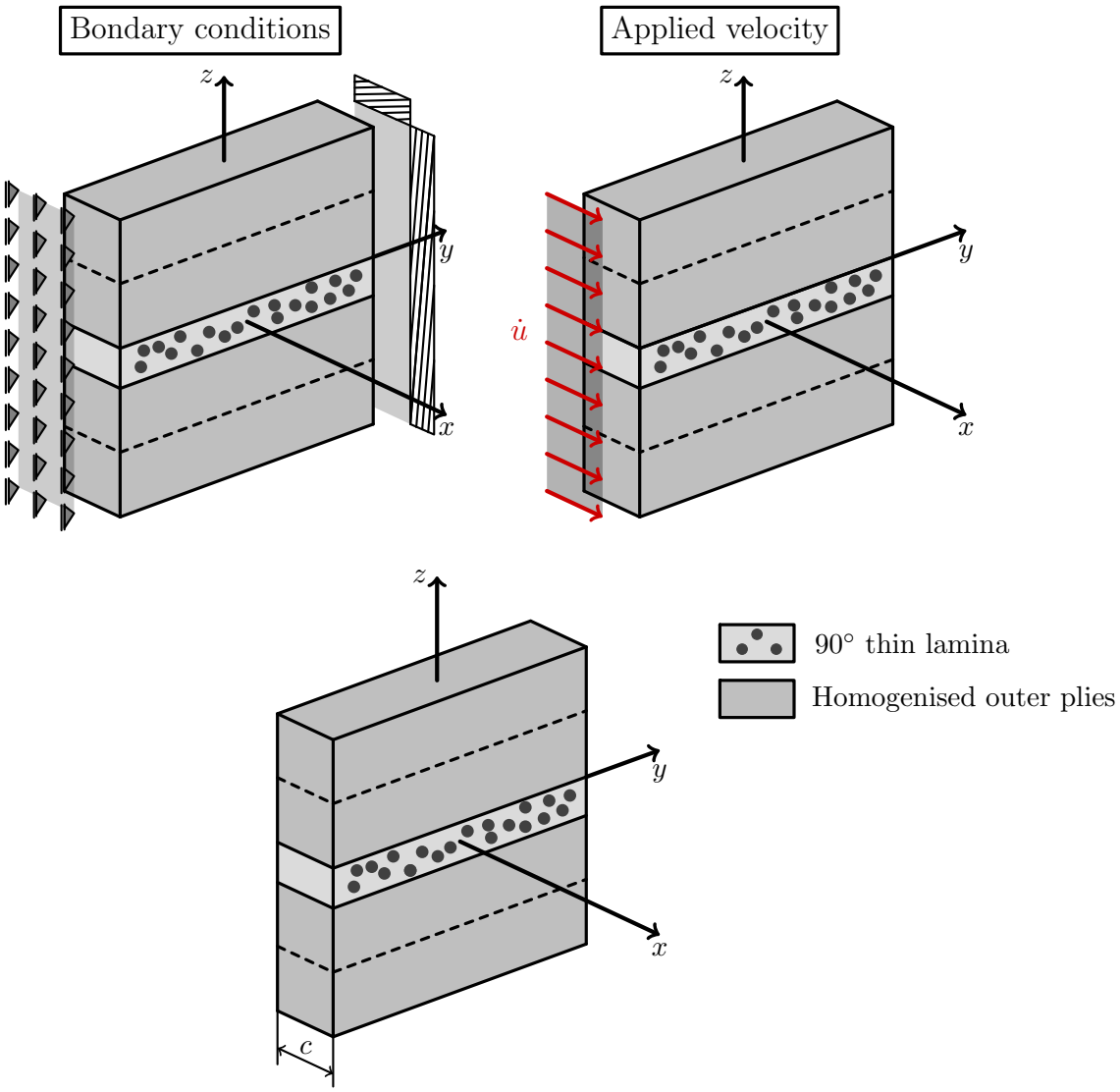

Figure A.1: Schematic suggestion of the loading and boundary conditions to apply to the micromechanical model for the in-plane shear analysis (for simplicity, the loading and boundary conditions are represented separately here, but should be applied simultaneously in the FE model).